Characterization of an enhancer upstream of *msx3* and its role in development of the neural tube of embryonic and larval zebrafish

Shea Keil

Thesis submitted to the University of Ottawa in partial fulfilment of
the requirements for the Master of Science in Biology Program

Department of Biology
Faculty of Science
University of Ottawa

Abstract

The vertebrate nervous system arises during embryogenesis from an epithelial sheet of cells called the neural plate that subsequently folds to become a rod of cells called the neural tube. Several signaling pathways act on the neural progenitors of the neural tube to give rise to the diverse set of neurons and glia that will make up the spinal cord and brain in adulthood. In vertebrates, Muscle segment homeobox (*Msx*) genes are expressed in the dorsal neural tube during development, and pattern dorsal neural progenitors to give rise to dorsal neuronal subtypes. Additionally, *Msx* genes are involved in the regulation of neurogenesis and proliferation in the neural tube. In zebrafish, three *msx* genes are expressed in the neural tube: *msx1a, msx1b,* and *msx3*. The Akimenko lab has identified a potential enhancer of *msx3* called Fragment C that drives expression in the dorsal neural tube. We hypothesized that Fragment C is a *bona fide* enhancer of *msx3* specifically in the neural tube, and that this enhancer contributes toward proper patterning and neurogenesis/proliferation in the developing neural tube of zebrafish. To test this hypothesis, I have generated zebrafish mutants with a deletion of the Fragment C enhancer using CRISPR/Cas9 that also have a transgenic Fragment C enhancer driving reporter expression of enhanced green fluorescent protein (Egfp). The deletion of Fragment C abolishes *msx3* expression in the neural tube excluding the dorsal-most cells likely corresponding to the roof plate. The spatial domain in which msx3 is lost corresponds to where Fragment C drives expression in the neural tube, suggesting that Fragment C contains an enhancer of *msx3*. This domain of expression corresponds to where dorsal neural progenitors reside. Analysis of markers for the cells with Fragment C-driven Egfp expression shows that at least some of these cells are indeed neural progenitors, many of which give rise to neurons during embryonic and larval development. The deletion of Fragment C and loss of *msx3*

expression in neural progenitors did not affect the numbers of neurons or neural progenitors amongst cells with Fragment C-driven expression, nor did it affect the dorsoventral location of cells in the neural tube. Taken together, we conclude that Fragment C-driven *msx3* expression does not contribute to the dorso-ventral position of neural progenitors nor the balance of proliferation and neurogenesis in the developing neural tube. However, a role for *msx3* in regulating neural progenitor identity along the dorso-ventral axis without affecting progenitor position cannot be ruled out.

Acknowledgements

First and foremost, I acknowledge my supervisors Dr. Marie-Andrée Akimenko and Dr. Tuan Bui as pivotal figures in the completion of my master's project. They provided invaluable guidance to maximize the significance and cohesiveness of my experimental results in the face of both successes and periods of troubleshooting. Additionally, my ability to write and communicate about scientific results has improved drastically thanks to their influences and examples.

I would like to thank my committee members, Dr. Marc Ekker and Dr. William (Bill) Willmore, for providing fresh guidance and perspectives at critical moments in my master's project. Furthermore, I would like to thank all the members of the Akimenko and Bui labs for their help and feedback regarding the daily challenges and considerations of research.

I acknowledge the members of the aquatics facility of the animal care and veterinary services for their ongoing support and care in taking care of the zebrafish that provided us with the experimental results of this thesis. A special thanks goes to Vishal Saxena for carrying out several microinjections that were necessary for the completion of my project.

Finally, I acknowledge science itself, for teaching me the value of perseverance and humility to achieve that which, at times, I did not think was possible.

Table of Contents

List of Figures

List of Abbreviations

bHLH	basic helix-loop-helix
BLAST	basic local alignment search tool
Bmp	bone morphogenic protein
bp	base pairs
Cdks	cyclin-dependent kinases
cDNA	complementary DNA
ChIP-seq	chromatin immunoprecipitation sequencing
CNS	central nervous system
CRISPR	clustered regularly interspaced short palindromic repeats
DEPC	diethylpyrocarbonate
DIG	digoxigenin
dp1	dorsal progenitor type 1
EDTA	ethylenediaminetetraacetic acid
Egfp	enhanced green fluorescent protein
G1, S, G2, M phase	growth 1, synthesis, growth 2, and mitotic phase
GTF	general transcription factors
HD	homeodomain-containing
ISH	*in situ* hybridization
MZ	mantle zone
NEC	neuroepithelial cell
PAM	protospacer adjacent motif
PBST	phosphate buffered saline with Tween-20
PFA	paraformaldehyde
PIC	pre-initiation complex
pMN	motor neuron progenitors
POD	horse-radish peroxidase
PTU	1-phenyl 2-thiourea
Rdh10	retinol dehydrogenase 10

RGC	radial glial cell
Shh	sonic hedgehog
SSC	saline-sodium citrate
TBST-B	(tris-buffered saline with Tween-20 and blocking powder
vp0	ventral progenitor type 0
VZ	ventricular zone
Wnt	wingless-type MMTV integration site proteins
βG	beta-globin minimal promoter

Glossary

Anterior/posterior	Toward the head and tail of the zebrafish, respectfully.
Astrocytes	A star-shaped glial cell of the central nervous system serving many functions including metabolic support of neurons, response to neuronal injury, and regulation of the formation, pruning, and function of synapses.
Autofluorescence	Natural emission of light by biological structures when they absorb light (excludes light originating from artificially-added fluorescent markers).
Blbp	A transcription factor that, in the neural tube, is a marker for radial glial cells.
Caudal fin	A fin at the posterior extremity of a fish's body.
cDNA	DNA that is complementary to a given RNA. Often used as a transcription template to generate the mRNA of a gene.
Dorsal/ventral	Toward the belly and back of the zebrafish, respectfully.
Enhancer	A short DNA sequence that can be bound by proteins to increase the likelihood that transcription of a gene will occur.
Floor plate	A group of cells at the ventral midline of the neural tube that releases morphogens to guide neurogenesis.
Gfap	A transcription factor that, in the neural tube, is a marker for radial glial cells.
Morphogen	A protein or chemical agent able to cause or determine the development of morphological characteristics.
Neocortex	The region of the cerebral cortex responsible for sight and hearing in mammals.
Nestin	A transcription factor that, in the neural tube, is a marker for neural progenitors.

Neural crest cells	A group of cells present in early development of vertebrates that are specified at the neural plate border and give rise to diverse cell lineages including melanocytes, bone, smooth muscle, peripheral and enteric neurons and glia.
Neural progenitor	Cells that give rise to neurons and glial cells of the central nervous system.
Neural tube	A hollow structure in the embryo from which the brain and spinal cord form.
Neuroepithelial cells	Earliest neural stem cells of the central nervous system that generate new neuroepithelial cells or early-born neurons and radial glial cells of the spinal cord.
Neurulation	The folding of the neural plate into the neural tube in vertebrate embryos.
Orthologue	One of two or more genes found in different species that share an evolutionary origin.
Paralogue	One of two or more genes found within a species that share an evolutionary origin.
Radial glial cells	Predominant neural stem cell of the central nervous system arising from neuroepithelial cells to generate the bulk of neurons and glial cells of the spinal cord.
Roof plate	A group of cells at the dorsal midline of the neural tube that releases morphogens to guide neurogenesis.
Sequence identity	A measurement of the similarity between two sequences based on the number of conserved nucleotides.
Somite	Bilaterally-paired blocks of paraxial mesoderm along the anterior-posterior axis in segmented animals.
Sox2	A transcription factor that, in the neural tube, is a marker for neural progenitors.

Teleost	All ray-finned fishes excluding primitive bichirs, sturgeons, paddlefishes, freshwater garfishes, and bowfins.
Transcription factors	A protein that regulates transcription of a gene by binding to specific DNA sequences.

1 Introduction

1.1 General Introduction

1.1.1 Overview and objectives of Masters project

In vertebrates, the spinal cord coordinates several important processes such as motor control and sensory processing (Grillner & Jessell, 2009; Umeda & Shoji, 2017). The transduction of motor and sensory signals through the spinal cord is achieved by chains of neurons organized into circuits. The identity of neurons in these circuits correlates with properties of the neural progenitors from which they derive, including the progenitors' initial positions in the neuroepithelium and the onset of the progenitors' differentiation (Lobjois et al., 2008). Many of the genes that contribute to the diversity of neural progenitors and neurons have been identified in vertebrates such as mice and zebrafish (Satou et al., 2013; Goulding, 2009; Zhuang & Sockanathan, 2006). However, there remain gaps in our knowledge of the roles these genes play in spatiotemporal patterning and regulation of differentiation in neural development (Satou et al., 2013).

The muscle segment homeobox (*Msx)* gene family is expressed in the dorsal neural tube of vertebrates (Ekker et al., 1997; Liu et al., 2004; Ramos & Robert, 2005) where both sensory neurons and interneurons involved in sensory processing are formed (Nguyen et al., 2000). Additionally, *Msx* genes are expressed in the neural crest cells, a cell type that gives rise to a wide range of cell types in vertebrates including neurons in the peripheral nervous system (Phillips et al., 2006; Raible & Ungos 2006; Wang et al., 1996). Taken together, expression of *Msx* genes in the developing vertebrate neural tube is essential for proper spinal cord development. For example, in mice with double knockout mutations for *Msx1* and *Msx2,* the

dorsal-most neural progenitor subtype fails to be specified (Duval et al., 2014). These neural progenitors give rise to a distinct class of dorsal interneurons (Duval et al., 2014). Furthermore, electroporation of a plasmid driving expression of the complementary DNA (cDNA) of mouse *Msx1* into chick spinal cords reduces markers of neuronal differentiation in neural progenitors, while electroporation of a plasmid driving expression of the cDNA of mouse *Msx3* enriches two classes of interneurons at the expense of other classes of interneurons (Liu et al., 2004). In zebrafish where *msx1a, msx1b,* and *msx3* are simultaneously knocked down, several abnormalities occur in the developing neural tube, including the loss of commissural neurons in the presumptive hindbrain, and a reduction in the number of sensory neurons throughout the entire neural tube (Phillips et al., 2006). Despite this observation that typical neuronal differentiation is disrupted when *msx1a, msx1b,* and *msx3* are knocked down, the underlying mechanisms towards which *msx* genes contribute in neural progenitors during spinal cord development has not yet been elucidated.

Expression of genes such as the *msx* genes is regulated by DNA sequences known as enhancers. Enhancers contain short DNA sequences that can be bound by transcription factors (Pennacchio et al., 2013). The binding of transcription factors to enhancers can modulate the rate of transcription of a gene (Pennacchio et al., 2013). The combination of enhancers that act on a gene and available transcription factors in each cell type contribute toward a gene's spatiotemporal expression (Pennacchio et al., 2013). Interestingly, in the developing neural tube, the mouse *Msx3* and zebrafish *msx3* gene show similar expression in the dorsal spinal cord (Wang et al., 1996; Ekker et al., 1997). These genes are orthologues (derived from the same gene in a common ancestor) (Finnerty et al., 2009), and thus its possible that the enhancers that regulate their expression may also be conserved, leading to their similar expression patterns in

the developing spinal cord. The sequences upstream of the zebrafish *msx3* gene and mouse *Msx3* gene were compared in the Akimenko lab, and regions of high sequence conservation were identified. One sequence upstream of *msx3* in the zebrafish genome, here onwards called Fragment C, contains 2 short sequences that share a high percentage of sequence identity with regions of DNA upstream of the mouse *Msx3* gene. Conservation of sequences outside of a gene can indicate the presence of a regulatory element such as an enhancer (Ruvinsky & Ruvkun, 2003). Thus, Fragment C may contain an enhancer of *msx3*. Fragment C was cloned upstream of the enhanced green fluorescent protein (Egfp) coding sequence driven by the beta-globin minimal promoter, and the resulting *Tg(Fragment C-βG:Egfp)* DNA construct was injected into zebrafish embryos. Like *msx3, egfp* is expressed in the dorsal neural tube throughout the spinal cord, hindbrain, and a subset of the midbrain and forebrain, suggesting that Fragment C may contain a neural-specific enhancer of *msx3.*

This project aims to contribute toward an understanding of how the gene *msx3* contributes to the development and patterning of the dorsal spinal cord in zebrafish. To this end, I will analyze the function of a sequence containing a potential enhancer of *msx3*, Fragment C, to study the mechanism by which *msx3* is expressed to exert its role in the dorsal spinal cord. Understanding the function that enhancers play in gene expression is critical for the knowledge of interactions between complex developmental pathways and can aid in the characterization of neuropathological states (Visel et al., 2009). Moreover, identifying a neural-specific enhancer of *msx3* in Fragment C may lead to targeted transgenic strategies to study both a sub-population of neural progenitors and a distinct role of *msx3* in the neural tube. Listed below are the main objectives for my master's project:

Objective 1: Determine if Fragment C contains an enhancer of *msx3*

Objective 2: Characterize the cells with Fragment C-driven expression

Objective 3: Identify the function of Fragment C-driven expression in the developing neural tube.

1.1.2 Zebrafish – a model of spinal cord development

Research in developmental neurobiology has been carried out in several models including frogs, chickens, mice, and zebrafish (Sakai, 2018). Among them, zebrafish have emerged as an attractive model for studying developmental processes (Ijaz & Hoffman, 2016; Sakai, 2018). Unlike mice, zebrafish embryos have a fast, external development and are transparent, allowing for direct visualization of early developmental processes. The bulk of neurogenesis occurs during the period that zebrafish embryos are transparent (Kim et al., 2008), making study of neural development readily available. Breeding produces large numbers of progeny which is convenient in studies where large sample sizes with a similar genetic background are required (Sakai, 2018).

A wide variety of genetic tools are available to study the function of zebrafish genes. The clustered regularly interspaced short palindromic repeats (CRISPR)/Cas9 system has been employed to introduce genetic modifications such as deletions (Hwang et al., 2013; Moreno-Mateos et al., 2015). This system has proven fruitful in loss-of-function studies and is consistently being adapted to study the zebrafish genome in new ways (Raj et al., 2018). To complement the available genetic tools, high throughput -omic-level data is steadily emerging using the zebrafish model to direct study of genes and their regulation (Tambalo et al., 2020; Raj et al., 2018; Lee et al., 2020).

While evolutionary divergence between zebrafish and humans is greater than that of mouse and humans, the central nervous system (CNS) is well conserved at a genetic and functional level. The divisions of the CNS (forebrain, midbrain, hindbrain, and spinal cord) are

present in both humans and zebrafish (Guo, 2009). The cells that make up the spinal cord share similar organization and function between humans and zebrafish (Ferretti et al., 2006; Schmidt et al., 2013). Finally, there is a high degree of spatial and temporal homology between gene expression in the zebrafish and mouse CNS, further underscoring the value of studying the development of the zebrafish spinal cord to understand its development across vertebrates (Ghosh & Hui, 2016).

1.2 Spinal cord development – from progenitor to neuron

1.2.1 Cells in the developing nervous system

The vertebrate CNS is comprised of the brain and spinal cord. The CNS is derived from the ectoderm, one of the three primary germ layers. The ectoderm is specified to give rise to a neural ectoderm (or neurectoderm) that forms the CNS, non-neural ectoderm that forms the epidermis, or neural crest that contributes to a variety of tissues, including the peripheral nervous system (Patthey & Gunhaga, 2014). The neural ectoderm is first organized as a monolayer epithelial sheet called the neural plate (or neuroepithelium) that folds in a process called neurulation (Colas & Schoenwolf, 2001). In zebrafish, the neural plate forms in an anterior to posterior direction between 10 and 11 hours post fertilization (hpf). The neuroepithelium then folds to bring the lateral neural plate to the dorsal midline and the medial neural plate to the ventral midline, forming a solid mass of cells called the neural keel by 12-13hpf (Konno et al., 2008). Cell movements shape the neural keel into a solid, rod-like structure called the neural rod by 15-17hpf (Konno et al., 2008). The neural rod cavitates at 18-20hpf to form a fluid-filled lumen, and from that point onwards is called the neural tube (Konno et al., 2008). The lumen of the neural tube continues to expand between 48hpf and 72hpf, forming the central canal of the developing spinal cord (Hudish et al., 2013; Taverna & Huttner, 2010).

At the cellular level, the vertebrate neural tube is composed of neurons, glia, and the progenitors that give rise to neurons and glia. Both differentiated neurons and glia reside in lateral positions of the neural tube in the mantle zone (MZ) (Molina & Pituello, 2017) (**Figure 1.1 left side, orange cells**). In the developing spinal cord, two progenitors cell types exist—neuroepithelial cells (NECs) and radial glial cells (RGCs) (Götz. & Barde, 2005). Both NECs and RGCs reside in the medial neural tube adjacent to the lumen in the ventricular zone (VZ) (Molina & Pituello, 2017) (**Figure 1.1 left side, yellow cells**), display radial morphology, and extend an apical and basal process to contact the lumen and outer surface of the neural tube, respectively (Götz. & Barde, 2005). These processes serve as a scaffold along which immature neurons travel from the VZ where they are born to the MZ where they will reside (McDermott et al., 2005). Both NECs and RGCs express neural progenitor markers including Sox2 and Nestin (Johnson et al., 2016). RGCs express additional glial markers such as Blbp and Gfap (Kriegstein & Alvarez-Buylla, 2009; Johnson et al., 2016).

NECs are the first progenitors of the neural tube (Hollyday, 2001), and initially undergo several rounds of symmetric proliferative divisions (generating 2 NECs) to expand the progenitor pool in the ventricular zone formed by neurulation (Tawk et al., 2007; Araya et al., 2016). These divisions equally contribute 1 NEC to both the left and right side of the neural tube (Tawk et al., 2007). After initial symmetric divisions, NECs undergo asymmetric divisions, giving rise to the first neurons of the neural tube, in addition to RGCs (Tawk et al., 2007). In zebrafish, the first neurons are born at approximately 10-11hpf. Alongside NEC neurogenesis, RGCs undergo neurogenic symmetric (Götz & Huttner, 2005) or asymmetric (Araya et al., 2016; Azaïs et al., 2019) divisions to continue cell population expansion. In zebrafish, by 24hpf, most neural progenitors are RGCs, and by 48hpf, nearly all neural progenitors are RGCs (except at the

ventral-most region of the spinal cord). Most neurons are born during the period when RGCs are the predominant progenitor cells, between 18hpf and 30hpf (Kim et al., 2008). Onwards of this period, RGCs continue to serve as progenitors of the central nervous system into adulthood in teleosts including zebrafish (Kim et al., 2008) but differentiate into astrocytes in mammals postnatally (Rakic, 2003). Additionally, some NEC-like cells persist into adulthood (März et al., 2010). In zebrafish, RGCs have been reported to serve some astrocytic functions such as metabolic support of neurons, responding to neuronal injury, and regulating the formation, pruning, and function of synapses (Ghosh & Hui, 2018; Corbo et al., 2012; Lyons & Talbot, 2014; Dallérac et al., 2013; Bouzier-Sore & Pellerin, 2013). However, recent evidence suggests that mature astrocytes exist in zebrafish (Chen et al., 2020), and it is unclear if previous reports about the astrocytic functions of RGCs were erroneously describing mature astrocytes rather than RGCs (Neely & Lyons, 2021). A switch from primarily neurogenic divisions (forming neurons) to gliogenic divisions (forming RGCs or differentiated glia) occurs in RGCs during development of mammals and zebrafish (Kim et al., 2008).

Several markers delineate the different stages of neural progenitor differentiation toward mature neurons. Members of the SoxB1 family such as Sox2 initially restrict the ectoderm into neural ectoderm, and activate repressors of neuronal differentiation (Sasai, 1998; Okuda et al., 2010). These "type A" neural progenitors are highly proliferative and display high Notch signalling (Sasai, 1998; Schmidt, et al., 2013). The expression of pro-neural genes such as *neurogenin1* and *achaete-scute1* mark the onset of "type B" progenitors (Sasai, 1998; Appel, B. & Chitnis, A., 2002; Allende, M. & Weinberg, E., 1994). These progenitors are still proliferative but are fated to give rise to neurons (Appel et al., 2001). They carry the Delta ligand that activates Notch receptors of neighboring progenitors (Appel et al., 2001). These type B

progenitors reside in clusters amongst non-neurogenic type A progenitors (Blader et al., 1997). The onset of expression of post-mitotic genes such as *elavl3* (formerly called *huc*) represents the transition of pro-neural progenitors to immature neurons that have exited the cell cycle (Peukert et al., 2011; Kim et al., 1996). Finally, immature neurons begin to express neurotransmitter and ion channel markers, indicative of the formation of mature neurons with axons and defined electrophysiological characteristics (Filippi et al., 2014).

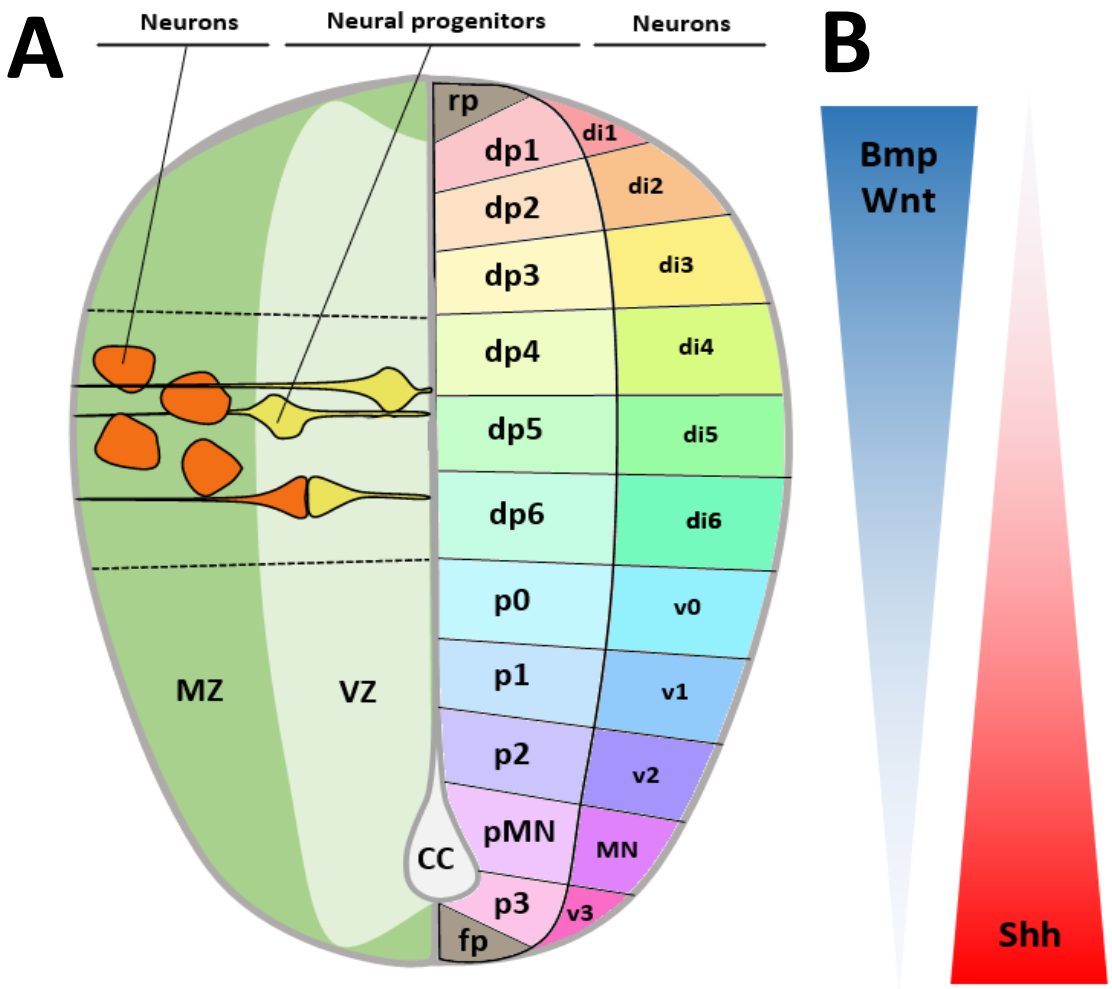

Figure 1.1. Schematic of the organization and patterning of cells in a transverse section of a zebrafish embryonic spinal cord. A (left side). the developing spinal cord contains a medial ventricular zone (VZ) and a lateral marginal zone (MZ) that spans the dorso-ventral axis of the spinal cord. Neural progenitors (neuroepithelial cells and radial glia) reside in the VZ, while neurons are fated for the MZ. Neural progenitors extend processes to touch the medial ventricular surface (midline) and lateral pial surface. Neural progenitors give rise to new neural progenitors or neurons. **A (right side).** The dorsoventral axis is divided into discrete zones that give rise to specific subtypes of progenitors (dorsal progenitor type 1 (dp1), dp2, dp3, dp4, dp5, dp6, ventral progenitor type 0 (p0), p1, p2, motor neuron progenitors (pMN), and p3). These progenitor subtypes then give rise to corresponding neuronal subtypes (dorsal interneuron typ1 1 (di1), di2, di3, di4, di5, di6, ventral interneuron type 0 (v0), v1, v2, motor neurons (MN), and v3). **B.** Bmp and Wnt factors secreted from the dorsal ectoderm and roof plate cells (rp) and Shh secreted from ventral notochord and floor plate (fp) create morphogen gradients that result in downstream expression of transcription factors that characterize each dorsoventral domain.

1.2.2 Patterning of cells in the developing spinal cord

The signalling pathways involved in the development of spinal neurons are well described. First, neural progenitors and neurons are specified by exposure to morphogens secreted from tissues surrounding the neurectoderm (Pierani et al., 1999; Lee & Jessell, 1999). This specification begins at the neural plate stage when the notochord, located at the midline ventral to the neural plate, secretes sonic hedgehog (Shh) that acts on the neural plate (van Straaten et al., 1988). Likewise, the non-neural ectoderm, initially located lateral to the neural plate, secretes bone morphogenic proteins (Bmps) that act on the adjacent lateral neural plate (Liem et al., 1995) and after neurulation will be located dorsal to the neural tube (Chizhikov & Millen, 2004). In response to the notochord and dorsal ectoderm secreting morphogens, the roof plate and the floor plate are subsequently established at the dorsal and ventral limits of the neural tube, respectively (Chizhikov & Millen, 2004; Jessell & Dodd, 1990). Bmps and wingless-type MMTV integration site proteins (Wnts) are then secreted from the roof plate, while Shh is secreted from the floor plate (Megason & McMahon, 2002).

Exposure to Bmp, Wnt and Shh induces the expression of Homeodomain-containing (HD) and basic helix-loop-helix (bHLH) transcription factors, the combination of which define neural progenitor subtype (Lai et al., 2016). In most vertebrates, including fish and mammals, the following progenitor subtypes are defined (from dorsal to ventral): dorsal progenitor type 1 (dp1), dp2, dp3, dp4, dp5, dp6, ventral progenitor type 0 (vp0), vp1, vp2, motor neuron progenitors (pMN) and p3 (Andrews et al., 2019; Satou et al., 2013) (**Figure 1.1A, right side**). In mice, the bHLH transcription factors Atoh1, Neurog1/2, Ascl1 and Ptf1a are necessary and sufficient to establish all dorsal neural progenitor subtypes (Bermingham et al., 2001; Glasgow et al., 2005; Gowan et al., 2001; Helms et al., 2005; Mizuguchi et al., 2006), while the HD

transcription factors Pax7, Irx3, Dbx1, Dbx2, Pax6, Nkx6.1 and Nkx2.2 are necessary and sufficient to establish all ventral neural progenitor subtypes (Goulding et al., 1993; Ericson et al., 1997; Briscoe et al., 1999; Pierani et al., 1999; Briscoe et al., 2000). However, HD transcription factors such as Msx1, Msx2, Msx3, and Gsx2 are still required in the dorsal neural tube to regulate the expression of bHLH transcription factors (Liu et al., 2004; Duval et al., 2014; Kriks et al., 2005; Pei et al., 2011).

In zebrafish, the transcription factor code contributing to the dorsal neural progenitor fates in the spinal cord has received less attention compared that in the ventral zebrafish spinal cord or the mouse spinal cord (Alaynick et al., 2011; Ferg et al., 2014; Ekker et al., 1997; Phillips et al., 2006; Gribble et al., 2007; Moore et al., 2013; Bergeron et al., 2015; Filippi et al., 2005; Lewis et al., 2005; Allende & Weinberg, 1994; McGaughey et al., 2010). The dorsal neural progenitor domains give rise to key neuronal and non-neuronal cell types including Rohon-Beard sensory neurons, a subset of neural crest cells, and interneurons involved in sensory processing, thus necessitating the characterization of the molecular hallmarks of these progenitors (Nguyen et al., 2000). In zebrafish, 3 Msx HD transcription factors (Msx1a, Msx1b, and Msx3) are expressed early in the developing spinal cord and have a dorsally restricted like that of the mouse Msx1, Msx2, and Msx3 (Ekker et al., 1997; Wang et al., 1996). Loss and gain of function studies show that mouse Msx genes regulate dorso-ventral patterning of neural progenitors and their neuronal progeny (Liu et al., 2004). Single knockdown studies have been carried out for each of the zebrafish *msx* genes expressed in the spinal cord in addition to a triple knockdown of all three *msx* genes, but the analysis of these knockdown mutants focussed primarily on consequences to neural crest cells rather than neural progenitors and neurons (Phillips et al., 2006). As the mouse

Msx genes have known roles in dorsoventral patterning of neural progenitors in the developing spinal cord, there is a possibility that the zebrafish *msx* genes have conserved a similar role.

1.2.3 Regulation of proliferation and neurogenesis in the developing spinal cord

Development of the spinal cord requires not only precise patterning of neural progenitors to produce the range of neuronal and non-neuronal cell populations found in the CNS, but also regulation of the proliferation and differentiation of these neural progenitors. Neural progenitors are faced with a choice at the time of cell division to generate 2 neural progenitors, 2 neurons, or 1 neuron and 1 neural progenitor, which are referred to as symmetric proliferative, symmetric neurogenic, and asymmetric neurogenic divisions, respectively (Götz & Huttner, 2005). In the case of asymmetric neurogenic divisions, asymmetric inheritance of proteins determines which daughter cell will become a neuron and which will remain a neural progenitor. For example, in the zebrafish CNS, Mindbomb1 localizes to one centriole during mitosis of neural progenitors, and the inheritance of this centriole is correlated with the neurogenic daughter cell (Tozer et al., 2017). The determination of the progeny of a neural progenitor is a crucial factor in producing neurons while maintain the progenitor pool. In a knockout mouse line for retinol dehydrogenase 10 (*Rdh10*), there is an increase in the number of newborn neurons and decrease in the number of neural progenitors in the neocortex at E11.5, suggesting a shift towards neurogenic divisions in neural progenitors (Haushalter et al., 2017). However, by E13.5, the neocortex is smaller in size, and is comprised of less neurons, illustrating that the maintenance of the progenitor pool and proper timing of neurogenesis are necessary for normal CNS development. Numerous studies have linked cell cycle dynamics to the mode of division of neural progenitors (Lanctot et al., 2017; Misumi et al., 2008; Arai et al., 2011), though cell cycle independent factors may also be

involved (Bonnet et al., 2018). Below I will briefly summarize the cell cycle and its role in regulation of mode of division of neural progenitors.

The cell cycle contains four phases: growth/gap 1 (G1) phase, synthesis (S) phase, growth/gap 2 (G2) phase, and mitotic (M) phase. In G1 and G2, the cell prepares for the S and M phases by undergoing protein synthesis, producing copies of organelles, and increasing cell size (Barberis et al., 2007; Sin & Harrison, 2016). During S phase, replication of chromosomes takes place, and during M phase, segregation of chromosomes occurs (Nurse, 2002). Cells complete the cell cycle to proliferate and exit from the cell cycle into a quiescent G0 phase to differentiate. Cyclins and Cyclin-dependent kinases (Cdks) are proteins that serve as checkpoints through each phase of the cell cycle, ensuring the necessary cellular events have occurred properly and push the cell unidirectionally through the phases of the cell cycle (Hardwick et al., 2015). Accumulation of cyclins leads to greater activation of Cdks that phosphorylate targets necessary for progression through the cell cycle (Bertoli et al., 2013; Nurse, 2002). Each phase of the cell cycle is regulated by different Cdks. CyclinD /Cdk4/6 regulates early progression through G1 phase, CyclinE /Cdk2 regulates entry into S phase, and CyclinA/B /Cdc2 regulates progression through G2 phase and entry into M phase (Hardwick et al., 2015). In vertebrate neural progenitors, lengthening of the G1 phase is associated with neurogenic divisions (Blader et al., 1997), while shortening of the G1 phase is associated with proliferative divisions (Allende & Weinberg, 1994) (summarized in **Figure 1.2**). CyclinD1 accumulation reduces the length of the G1 phase and is therefore negatively correlated with neurogenic modes of neural progenitor divisions (Lobjois et al., 2004). In mice, *Msx1* and *Msx2* indirectly activate CyclinD1 and Cdk4 activity (which binds CyclinD1) (Hu et al., 2001; Catron et al., 1995), however this activation has not been studied in the neural tube. However, electroporation of a plasmid driving expression

of the cDNA of mouse *Msx1* into chick spinal cords reduces markers of neuronal differentiation in neural progenitors (Liu et al., 2004). This reduction in neuronal differentiation could be due to CyclinD1-mediated reduction in neurogenic progenitor divisions, though it is also feasible that Msx1 represses neuronal differentiation markers directly.

In addition to regulating the proliferative and neurogenic potential of neural progenitors in the developing spinal cord, neurogenesis is also regulated through Notch-mediated lateral inhibition (Appel et al., 2001). In this process, the earliest progenitors that express pro-neural genes also express a ligand on their cell surface that activates the Notch receptor on the surface of neighbouring progenitors (Cau & Blader, 2009). The intracellular signalling mechanism that follows Notch receptor activation ultimately inhibits expression of pro-neural genes in the responding cell, keeping these cells undifferentiated (Appel et al., 2001). Human MSX1 upregulates *NOTCH3* at a transcriptional level, but additionally promotes activation of NOTCH3 protein from its inactive form through an unknown mechanism. Taken together, there is a potential role for *Msx* genes in regulating proliferation and differentiation of neural progenitors of the developing spinal cord may be mediated by Notch signaling.

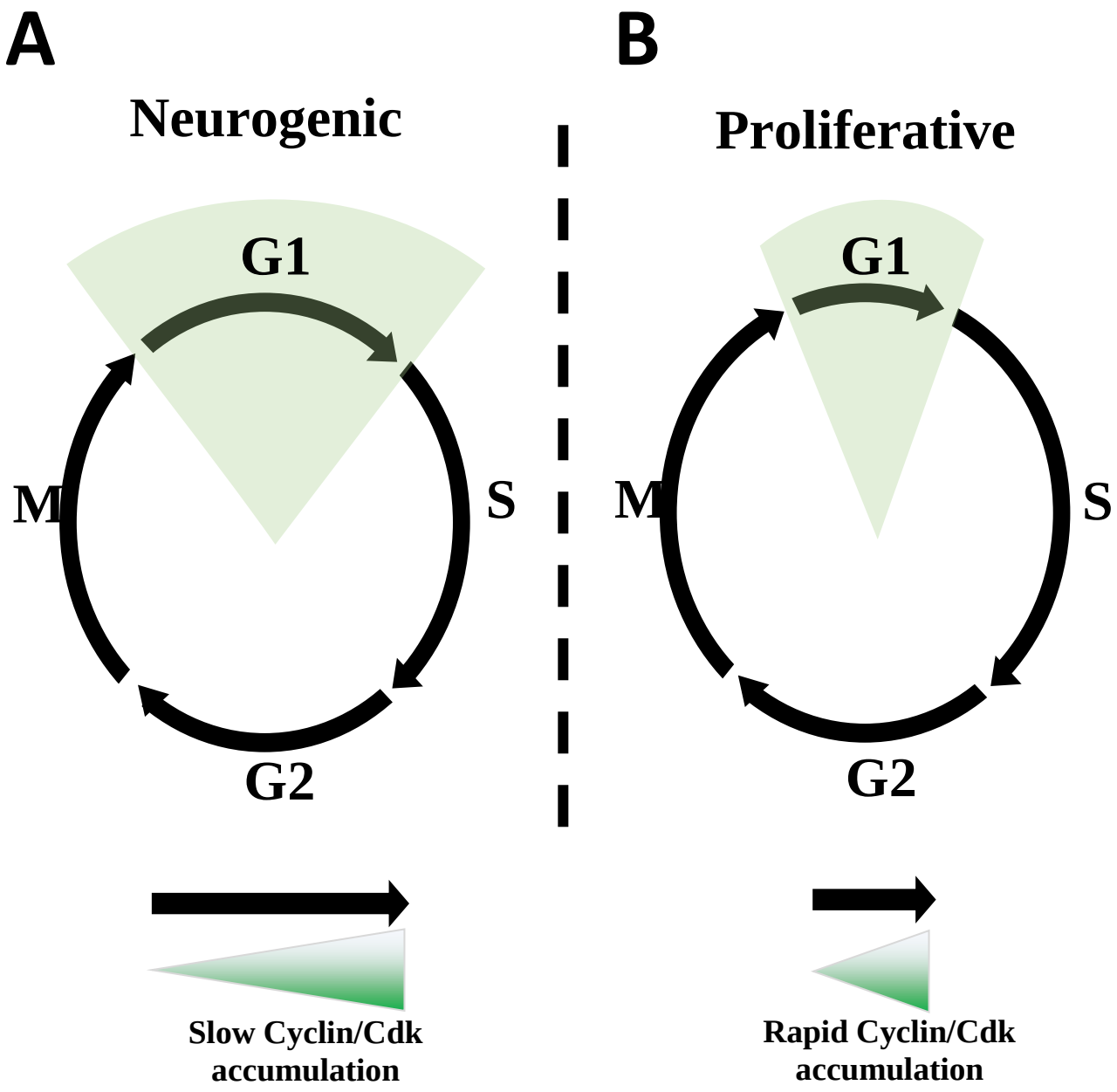

Figure 1.2. Cell cycle dynamics affect the balance between proliferation and differentiation for neural progenitors. Neural progenitors cycle through the four phases of the cell cycle. Cyclins and cyclin-dependent kinases (Cdks) act as checkpoints that trigger cells to proceed to the next phase of the cell cycle. When cyclins accumulate along with cyclin-dependent kinases, their downstream signalling events lead to progression to the next cell cycle phase. **A.** during proliferative divisions that generate two neural progenitors, the G1 phase of the cell cycle is stereotypically short. **B.** During neurogenic divisions that generate one or two neurons, the G1 phase of the cell cycle is stereotypically long.

1.2.4 *msx* gene expression in the developing nervous system

Collective evidence from several vertebrates (provided in sections **1.2.2 and 1.2.3**) suggests that *Msx* genes are involved in both patterning of the developing spinal cord and the regulation of proliferation and neurogenesis. However, little is known about the role of *msx* genes in neural progenitors of the developing zebrafish spinal cord. Below I will provide an overview of the function of Msx proteins, with particular focus on the zebrafish spinal cord.

The muscle segment homeobox (*Msx*) gene family are highly conserved, homeobox-containing genes that encode homeodomain-containing transcription factors (Bendall & Abate-Shen, 2000). Msx proteins form heteromeric complexes with other homeodomain transcription factors that can then associate with additional proteins. Like other homeodomain-containing proteins, Msx proteins modulate transcription through associations with other DNA-binding proteins (Ferg et al., 2014; England et al., 2011; Dessaud et al., 2008; Sin & Harrison, 2016) in addition to direct DNA binding (Barberis et al., 2007; Sin & Harrison, 2016). The effect of Msx proteins on transcription is determined by the protein with which Msx heterodimerizes (Sun et al., 2019) and additional protein partners that form complexes with the heterodimer (Sin & Harrison, 2016). Typically, Msx-dependent heterodimers function as transcriptional repressors (Dessaud et al., 2008), though heterodimerization with some transcription factors results in transcriptional activation (Sun et al., 2019; Mo et al., 2021).

Throughout evolution, the vertebrate genome underwent two whole-genome duplications, resulting in four *Msx* paralogues from a single ancestral *Msx* gene (Finnerty et al., 2009). One of these *Msx* genes was likely lost prior to the divergence of ray-finned fish from lobe-finned fish and tetrapods (four-limbed animals). In some vertebrates, such as humans, one of the three remaining *MSX* genes was additionally lost, leaving only two (*MSX1* and *MSX2*), while in other

vertebrates, such as mice, the three *Msx* genes (*Msx1-3*) are still present (Zhong & Holland, 2011). In teleosts, a third whole-genome duplication brought the 3 *Msx* paralogues to a total of 6. After the loss of a single *msx* gene in teleosts (including zebrafish), 5 *msx* genes remain: *msx1a, msx1b, msx2a, msx2b,* and *msx3* (Finnerty et al., 2009).

In zebrafish, three of the five *msx* genes are expressed in the developing spinal cord: *msx1a, msx1b,* and *msx3* (Ekker et al., 1997). *msx1b* expression at the lateral borders of the neural plate begins at 8hpf, and by 12hpf, these domains converge at the dorsal midline due to folding of the neural plate. Expression remains in the dorsal neural tube until at least 36hpf (Phillips et al., 2006). *msx3* shares a similar expression to *msx1b* in the neural plate/tube up until 36hpf, with unique expression domains outside the neural plate (Ekker et al., 1997; Phillips et al., 2006). *msx1a* is detected in the neural tube starting at 16hpf with expression levels lower than that of *msx3* or *msx1b* based on *in situ* hybridization (ISH) of antisense RNA probes analysis (Ekker et al., 1997). Expression of *msx3* extends more ventrally than *msx1b* in the dorsal neural tube, though it has not been determined what cell types express these genes except for neural crest cells, in which all three *msx* genes are expressed (Ekker et al., 1997; Phillips et al., 2006). *msx1b* and *msx3* are expressed in the ectoderm overlying the neural tube (Ekker et al., 1997). *msx3* expression extends anteriorly past the midbrain-hindbrain border and shows reduced expression in rhombomere 3 and 5 of the hindbrain. *msx1b* expression extends more anteriorly in the neural tube relative to *msx3* (Ekker et al., 1997).

1.3 Fragment C enhancer

1.3.1 Function of enhancers in the genome

Expression of *msx1a, msx1b,* and *msx3* in zebrafish shows both similarities and differences with that of other vertebrates such as mice. In mice, *Msx1, Msx2,* and *Msx3* are all expressed in the dorsal neural tube until E10.5, at which point *Msx1* and *Msx2* expressions are restricted to the roof plate, while *Msx3* expression persists in the dorsal ventricular zone (Wang et al., 1996). In zebrafish, all three *msx* genes are expressed broadly in the dorsal third of the developing spinal cord including the dorsal ventricular zone where neural progenitors reside (Ekker et al., 1997; Phillips et al., 2006; Thisse et al., 2001). Thus, the zebrafish *msx3* and mouse *Msx3* share similar expression profiles in the developing spinal cord. It is possible that the expression of these genes is regulated by a similar mechanism. Here I will give a brief overview of the mechanisms by which genes are expressed.

Transcription in eukaryotes involves three broad phases: initiation, elongation, and termination. The initiation of transcription in eukaryotes is a concerted effort from numerous protein factors. A pre-initiation complex (PIC) that includes RNA polymerase II and general transcription factors (GTFs) nucleate at a core-promoter sequence (a short DNA sequence containing the transcription start site at the 5' end of a gene) (Roeder, 1996). While the PIC can initiate transcription at basal levels, elevated levels of transcription are often required for tissue and cell-type specific gene expression (Shlyueva et al., 2014).

Enhancers are DNA sequences located outside of the core promoter that, through binding of *trans*-acting transcription factors, can modulate the rate of initiation of transcription or transition from initiation to elongation. Transcription factors bind to short (often 6-10 base pairs (bp)) sequences in enhancers (Shlyueva et al., 2014). Often, the binding site permits some degree

of sequence flexibility, allowing several similar sequences to serve as a binding site for a transcription factor (Giniger et al., 1985). The combination of transcription factors binding sites within an enhancer and the availability of transcription factors to bind the enhancers determine the spatial and temporal activity of an enhancer (Kaaij et al., 2018; Yáñez-Cuna et al., 2012).

Transcription factors that have binding sites within enhancer sequences can recruit cofactors, which can act to modify histones, remodel chromatin, or mediate interactions with GTFs at the core promoter (Spitz & Furlong, 2012). The mechanism by which enhancers and their bound transcription factors and cofactors affect transcription initiation at the core promoter bound by GTFs and RNA polymerase II is not fully elucidated. However, mechanisms that have been proposed involve bringing the enhancer and core-promoter near one another (Krivega & Dean, 2012; Bondarenko et al., 2003). From here, direct interaction of enhancer-bound transcription factors and associated cofactors and GTFs at the core promoter stabilize the PIC for RNA polymerase to then begin transcription (Reiter et al., 2017). Alternatively, or in parallel, cofactors nucleated around the enhancer sequence can create post-translational modifications to RNA-polymerase, GTFs, or other transcription factors that favor transcription initiation (Schröder et al., 2013; Roeder, 2005).

Identifying enhancers of genes is carried out by a variety of techniques. A classic technique of enhancer identification is to identify regions with an enrichment of transcription factor binding motifs (Berman et al., 2002), or conservation of a specific transcription factor binding motif across several species (Kheradpour et al., 2007), indicating conserved functional significance of the motif. These techniques depend on datasets of binding motifs and cannot definitively pair an enhancer to a specific gene. More generally, identifying DNA sequence conservation across species irrespective of transcription factor binding motifs has been employed

as a method of enhancer identification (Odenwald et al., 2005; Yavatkar et al., 2008; Brody et al., 2008). This approach is based on the idea that enhancers serve a functional purpose (such as containing transcription factor binding sites) that, if mutated, may alter the function of the sequence, placing these sequences under greater functional constraint relative to non-enhancer sequences, thus resisting mutations (Odenwald et al., 2005). While this technique has been used for large-scale identification of enhancers of a gene in combination with other criteria for sequence selection (Yavatkar et al., 2008; Brody et al., 2008), it cannot form a link between enhancers and their target gene. Linking enhancers to specific genes in this technique assumes that enhancers act on genes in close nucleotide proximity to the enhancer. Using this assumption has been successful in relating genes to their enhancers (Werner, T et al., 2007; Hornig et al., 2013; Forghani et al., 2001). A shortcoming of this technique is the necessity of manual selection of a gene or set of genes for which modulation of expression by a given enhancer will be tested. Modern techniques such as chromatin immunoprecipitation sequencing (ChIP-seq) using enhancer-associated proteins provide omic-level identification of enhancers (Blow et al., 2010).

While identification of potential enhancer sequences can be accomplished by a variety of techniques, determining if these sequences contain functional enhancers is primarily achieved using a transgenic approach whereby a plasmid containing the potential enhancer upstream of a promoter with minimal activity (Banerji et al., 1981) and a reporter gene (fluorescent or colorimetric) is injected into an appropriate organism. This technique has been described as the gold-standard for identification of enhancer activity and can indicate spatial and temporal activity of enhancers (Shlyueva et al., 2014; Banerji, et al., 1981; Zinzen et al., 2009; Visel et al., 2009). In zebrafish, stable transgenic lines can be generated by growing primary injected embryos to adulthood and outcrossing the offspring with the transgene present in germ-line cells

with wild-type adults (Suster, 2009). Reporter expression can then be screened for in offspring of these crosses (Kvon, 2015).

1.3.2 Identification of the Fragment C enhancer

The zebrafish *msx3* and mouse *Msx3* show similar expression profiles in the developing spinal cord, and thus it is possible these genes are regulated by a conserved regulatory element such as an enhancer. This hypothesis was tested in Marie-Andree Akimenko's lab, where sequences upstream of the *msx3* gene were compared across teleost and rodent species, and regions of high sequence conservation were identified. The last common ancestor of rodents and teleosts occurred before the divergence of lobe-finned fishes and ray-finned fishes between 427 and 445 million years ago (Takezaki, 2018). Thus, the genomes of rodents and teleosts have independently evolved over a long period of time. High sequence conservation throughout a long period of independent evolution could indicate the presence of a functional enhancer. PCR amplification of a region upstream of *msx3* isolated two such regions of high sequence conservation with the mouse genome separated by 824bp. The entire sequence contained in this PCR amplicon is 1566bp and was called Fragment C. Fragment C is located 9.8kb upstream of the *msx3* gene on chromosome 13. The two regions within Fragment C with a high sequence homology between zebrafish and mouse, which I will call Fragment C1 and Fragment C2, map to two sequences 15.2kb and 12.2kb upstream of the mouse *Msx3* gene on chromosome 7, respectively, and are separated by 3.0kb. Fragment C1 contains 179bp, and Fragment C2 contains 80bp (See **Figure 1.3** for a summary of the locations of Fragment C in the mouse and zebrafish genome). I have repeated an analysis of sequence conservation between various fish and rodent species as was initially performed in the Akimenko lab. I used a basic local alignment search tool (BLAST) on the zebrafish Fragment C sequence and the mouse genome, identifying

conserved nucleotides upstream of *msx3/Msx3*. The mouse and zebrafish sequences corresponding to Fragment C1 have 74% shared sequence identity while the mouse and zebrafish sequences corresponding to Fragment C2 have 78% shared sequence identity (**Figure 1.4A** and **1.4B**, respectively). For comparison, the 3kb region in the mouse genome between Fragment C1 and Fragment C2 has only 44.4% shared sequence identity with a 3kb region in the zebrafish genome between Fragment C1 and Fragment C2 (results obtained from EMBOSS Needle alignment tool). Furthermore, I used the UCSC BLAST-like alignment tool (BLAT) as described in Odenwald et al. (2005) to identify conserved nucleotides between Fragment C and the genomes of three fish (fugu, medaka, and stickleback) and two rodents (mouse and rat). Of the 179bp in the zebrafish Fragment C1, 65bp are conserved among the three fish genomes analyzed (**Figure 1.4C, blue nucleotides in Fragment C1**), while 27bp are conserved among the three fish and two rodent genomes analyzed (**Figure 1.4C, red nucleotides in Fragment C1**). Likewise, Of the 80bp in the zebrafish Fragment C2, 34bp are conserved among the three fish genomes analyzed (**Figure 1.4C, blue nucleotides in Fragment C2**), while 26bp are conserved among the three fish and two rodent genomes analyzed (**Figure 1.4C, red nucleotides in Fragment C2**).

To test if Fragment C has enhancer activity, Fragment C was cloned upstream of the beta-globin minimal promoter (βG), which was cloned upstream of the coding sequence for the green fluorescent protein Egfp. Fragment C will drive *egfp* expression if it contains an active enhancer. A plasmid containing these sequences, denoted *Tg(Fragment C-βG:Egfp)*, was injected into zebrafish embryos at the 1-cell stage, and embryos were grown to adulthood and bred to identify fish with germ-line incorporation of transgenic DNA. In the progeny of the transgenic founder fish, *egfp* expression was observed in the dorsal neural tube, with an anterior boundary in the

forebrain (**Figure 1.5**) and a posterior boundary at the posterior end of the neural tube, and expression persists into the juvenile stage (**Figure 1.5C-E**). This dorsal neural tube expression is similar to that of a transgenic line of mice with lacZ/Xgal reporter driven by the mm1489 enhancer, which contains the mouse counterpart of the conserved Fragment C2 sequence in addition to 646bp upstream (toward Fragment C1) and 1528bp downstream of Fragment C2. **(Supplementary Figure 6.1**) (Visel et al., 2007). Based on the similarity of Fragment C reporter expression to *msx3* expression in the neural tube (Akimenko et al., 1995; Bonner et al., 2008; Flowers et al., 2012), it was hypothesized that Fragment C may contain an enhancer of *msx3*. *msx3* is also expressed in the neural crest that initially reside adjacent to the neural ectoderm, but cells derived from the neural crest ultimately migrate away to contribute to other tissues (Achilleos & Trainor, 2012; Phillips et al., 2006) whereas expression driven by potential enhancers in Fragment C is retained in the neural tube. Fragment C could contain an enhancer driving a subset of *msx3* expression restricted to the dorsal neural tube.

My project aims to test if Fragment C contains a *bona fide* enhancer of *msx3* (which will hereby be referred to as the Fragment C enhancer), characterize the identity of cells with Fragment C-driven expression and assess the function of Fragment C-driven expression in the dorsal neural tube.

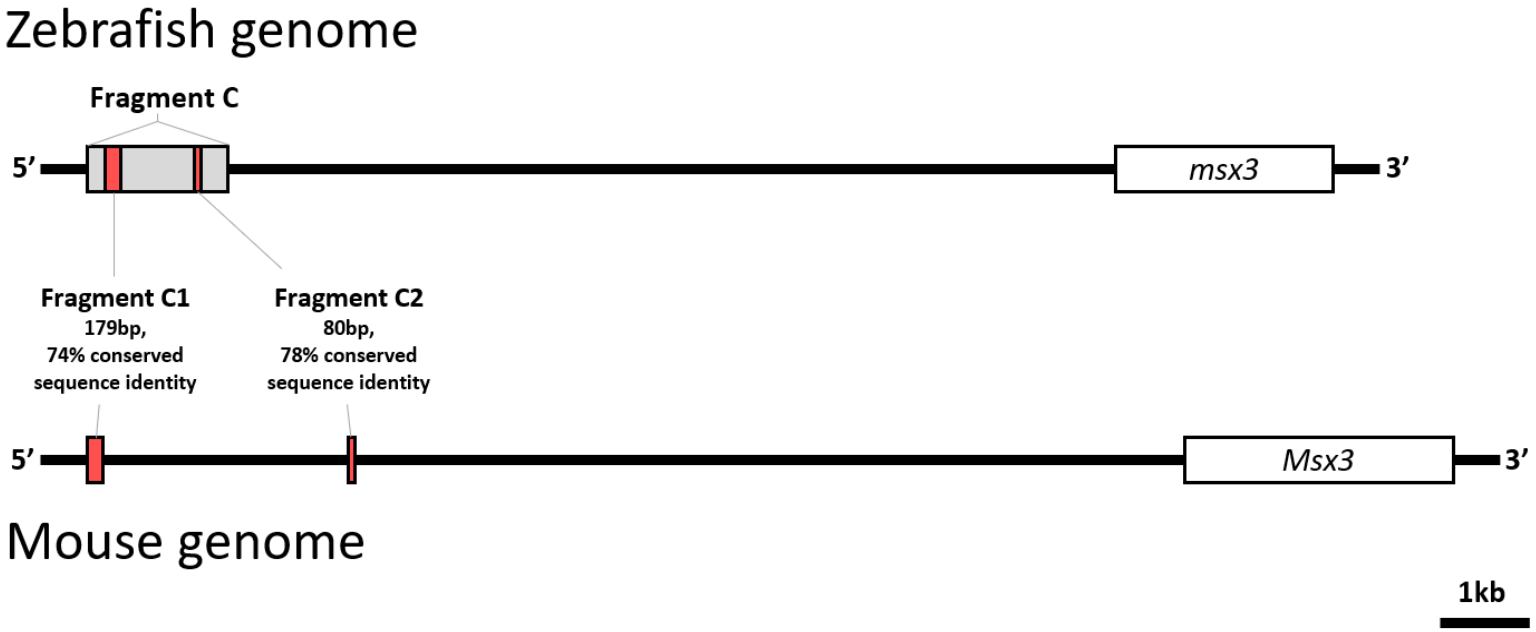

Figure 1.3. Location of the Fragment C1 and C2 conserved sequences in the mouse and zebrafish genome. Sequences upstream of the *msx3* gene were compared across fish and rodent species, and two regions of high sequence conservation were identified as Fragment C1 and C2. PCR was used to amplify this region containing Fragment C1 and C2 within a larger amplicon called Fragment C. In the zebrafish genome, Fragment C1 is 179 base pairs (bp) long and has 74% conserved sequence identity with a sequence in the mouse genome, while Fragment C2 is 80bp long and has 78% conserved sequence identity with a sequence in the mouse genome. Scale bar (black line, bottom right) represents a length of 1 kilobase pairs (kb).

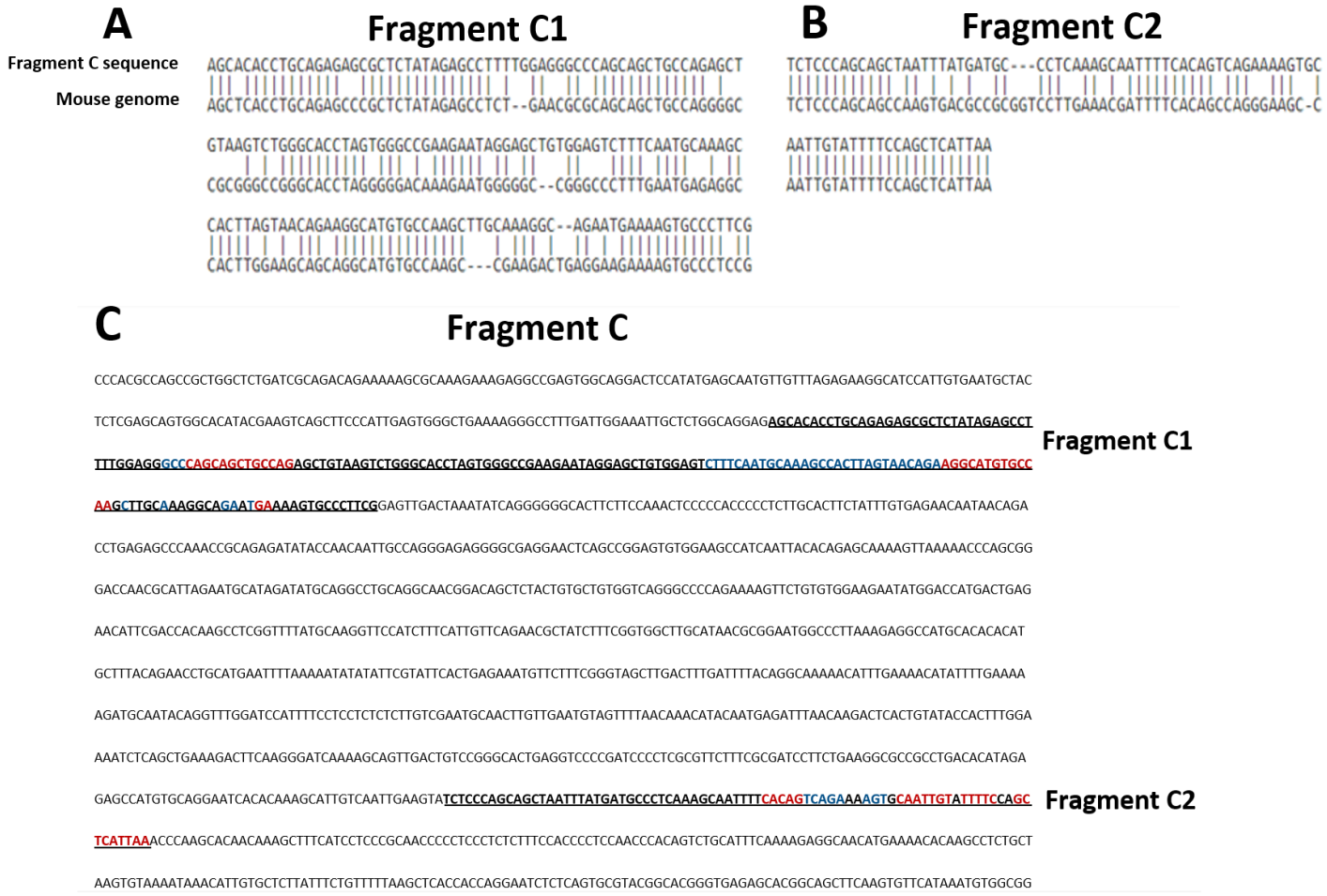

Figure 1.4. Conserved sequence analysis between the zebrafish Fragment C sequence and the genomes of other vertebrates. A, B. BLAST-n search using the zebrafish Fragment C as a query against the mouse genome. Two regions of high shared sequence identity are identified, denoted Fragment C1 (**A)** and Fragment C2 (**B)**. Fragment C1 (179bp) and Fragment C2 (80bp) have 74% and 78% shared sequence identity with corresponding sequences of the mouse genome, respectively. **C.** Position of Fragment C1 (1st bolded, underlined sequence) and Fragment C2 (2nd bolded, underlined sequence) in Fragment C. The UCSC BLAT search was used as described in Odenwald et al. (2005) to identify conserved nucleotides between Fragment C and the genomes of three fish (fugu, medaka, and stickleback) and two rodents (mouse and rat). Blue nucleotides in Fragment C are conserved across the three fish species, and red nucleotides in Fragment C are conserved across all fish and rodent species examined.

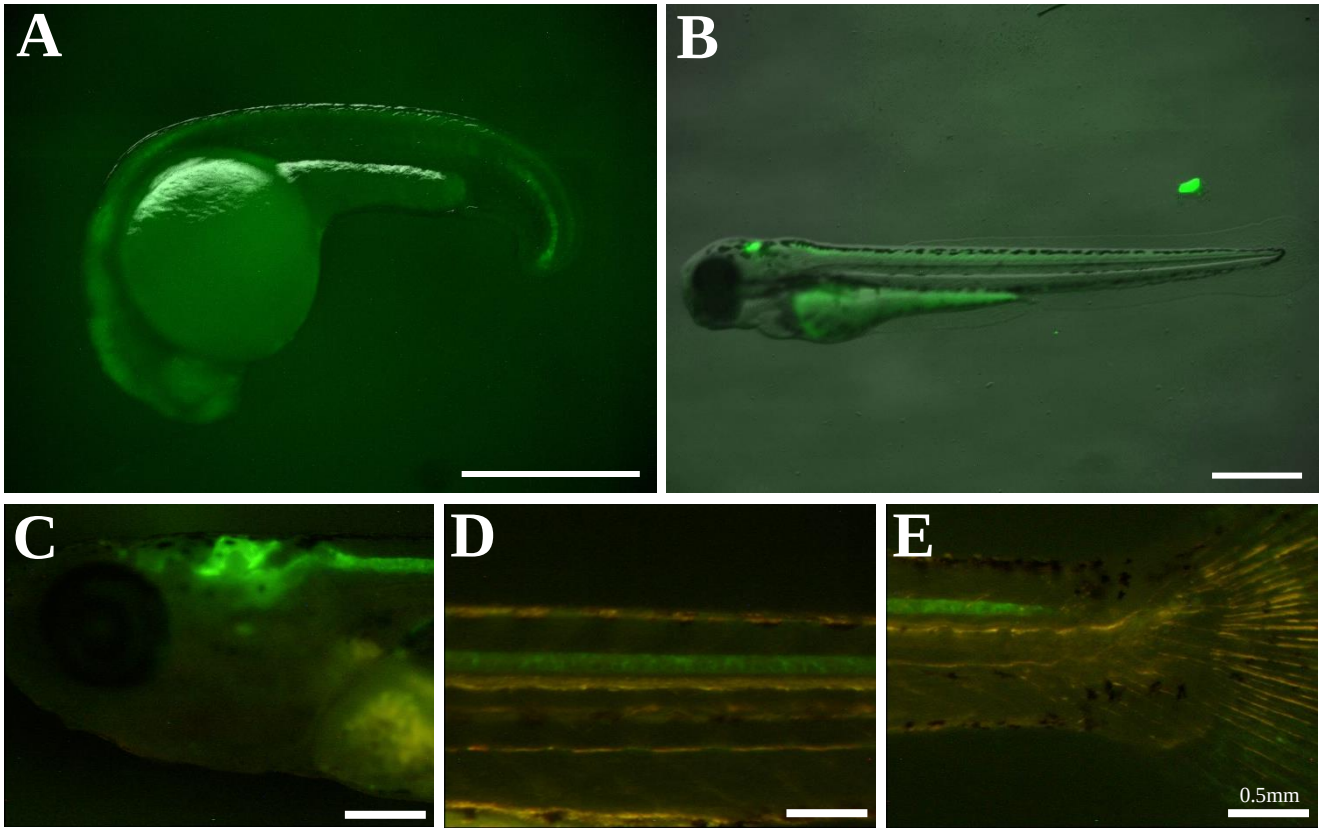

Figure 1.5. Fragment C-driven Egfp reporter expression in two transgenic lines of zebrafish. A, B. Fragment C-driven Egfp expression in the current *Tg(Fragment C-βG:Egfp)ot1* line at embryonic (**A**) and larval (**B**) stages. **C-E.** Fragment C-driven Egfp expression in a previous *Tg(Fragment C-βG:Egfp)* line at 30dpf. Images are either merges of brightfield and fluorescent images (**A, B**) or images taken with both brightfield and fluorescent light (**C-E**). Scale bars represent a length of 0.5mm. Anterior toward the left of images. Dorsal toward the top of images.

1.4 Hypothesis

Fragment C-driven *msx3* expression in the dorsal neural tube contributes to the identity and/or fate of neural progenitors in the neural tube during embryonic and larval development.

2 Methods

2.1 Zebrafish maintenance and care

Work with zebrafish follows the guidelines of the Canadian Council on Animal Care and the protocols in place at the University of Ottawa Animal Care Committee (approval ID:BL-2589).

Adult zebrafish were housed at 28.5^{o}C in 10L tanks at an approximate density of 30 fish per tank, with constant water flowing in and out of tanks for maintenance and regulation of water quality. Adult zebrafish are housed in a room with a 14 hour light cycle (9am – 11pm light, 11pm – 9am dark), and fed twice daily.

Adult zebrafish currently being housed were bleached as embryos for 10 minutes in 0.003% NaOCl solution between 5-28hpf and raised in embryo medium until 5dpf before being transferred to a nursery with tanks receiving water exchange and a feeding regimen. Food is determined by the age and size of fish. Larger particles of food were given to older and larger fish (progression from rotifers to Gemma 75 to Gemma 150 to Gemma 300 as fish mature from larvae to juvenile to adult).

To breed adult zebrafish, one male and female are placed into a 1L tank filled with system water in the afternoon, and a divider is placed between the male and female in this tank. At 9:00am of the next day, the divider is removed, and fish are allowed to breed. Embryos are then collected, and adults are returned to their tanks. Embryos to be grown to adulthood are then bleached within the first 25 hours after fertilization, and embryos to be used in experiments at embryonic and larval stages were not bleached.

2.2 Generation of *Tg(Fragment C-βG:Egfp)ot1* transgenic zebrafish

From 5’ to 3’, the sequence of Fragment C, β-globin minimal promoter (βG), and cDNA for Egfp were cloned in the multiple cloning site of the *Tg(Fragment C-βG:Egfp)* plasmid (see **Supplementary Figure 6.2** for plasmid map). To prepare for microinjection of this DNA construct into zebrafish embryos, 2μL of the following injection solution was prepared on the day of microinjection and kept on ice until injected: 100ng/μL of the *Tg(Fragment C-βG:Egfp)* DNA construct, 50ng/μL transposase mRNA, 0.05% phenol red, and 200mM KCl. 10pL of the injection solution were injected into individual wildtype zebrafish embryos at the one cell stage. These embryos were bleached before 24hpf and screened for Egfp fluorescence under UV light filtered to excite the Egfp protein at 24hpf, 48hpf, and 72hpf. Embryos with any Egfp expression at any time point were kept and grown to adulthood. These primary injected adults (F0 generation) were outcrossed with wildtype zebrafish, and offspring of these crosses were bleached and screened for Egfp fluorescence. Embryos from two separate crosses presenting Egfp fluorescence in the embryonic neural tube were grown to adulthood and used to establish two separate transgenic lines. However, only one of these transgenic lines was maintained and used for the experiments comprising my master’s project.

2.3 Generation of mutant zebrafish with the deletion of Fragment C

2.3.1 Induction of the Fragment C deletion by the CRISPR-Cas9 system

Guide RNAs (gRNAs) are composed of a scaffolding sequence that interacts with the Cas9 protein, and a spacer sequence that is designed complementary to a sequence in the region of DNA where a double-stranded DNA break will be introduced (Jinek et al., 2012; Marina et al., 2020). The 5’ end of the spacer sequence must contain the DNA nucleotides NGG (where each letter is the IUPAC single letter codes for DNA nucleotides), called a protospacer adjacent motif

(PAM) (Marina et al., 2020). 4 gRNAs were designed and created with spacer sequences targeting the zebrafish genome flanking Fragment C (**Figure 3.1B**, green sequences). To do so, an overlapping polymerase chain reaction (PCR) using a sequence-specific forward primer and common reverse primer was performed for each gRNA. Each forward primer contains in tandem a T7 promoter sequence, the spacer sequence that targets a sequence flanking Fragment C, and a sequence that overlaps with the reverse primer. gRNA spacer sequences must begin with the PAM sequence for efficient DNA cleavage to occur by the CRISPR-Cas9 system (Jinek et al., 2012). Since the PAM motif is any nucleotide followed by 2 guanines, if the chosen spacer sequences did not start with any Gs, 2 Gs were added to introduce the PAM sequence at the 5' end of the spacer sequence. If they started with 1 G, 1 additionally G was added. Primers used to synthesize each gRNA are given in **Figure 3.1A**. The sequence-specific regions of the forward primers were designed using the web tool CHOPCHOP (Labun et al., 2016). The PCR program for amplification of the gRNA template DNA was as follows: 95^{o}C for 30 seconds, 10 cycles of (90^{o}C for 10 seconds, 62^{o}C for 20 seconds, 72^{o}C for 20 seconds), 25 cycles of (98 °C for 10 seconds, 72 °C for 30 seconds), 72^{o}C for 5 minutes.

Following purification of PCR products with the Illustra GFC PCR DNA and Gel Band Purification Kit (product number GE28-9034-70), the HiScribe T7 *In Vitro* Transcription Kit (New England Biolabs, product number E2050) was used to transcribe PCR products to gRNAs. Transcription reactions were incubated for 2 hours at 37^{o}C and precipitated with 2.5µL of 4M LiCl and 75µL of 100% cold ethanol. Solutions were vortexed and kept at -80^{o}C for 30 minutes, followed by a 15-minute centrifuge at 13,000rpm, and a wash with cold diethylpyrocarbonate (DEPC) treated 70% ethanol. gRNAs were dried in a fume hood and resuspended in H_2O.

An injection mix containing the gRNAs was prepared with the following reagents: 1µL of 1µg/µL *cas9* mRNA, 1µL of 100µg/µL prepared gRNA (for each of the four gRNAs), 2µL phenol red, and 2µL H_2O. Wild-type adult zebrafish were bred. Offspring were born between 9:00am and 9:10am were transferred onto a petri dish containing 0.8% agarose Tris-borate-EDTA (TBE) gel (10.8g Tris base, 5.5g boric acid and 4mL 0.5M EDTA pH 8.0 per 1L H_2O, 1% agarose W/V). Microinjections were carried out at the one-cell stage. Injection volume per embryo was 10pL. Embryos were bleached and raised to adulthood.

2.3.2 Screening for the deletion of Fragment C

The adult zebrafish that were injected with the gRNAs and *cas9* mRNA at the one cell stage were outcrossed with wild-type zebrafish, and the offspring were screened for the deletion of Fragment C. This screening required the extraction of genomic DNA from larvae of the cross. To do so, 20 3dpf larvae were transferred into separate PCR tubes (1 larva per tube). Liquid was removed from PCR tubes containing larvae and filled with 20µL of 50mM NaOH. Tubes with individual larva were placed in boiling water for 10 minutes, followed by 5 minutes on ice. Samples were then left at room temperature while 2µL of 1M Tris-HCl (pH 8.0) was added. Samples were then vortexed for 20 seconds and centrifuged for 1 minute at high speed. The supernatants of the resulting samples were used as the source of genomic DNA for subsequent genotyping of embryos for the deletion of Fragment C.

Two PCR reactions were set up per sample: one reaction to detect the deletion of Fragment C, and one reaction to detect the presence of Fragment C. DNA primers were obtained from Invitrogen (custom primers, catalogue number 10336022). Both reactions use the forward primer 5'-CAGCACATTTATTCGACAACACAGA-3'. The reaction detecting the deletion of Fragment C uses the reverse primer 5'-CAAGAGCCATCTATCAAGAGTGC-3', while the

other uses the reverse primer 5'-TGCTGGCAAGCTGAGACATCTA-3'. The location of primers and size of PCR products if Fragment C is deleted/not deleted is summarized in **Figure 3.1A.** Primers were diluted to 20mM in H_2O. Each reaction was made with 1µL of forward primer, 1µL of reverse primer, 12.5µL of GoTaq (Promega ref #M7123), 7.5µL of nuclease-free H_2O, and 3µL of supernatant from previous genomic DNA extractions. Tubes were placed in a PCR machine with the following program: 5 minutes at 95ºC, 35 cycles of (30 seconds at 95ºC, 45 seconds at 60.5 ºC, 45 seconds at 72 ºC), and 10 minutes at 72 ºC. 10µL of PCR products were run on a 1% agarose gel with Redsafe (2.5µL/50mL gel, FroggaBio catalog number 21141) at 140V and imaged under UV light.

For one cross where a subset of offspring had the PCR band indicative of a successful deletion of Fragment C, purified genomic DNA at a concentration of 100ng/µL from these embryos were processed at the Ottawa Hospital Research Institute StemCore Laboratories for sequencing using the Fw1 and Rev2 primers (see **Figure 3.1A** for the location where these primers will hybridize in the zebrafish genome) to confirm that the PCR product corresponds to the deletion of Fragment C. The parent of this cross that received the gRNAs is denoted as the founder of the Fragment C deletion line, or F0 generation.

The remaining offspring of the Fragment C deletion founder fish were bleached, grown to adulthood, and subsequently screened using genomic DNA extracted from the caudal fin to identify heterozygotes for the Fragment C deletion (Fragment $C^{+/-}$). These Fragment $C^{+/-}$ F1 adults were inbred, and offspring of these crosses were grown to adulthood and screened using genomic DNA extracted from the caudal fin to find homozygotes for the deletion of Fragment C (Fragment $C^{-/-}$). These homozygotes (F2 generation) were then crossed with the *Tg(Fragment C-βG:Egfp)ot1* line, and embryos of this cross (F3 generation) were screened for the presence of

Egfp in the neural tube, bleached and grown to adulthood. These F3 adults were screened using genomic DNA extracted from the caudal fin to find heterozygotes for the Fragment C deletion that simultaneously express Egfp *(Tg(Fragment C-βG:Egfp)ot1; Fragment C$^{+/-}$).* Offspring of these fish were then used for subsequent experiments.

2.4 Egfp expression and growth time course

Adult zebrafish that are heterozygous for the deletion of Fragment C and containing the *Fragment C-βG:Egfp* transgene (*Tg(Fragment C-βG:Egfp)ot1; Fragment C$^{+/-}$*) were bred. Offspring were born between 9:00am and 9:10am and were transferred to Petri dishes filled with embryo medium (0.5mg/L methylene blue in system water) at a density of 60 embryos/dish and incubated at 28.5^{o}C. At 5hpf, embryos were imaged using the ZEISS Axio Zoom V16 microscope with brightfield light and UV light filtered to 488nm (excites Egfp/Gfp). Embryos were then placed in individual wells filled with 2mL embryo medium and incubated at 28.5^{o}C between future time points for imaging (8hpf, 9.5hpf , 11hpf, 14hpf, 19hpf, 24hpf, 48hpf, 72hpf, and 7dpf). Following imaging, larvae were genotyped.

Brightfield images from Fragment C$^{+/+}$ and Fragment C$^{-/-}$ embryos were used for either measuring standard body length (2dpf and 3dpf images) or counting somites (14hpf and 19hpf images). ImageJ was used to create merged images from brightfield and Egfp channel images.

2.5 Molecular analysis of Fragment C deletion mutant zebrafish

2.5.1 Probe preparation for *in situ* hybridization

Probes for *in situ* hybridization were made by the following steps. 10µg of purified plasmid DNA containing the CDS of either *msx3, msx1b,* or partial CDS of *egfp* (fragment bounded by 5'-AAGGGCGAGGAGCTGTTCAC-3' ; 5'-GAACTCCAGCAGGACCATGT-3') were linearized with the BamHI restriction enzyme (New England Biolabs, catalog number

R3136S) in 1X CutSmart buffer (New England Biolabs, catalog number B6004), and purified using the Illustra GFC PCR DNA and Gel Band Purification Kit. 3µL of purified linearized plasmid DNA was used as a template in a transcription reaction with 2µL digoxigenin (DIG) labeling mix (Sigma Aldrich, product number 11277073910) for *msx3* and *msx1b*, or 2µL fluorescein labeling mix (Sigma Aldrich, product number 11685619910) for *egfp*, 2µL 5x transcription buffer (Thermo Scientific), 0.5µL RNase inhibiter (Thermo Scientific, product number EO0381), 2µL of RNA polymerase (T7, T3, and Sp6 for *msx3*, *msx1b* and *egfp*, respectively. Each RNA polymerase is ordered from Thermo Scientific, product numbers EP0111, EP0101 and EP0131, respectively), and 10.5µL H_2O. Reactions were incubated for 2 hours at 37^{o}C and precipitated with 2.5µL of 4M LiCl and 75µL of 100% cold ethanol. Solutions were vortexed and kept at -80^{o}C for 30 minutes, followed by a 15-minute centrifuge at 13,000rpm, and a wash with cold DEPC-treated 70% ethanol. Probes were dried in a fume hood and resuspended in 25µL of RNase-free H_2O. 1µL of probe was run on an RNase-free agarose gel to ensure quality of the probe (single band of RNA; no smear). 1µL of 0.5M ethylenediaminetetraacetic acid (EDTA) and 9µL of RNALater (Sigma Aldrich R0901) were added to each probe mix. Probes were stored at -80^{o}C until use.

2.5.2 Preparation of embryos for *in situ* hybridization and immunohistochemistry

Tg(Fragment C-βG:Egfp)ot1; Fragment C$^{+/-}$ adult zebrafish were bred. Offspring were born between 9:00am and 9:10am and were transferred to Petri dishes filled with embryo medium (0.5mg/L methylene blue in system water) at a density of 60 embryos/dish and incubated at 28.5^{o}C. For embryos that would undergo the *in situ* hybridization protocol, 40µL of 1-phenyl 2-thiourea (PTU) solution (0.3g PTU in 3mL H2O and 7mL dimethyl sulphoxide) was added to each dish at 5:00pm, whereas for embryos that would undergo the

immunohistochemistry protocol, PTU was not added. At 20hpf, embryos were screened for Egfp fluorescence in the dorsal neural tube, and embryos positive for Egfp were kept. Immediately afterwards, embryos were manually dechorionated with forceps, and placed back at 28.5ºC until 24hpf.

At either 24hpf, 36hpf, or 48hpf, 1mL of tricaine solution (400mg Tricaine powder in 97.9mL H_2O and 2.1mL of 1M Tris-HCl pH 9.0) was added to each dish, and embryos were placed into 1.5mL Eppendorf centrifuge tubes. Embryo medium was removed from the tubes and replaced with 1mL of 4% paraformaldehyde (PFA) in DEPC-treated phosphate-buffered saline (PBS). Embryos were left on a shaker at room temperature for 2 hours in PFA solution and were subsequently washed twice with diethylpyrocarbonate (DEPC) treated PBS with 0.25% Tween-20 (PBST). Embryos were placed in a final volume of PBST and left at 4ºC overnight.

Embryos were then manually deyolked with forceps and washed twice to remove loose yolk. The heads of embryos were then dissected with a scalpel and transferred to individual PCR tubes for genotyping. 70% ethanol was used to clean all equipment and the dissection surface between each dissection. The trunks of the embryos were placed in 24-well plates filled with PBST and left at 4ºC for later use.

PBST was removed from PCR tubes containing a single embryo's head, and these heads were genotyped. The trunks of embryos that were stored at 4ºC were sorted based on the genotype of their head tissue: Fragment $C^{+/+}$ (wild-type siblings), Fragment $C^{+/-}$ (heterozygous siblings), or Fragment $C^{-/-}$ (homozygous siblings). The remaining embryo tissue that would undergo the immunohistochemistry protocol were prepped to be cryo-sectioned by incubating them overnight at 4ºC in 30% sucrose dissolved in PBST.

2.5.3 Cryo-sectioning embryos for immunohistochemistry

Tails of the embryos that were previously stored at 4^{o}C in 30% sucrose dissolved in PBST were embedded in 7mm x 7mm x 5mm blocks of Shandon Cryomatrix (Thermo Scientific, product number 6769006) and chilled in cold isopentane until Cryomatrix solidified. Blocks were stored at -80^{o}C until they were sectioned. Blocks were sectioned in a cryostat with an orientation providing transverse sections of the embryos/larvae, with thickness 10µm. Sections were adhered to Superfrost plus microscope slides (Fisherbrand, catalog number 12-550-15), and allowed to dry for at least 30 minutes before being stored at -20^{o}C until use in the immunohistochemistry protocol.

2.5.4 *In situ* hybridization

Previously prepared trunks of 24hpf embryos underwent a fluorescent *in situ* hybridization procedure. All solutions for the first day of this procedure were made with DEPC-treated water. All washes/treatments were carried out in 4mL volumes in 6-well plates unless otherwise stated. trunks were sorted based on genotype, and each set of trunks was placed in a unique embryo basket in a 6-well plate filled with PBST. Approximately 150 spare, whole 24hpf embryos were added to a fourth embryo basket for later use in pre-adsorption of polyclonal antibodies.

Embryos were rehydrated from methanol (MeOH) to PBST through a series of 5 minute washes (3:1 MeOH:PBS, 1:1 MeOH:PBS, 1:3 MeOH:PBS, PBST, PBST, PBST). Spare embryos and genotyped trunks were placed in 2µl of 20mg/ml proteinase K in 4mL PBST for 5 minutes and washed twice with PBST. Embryos were fixed in 4% PFA and washed twice in PBST. Embryos were treated with an acetylation mix (37.5µL triethanolamine, 8.1µL acetic anhydride in 3mL H_2O), and washed twice in PBST. Embryos were then transferred to 2mL

tubes and incubated in a 70°C water bath for 2 hours in 700µL hybridization buffer (50% deionized formamide, 5x SSC, 0.125% Tween-20, 20mM citric acid, 100µg/mL yeast tRNA, and 50µg/mL heparin in H_2O). During this 2-hour incubation, spare embryos were divided amongst two 2mL tubes, and liquid was removed. 1mL of TBST-B (tris-buffered saline with Tween-20 and blocking powder) solution (0.25g Perkin Elmer Blocking Powder, 5 mL 1M Tris HCL pH 7.5, 1.5 mL 5M NaCl and 0.25 mL Tween-20 in 50 mL H2O) was added along with 4 µL of anti-DIG antibody conjugated with horse-radish peroxidase (POD) to one tube, and 4 µL anti-fluorescein POD to the other (Sigma Aldrich, products numbers 11207733910 and 11426346910, respectively). Tubes were left at room temperature on a shaker for two hours.

After the 2-hour incubation at 70°C, probes for *msx3*, *msx1b* and *egfp* were thawed from -80°C on ice. Depending on the desired probes to be used in each experiment, one of the following probe combinations were prepared: *msx3* and *egfp*, or *msx1b* and *egfp*. Probes were diluted to 0.75µL probe per 100µL hybridization buffer. The hybridization buffer containing the desired probes was heated at 70°C for 15 minutes. The 700µL of hybridization buffer in each tube with genotyped trunks was removed, and 200 µL of hybridization buffer mixed with the probes was added. Embryos were incubated in this solution overnight at 70°C. Tubes containing TBST-B and antibody were transferred to 4°C overnight.

The next day, the following solutions were prepared: 5X buffer (50% deionized formamide, 5X saline-sodium citrate (SSC, 175.3g NaCl, 88.2g tri-sodium citrate in 1L H_2O, pH 7) and 0.25% Tween-20 in H_2O), 2X buffer (2X SSC and 0.25% Tween-20 in H_2O), and 0.2X buffer (0.2X SSC and 0.25% Tween-20 in H_2O). Trunks of embryos were transferred back to 6 well plates and underwent the following washes at 70°C: 5 minutes in 5X buffer, 5 minutes in 3:1 5X:2X buffer, 5 minutes in 1:1 5X:2X buffer, 5 minutes in 1:3 5X:2X buffer, 5 minutes in 2x

buffer, and three 20 minute washes in 0.2X buffer. Afterwards, embryos were placed back at room temperature and washed twice with PBST, followed by a 1 hour treatment in 267 µl 30% H_2O_2 in 4mL PBST. Embryos were washed 4 times in TNT buffer (0.1M Tris-HCl pH 7.5; 0.15M NaCl; 0.5% Tween-20, in H_2O). Embryos were transferred to TBST-B for 2 hours. Subsequently, the 1mL of embryos in TBST-B with anti-fluorescein antibody was mixed with 3mL of TBST-B, and embryos were incubated in this solution at 4^oC overnight. The following day, embryos were washed 7 times in TNT (2x5 min, 2x10 minutes, 20 minutes, 30 minutes, 40 minutes). Embryos were transferred to 2mL tubes, and excess liquid was removed. Embryos were incubated in 50µL Perkin Elmer Amplification Diluent (ordered in kit with product number NEL701A001KT) for 5 minutes, followed by a 1 hour incubation in 100µL amplification diluent with 1:100 tyramide conjugated with Cy3 (Perkin Elmer, NEL701A001KT) in the dark. Embryos were transferred back to 6-well plates wrapped in aluminum foil (to prevent light exposure) and washed twice in TNT. Embryos underwent a hydrogen peroxide treatment identical to that performed earlier and were washed 4 times in TNT. Embryos were incubated in TBST-B for 2 hours. Following this, the 1ml of embryos in TBST-B with anti-DIG POD antibody was mixed with 3mL of TBST-B, and embryos were incubated in this solution at 4^oC overnight. The next day, embryos were washed seven times in TNT (2x5 minutes, 2x10 minutes, 20 minutes, 30 minutes, 40 minutes). Embryos were transferred to 2mL tubes, and excess liquid was removed. Embryos were incubated in 50µL Perkin Elmer Amplification Diluent followed by an incubation of 100µL amplification diluent with 1:100 tyramide conjugated with fluorescein in the dark (Perkin Elmer, NEL701A001KT). Embryos were transferred back to 6-well plates wrapped in aluminum foil to prevent light exposure and washed twice in TNT. Embryos were

then incubated for 30 minutes in TNT with 4′,6-diamidino-2-phenylindole (DAPI), followed by two more TNT washes. Embryos were then imaged.

2.5.5 Immunohistochemistry

Sectioned 1.5dpf and 3dpf embryos sectioned on slides were thawed for 2 hours at room temperature, followed by rehydration in PBS for 30 minutes. slides to be treated with Sox2 antibody were left in this PBS wash, while slides to be treated with Elavl3/4 antibody were incubated for 30 minutes at 70^{o}C in 50mM Tris-HCl pH 8.0, followed by three washes in PBST + 0.1% DMSO at room temperature. All slides were then incubated in a blocking solution (0.2% triton X-100, 2% calf serum in PBS) for two hours. Sections on slides were incubated in blocking solution with one of the following primary antibody combinations at 4^{o}C overnight: Gfp-anti-chicken (1:300, Abcam #ab13970) + Elavl3/4-anti-mouse (1:300, Abcam #ab210554), or : Gfp-anti-chicken (1:300) + Sox2-anti-rabbit (1:300, Abcam #ab97949). On the next day, slides were washed in PBST for 10 minutes four times. One of the following secondary antibody combinations were applied to the slides dissolved in PBST: Goat-anti-chicken (1:300, Abcam # ab150169) + Donkey-anti-mouse (1:300, Abcam #ab150106), or Goat-anti-chicken (1:300) + Goat-anti-rabbit (1:300, Abcam # ab150078) and incubated at room temperature for three hours. Slides were then washed four times in PBST for 10 minutes each, with the first wash containing 0.5ng/mL DAPI). Slides were rinsed twice with H_2O for 5 minutes and allowed to dry before being mounted with Aqua-Poly/Mount (Polysciences, catalog number #18606-20) and imaged.

2.5.6 Imaging

Whole-mount and sectioned embryos were imaged using the Olympus FV1000 BX61 LSM confocal microscope. For whole-mount embryos, slides were prepared by adhering square coverslips to a microscope slide with Cryomatrix, placing and positioning embryos to be imaged

between the coverslips in TNT, and placing a long rectangular coverslip on top as a bridge between the square coverslips. Images were taken with 10X, 20X, and 40X objectives. Images were processed using ImageJ to adjust look-up tables and combine color channels. Lateral view images were directly taken by the microscope, while transverse view images were processed using the re-slicing tool in ImageJ. In lateral view images, images shown are maximum-intensity Z projections covering Z-stacks containing part of the neural tube. In transverse view images, images shown are maximum-intensity Z projections spanning 10μm along the anterior-posterior axis at the level of urogenital opening. For sectioned embryos, a 40X objective lens was used to take images of transverse sections of embryos.

2.5.7 Cell counting

From images of sectioned embryos, one z-stack with the clearest staining was picked for each section to perform subsequent cell counting. Color balance was adjusted in ImageJ to remove any background stain. Sox2 positive cells were denoted as cells with colocalization of DAPI and Sox2 stain. Elavl3/4 positive cells were denoted as cells with Elavl3/4 stain completely or almost-surrounding a DAPI-stained nuclei. Cells with Elavl3/4 staining that was weak and only partially surrounding DAPI-stained nuclei were not counted as Elavl3/4 positive. Egfp positive cells were denoted by the following criteria: A continuous boundary of Gfp stain (anti-Gfp antibodies also bind Egfp) around a DAPI stained nuclei, and some degree of cytosolic Gfp stain. These criteria excluded cells that were surrounded by a Gfp border but did not have Gfp staining within the cell body (see **Figure 2.1** for examples of both staining profiles). This distinction was made because cells may extend processes that travel near or around adjacent cells, which could create a border Gfp signal around a DAPI-stained nuclei. For all Gfp^+ cells that did not have staining throughout their cell body, the adjacent z-stacks were checked in the

anterior and posterior direction for staining in the cell body. If cell body staining was present, the cell was still counted as Egfp positive.

The dorso-ventral length of each neural tube section was measured by a line from ventral limit of the neural tube to the dorsal limit passing through the central canal. The most ventral Egfp positive cell was located, and a parallel line from the dorsal limit of the neural tube to this Egfp positive cell was measured. If Egfp was not present in the dorsal most nuclei, a parallel line from the dorsal limit of the neural tube to the dorsal most nucleus was also measured.

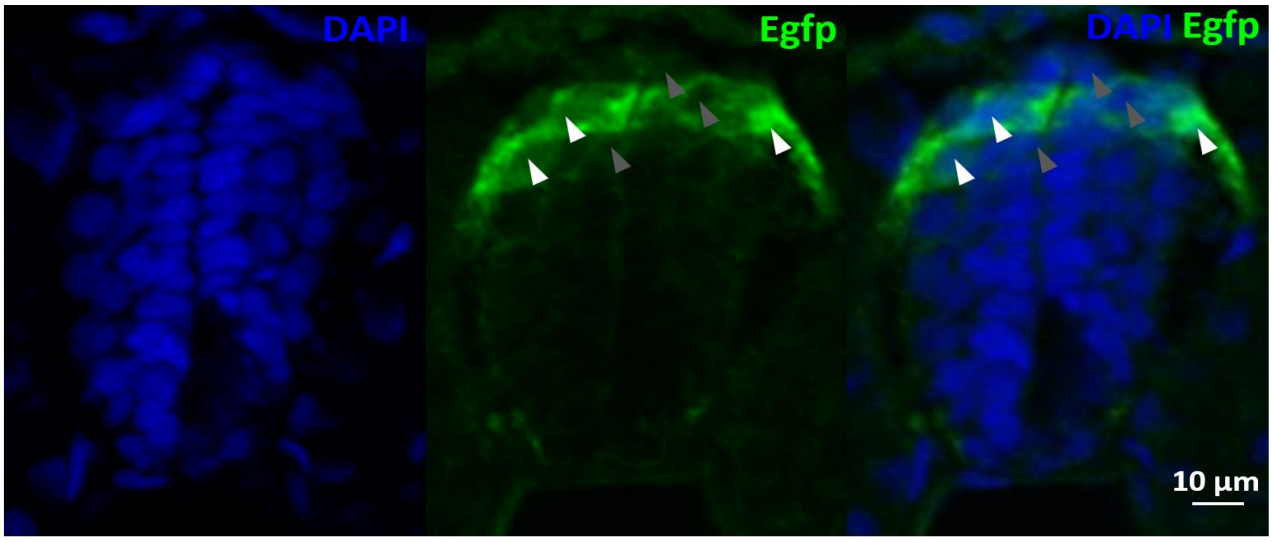

Figure 2.1. Profiles of Gfp staining in neural tube cells of embryonic and larval zebrafish. Immunohistochemistry with antibodies against Gfp (which recognizes the Egfp protein) and either Elavl3/4 or Sox2 was performed on embryonic and larval zebrafish followed by DAPI staining to label cell nuclei. Cells with Gfp staining showed two profiles: one where Gfp stain surrounds only the border of a $DAPI^+$ nucleus but does not stain the cell body (grey arrowheads), and one where Gfp stain both surrounds a $DAPI^+$ nuclei and stains the cell body (white arrowheads). Scale bar represents a length of 10µm.

3 Results

3.1 Generation of Fragment C$^{-/-}$ mutant zebrafish line

To understand the function of the Fragment C enhancer, we deleted the Fragment C enhancer using the CRISPR-Cas9 genome-editing system. We designed guide RNAs (gRNAs) that target either a sequence upstream or downstream of the Fragment C enhancer (**Figure 3.1B, green sequences**). Guide RNAs are sequence-specific, form a complex with the Cas9 protein, and bind to a complementary sequence in the genome, thus recruiting the Cas9 protein to a specific location in the genome (Mali et al., 2013). The Cas9 protein contains a domain with endonuclease activity, allowing it to introduce a double-stranded break in the DNA (Cong et al., 2013). After the Cas9 protein introduces a double-stranded break at the targeted site (i.e. the regions flanking Fragment C), there is a chance that, through the non-homologous end-joining DNA repair mechanism, the DNA upstream and downstream of Fragment C is rejoined with the exclusion of Fragment C (**Figure 3.2A**).

Wild-type embryos at the one cell stage were injected with a mix of two gRNAs targeted upstream of Fragment C, two gRNAs targeted downstream of Fragment C, and *cas9* mRNA. After growing the primary injected embryos (F0 generation) to adults and outcrossing them with wild-type adults, a subset of the embryos of these crosses (F1 generation) were screened by PCR for the successful deletion of Fragment C. Two different PCR reactions were used to screen for the deletion of Fragment C: one forms a PCR amplicon of 238bp if the deletion of Fragment C was unsuccessful, and the other forms a PCR amplicon of 137bp if the deletion of Fragment C was successful (Figure 3.2A). A sample gel showing these PCR products is provided in **Figure 3.2B**.

After finding embryos of the F1 generation that screened positive for the Fragment C deletion, the genomic DNA of these embryos was sent to be sequenced using the Fw1 and Rev2 primers shown in **Figure 3.2A** (green arrows) and **Figure 3.3A**. The sequencing result from these genomic DNA samples are shown in **Figure 3.3B**. Fragment C **(Figure 3.3A**, purple bold sequence) is absent from this sequencing result, and in its place, a 12 base-pair insertion (**Figure 3.3B**, black sequence) is found due to the error-prone DNA repair mechanism of non-homologous end-joining.

The remaining F1 generation were grown to adulthood and subsequently screened by PCR to identify heterozygotes for the Fragment C deletion (Fragment $C^{+/-}$). These Fragment $C^{+/-}$ adults were inbred, and offspring of these crosses were grown to adulthood and screened by PCR to find homozygotes for the deletion of Fragment C (Fragment $C^{-/-}$). These homozygotes (F2 generation) were then crossed with the *Tg(Fragment C-βG:Egfp)ot1* line, and embryos of this cross (F3 generation) were screened for the presence of Egfp in the neural tube and grown to adulthood. These F3 adults were screened by PCR to identify heterozygotes for the Fragment C deletion that simultaneously express Egfp *(Tg(Fragment C-βG:Egfp)ot1; Fragment* $C^{+/-}$*).* Offspring of these fish were used in subsequent experiments to obtain embryos that are homozygous for the Fragment C deletion (alongside heterozygous and wild-type siblings) that additionally express *egfp* driven by the Fragment C enhancer. Homozygous mutants for the deletion of Fragment C are viable, fertile, and do not display overt morphological abnormalities at any developmental stage.

A

gRNA	gRNA forward primer sequence (5' – 3')	gRNA reverse primer sequence (5' – 3')
Upstream gRNA 1	TAATACGACTCACTATAGGCTTTCACACTCATAT CAAGGTTTTAGAGCTAGAAATAGC	AAAAGCACCGACTCGGTGCCACTTTTTCAAGTTGATAACG-GACTAGCCTTATTTTAACTTGCTATTTCTAGCTCTAAAAC
Upstream gRNA 2	TAATACGACTCACTATAGGACTTTCGGCCGTCA GCATCGGTTTTAGAGCTAGAAATAGC	AAAAGCACCGACTCGGTGCCACTTTTTCAAGTTGATAACG-GACTAGCCTTATTTTAACTTGCTATTTCTAGCTCTAAAAC
Downstream gRNA 1	TAATACGACTCACTATAGGACTGAGAGAGCGT TTCAAGCGTTTTAGAGCTAGAAATAGC	AAAAGCACCGACTCGGTGCCACTTTTTCAAGTTGATAACG-GACTAGCCTTATTTTAACTTGCTATTTCTAGCTCTAAAAC
Downstream gRNA 2	TAATACGACTCACTATAGGGTGAGGTGCCTGC ATTCCCGTTTTAGAGCTAGAAATAGC	AAAAGCACCGACTCGGTGCCACTTTTTCAAGTTGATAACG-GACTAGCCTTATTTTAACTTGCTATTTCTAGCTCTAAAAC

B

Figure 3.1. gRNA design for the deletion of Fragment C. A. Each guide RNA was synthesized from an overlapping PCR using the listed forward and reverse primers to generate a DNA template that was subsequently used as a template in an *in vitro* transcription reaction with T7 RNA polymerase. All four gRNAs were subsequently injected into zebrafish embryos alongside *cas9* mRNA at the 1-cell stage. Each forward primer begins at the 5' end with the T7 promoter sequence (red), followed by a custom sequence complementary to a region flanking Fragment C (black, designed using the CHOPCHOP gRNA design software (Labun et al., 2016)), followed by a sequence overlapping with the reverse primer (blue). The same reverse primer is used in the overlapping PCR for all gRNAs and corresponds to scaffolding region of the gRNA (blue) that will interact with Cas9 protein. **B.** location of the sequence-specific regions of the four gRNAs injected into zebrafish, two of which bind upstream of Fragment C and two of which bind downstream (green). The Fragment C sequence is shown in purple.

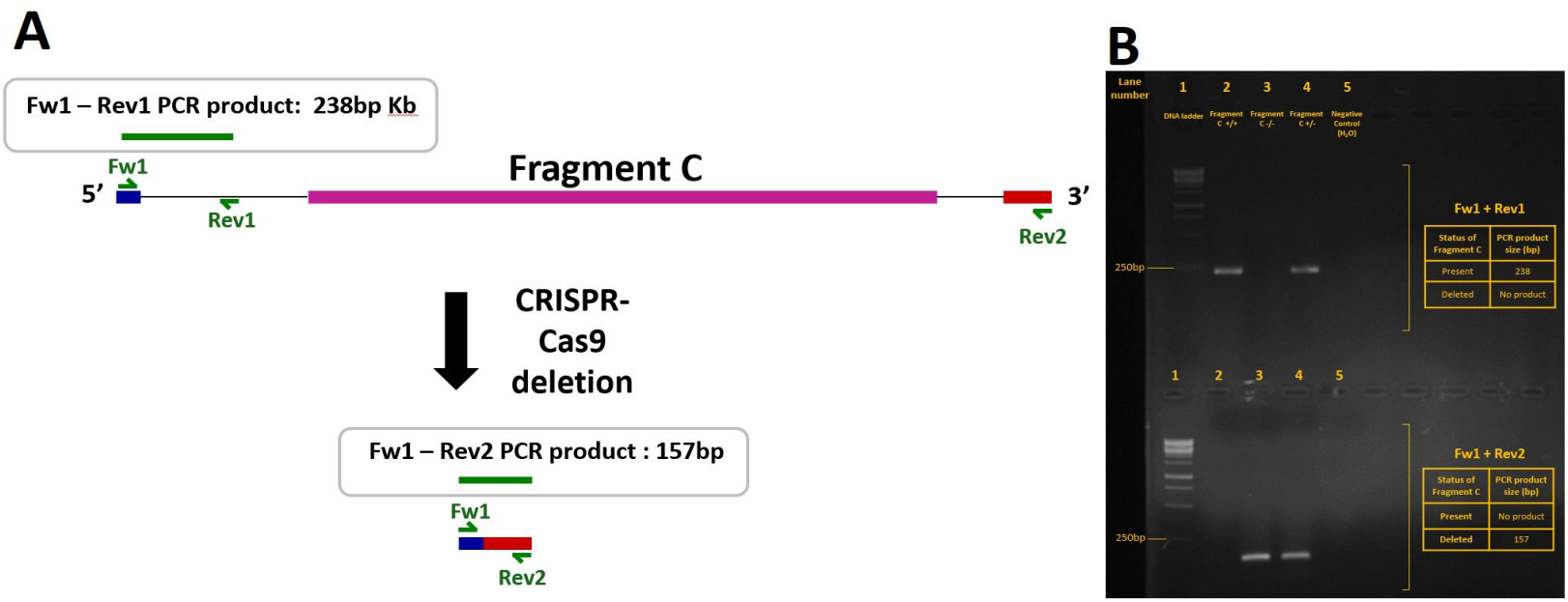

Figure 3.2. Screening of the Fragment C deletion by PCR. Guide RNAs targeting sequences upstream and downstream of the Fragment C enhancer were injected with *cas9* mRNA into zebrafish embryos at the one cell stage. Embryos were grown to adulthood and outcrossed with wild-type adults, and genomic DNA from offspring were screened via PCR for the deletion of Fragment C. **A.** Schematic of primer binding sequences and resulting PCR products if Fragment C is deleted or not deleted. Blue line: sequence upstream of Fragment C deletion. Red line: sequence downstream of Fragment C sequence. The sequence between Fw1 and Rev1 primers should be deleted, including Fragment C (pink line) and the flanking sequence (black lines). Length of lines are proportional to lengths of sequences that they represent. Green arrows: primer-binding sequences. Fw1 and Rev1 yield a 238bp PCR product if Fragment C and flanking sequences (pink + black lines) are not deleted and no product if deleted. Fw1 and Rev2 yield a 157bp product if Fragment C and flanking sequences (pink + black lines) are deleted, and no product if not deleted. **B.** Agarose gel of PCR products from reactions with genomic DNA and either Fw1/Rev1 (top lanes) or Fw1/Rev2 (bottom lanes) primer pairs. Each pair of lanes with the same lane number correspond to the same single embryo sample. Presence of only the Fw1-Rev2 DNA band represents Fragment $C^{+/+}$ samples (lane 2). Presence of only the Fw1-Rev1 band represents Fragment $C^{-/-}$ samples (lane 3), and presence of both represents Fragment $C^{+/-}$ fish (lane 4). Lane 5: PCR reaction set up with water instead of sample. DNA ladder is the ThermoFisher GeneRuler 1kb DNA Ladder.

Figure 3.3. DNA sequence of and surrounding the endogenous Fragment C enhancer before and after CRISPR-mediated deletion of Fragment C. A. Genomic DNA sequence of and surrounding the Fragment C enhancer in wild-type zebrafish. **B.** Sequencing results from genomic DNA of CRISPR-Cas9 mutant F1 generation with the Fragment C enhancer deleted. Blue nucleotides are upstream of the deletion, while red nucleotides are downstream of the deletion. Target sites of the four guide RNAs (upstream gRNA1, upstream gRNA2, Downstream gRNA 1, and Downstream gRNA2) used to induce the deletion of Fragment C and flanking sequences (pink and black sequences, respectively) are labelled above each corresponding sequence. Sequences of primers Fw1, Rev1, and Rev2 are labelled above or below each corresponding sequence. Note that the 12bp between the upstream and downstream sequences in **B** do not correspond to the original undeleted sequence, and instead represent an insertion due to the error-prone repair mechanism of the CRISPR-Cas9 system.

3.2 Loss of the Fragment C enhancer does not alter rate of embryonic and larval development

Firstly, we wanted to test if the rate of overall development is affected by the loss of the Fragment C enhancer. If the rate of development is affected, future experiments would have to correct for the differing developmental rates. In zebrafish, maturation is affected by several factors including water temperature, fish density, and water quality (Singleman & Holtzman, 2014). Due to the influence of these external factors and genetic factors, age is not necessarily a reflection of developmental stage (Parichy et al., 2009). During embryonic stages, somite number is an accurate measure of developmental stage (Kimmel et al., 1995). At post-embryonic stages, the most reliable assessment of developmental maturity requires analyzing factors including the standard length of the zebrafish, pigmentation pattern, and formation of bony fin rays (Singleman & Holtzman, 2014). However, within the first week of development, only one of five characterized pigmentation patterns are observed, and bony fin rays have not yet formed. Thus, to assess the developmental stage of larval zebrafish, standard length was measured, while number of somites were counted to assess the developmental stage at embryonic stages. *Tg(Fragment C-βG:Egfp)ot1;Fragment C*$^{+/-}$ siblings were crossed, and offspring were kept at a fish density of 60 fish per 50mL Petri dish until 5hpf, after which the density was adjusted to one fish per 2mL well of a 24-well plate. Temperature was kept at 28.5^{o}C except during imaging of embryos. Water was changed at 5hpf, 11hpf, 14hpf, 19hpf, 24hpf, and 48hpf.

The mean number of somites ± sample standard deviation was 8.29 ± 0.76 for 14hpf Fragment C$^{+/+}$ embryos (N = 7) and 8.57 ± 1.13 for 14hpf Fragment C$^{-/-}$ embryos (N = 7), 17.00 ± 0.63 for 19hpf Fragment C$^{+/+}$ embryos (N = 6), and 17.29 ± 0.76 for 19hpf Fragment C$^{-/-}$ embryos (N = 7) (**Figure 3.4**). At both 14hpf and 19hpf there was no statistically significant

difference in the number of somites between Fragment $C^{+/+}$ and Fragment $C^{-/-}$ embryos ($p = 0.589$ at 14hpf, $p = 0.480$ at 19hpf).

The mean standard length of larvae ± sample standard deviation was 3.30 ± 0.05 mm for 2dpf Fragment $C^{+/+}$ larvae (N = 5) and 3.25 ± 0.13 mm for 2dpf Fragment $C^{-/-}$ larvae (N = 6), 3.77 ± 0.04 mm for 3dpf Fragment $C^{+/+}$ larvae (N = 5), and 3.70 ± 0.16 mm for 3dpf Fragment $C^{-/-}$ larvae (N = 6) (**Figure 3.5**). At both 2dpf and 3dpf there was no statistically significant difference in standard length between Fragment $C^{+/+}$ and Fragment $C^{-/-}$ larvae ($p = 0.405$ at 2dpf, $p = 0.392$ at 3dpf).

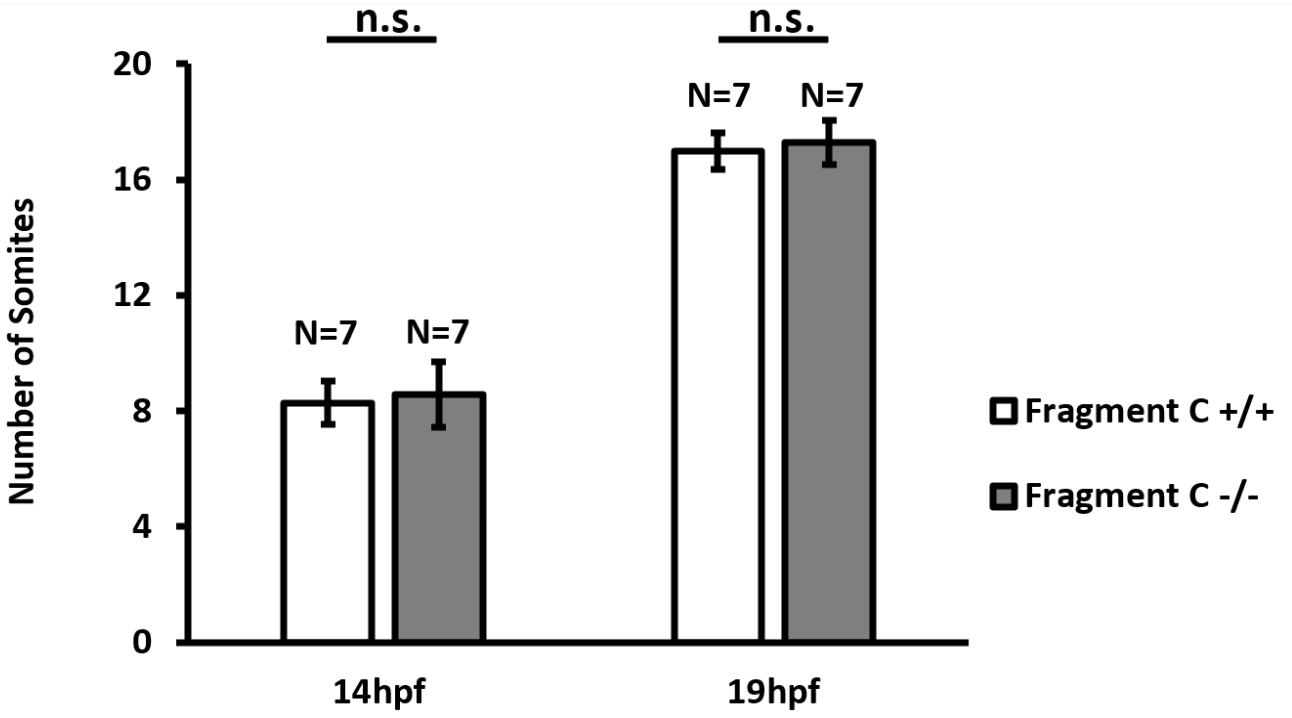

Figure 3.4. Number of somites of wild-type and Fragment C deletion mutants at 14hpf and 19hpf. Embryos from a cross of *Tg(Fragment C-βG:Egfp)ot1;Fragment C*$^{+/-}$ siblings of were collected within ten minutes of fertilization and grown in Petri dishes at a density of 60 embryos per dish until 5hpf, after which embryos were grown individually in wells of a 24-well plate. Embryos were imaged at 14hpf and 19hpf and somites were counted from these images. Each sample is a somite count from one embryo. Height of bars represent the mean number of somites among all embryos per genotype and age ± sample standard deviation (error bars). A two-tailed student's t-test was used to compare embryos with no deletion of Fragment C (Fragment C$^{+/+}$) and homozygous deletion of Fragment C (Fragment C$^{-/-}$) of the same age. Between genotypes at 14hpf, $p = 0.589$, and at 19hpf, $p = 0.480$. n.s.(not significant) = $p > 0.05$.

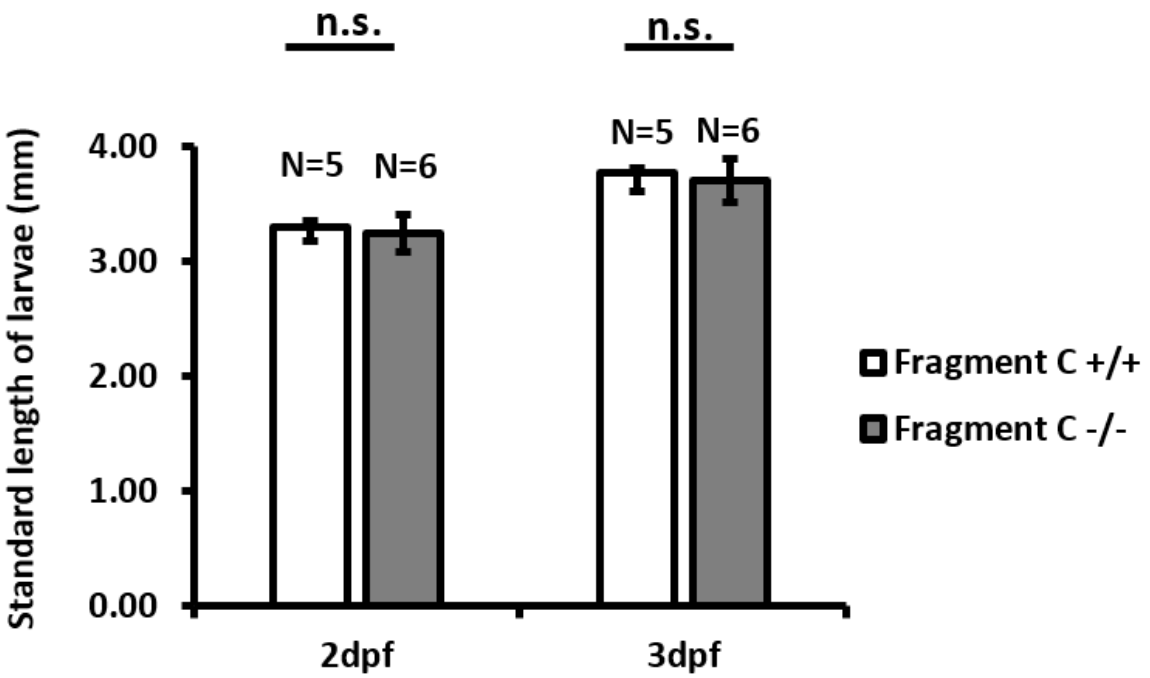

Figure 3.5. Standard length of wild-type and Fragment C deletion mutant at 2dpf and 3dpf. Embryos from a cross of *Tg(Fragment C-βG:Egfp)ot1;Fragment* $C^{+/-}$ siblings of were collected within 10 minutes of fertilization and grown in Petri dishes at a density of 60 embryos per dish until 5hpf, after which embryos were grown individually in wells of a 24-well plate. Larvae were imaged at 2dpf and 3dpf and the length from the anterior head of the zebrafish to the posterior tail (excluding the median fin fold) of the zebrafish was measured from these images (these lengths are referred to as standard length). Each sample is a single measurement of standard length from one larva. Height of bars represent the mean standard length among all larvae per genotype and age ± sample standard deviation (error bars). A two-tailed student's t-test was used to compare embryos with no deletion of Fragment C (Fragment $C^{+/+}$) and homozygous deletion of Fragment C (Fragment $C^{-/-}$) of the same age. Between genotypes at 2dpf, $p = 0.405$, and at 3dpf, $p = 0.392$. n.s. (not significant) = $p > 0.05$.

3.3 Loss of the Fragment C enhancer does not result in gross morphological changes nor gross changes in Egfp reporter expression.

It is possible that after the loss of the endogenous Fragment C enhancer, the fate and or location of cells with Fragment C-driven expression may be altered. These cells are labelled by Egfp driven by the transgenic Fragment C enhancer. Additionally, if a signaling pathway downstream of *msx3* ultimately has feedback on transcription factors binding to Fragment C, the transgenic Fragment C enhancer may drive differential expression in zebrafish lacking the endogenous Fragment C compared to those with the endogenous Fragment C. To test if either of these outcomes occur after the deletion of Fragment C, a time course analysis of Egfp fluorescence was carried out during embryonic and larval development.

Images of Egfp fluorescence in offspring of a cross between *Tg(Fragment C-βG:Egfp)ot1;Fragment C*$^{+/-}$ siblings were taken at 8hpf, 9.5hpf, 11hpf, 14hpf, 19hpf, 24hpf, 36hpf, 48hpf, 72hpf, and 7dpf (**Figure 3.6 – 3.14,** respectively). Fragment C$^{+/+}$ and Fragment C$^{-/-}$ embryos showed no overt differences in Egfp fluorescence at any time point examined. Egfp fluorescence was first observed in the neural plate at 8hpf in both Fragment C$^{+/+}$ and Fragment C$^{-/-}$ embryos (**Figure 3.6B, E**). At 8hpf, Egfp fluorescence is not much stronger than fluorescence in the yolk sac (which is auto-fluorescent, meaning it does not require the expression of Egfp to fluoresce). At 9.5hpf, Egfp fluorescence in the neural plate is slightly stronger than the autofluorescence of the yolk sac (**Figure 3.7B, E**). By 11hpf, Egfp expression in the neural plate increases in intensity drastically (**Figure 3.8B, E**). Onwards of 14hpf, Egfp is strongly expressed in the midbrain (more specifically the optic tectum), hindbrain, and dorsal neural tube

corresponding to the presumptive spinal cord. (**Figure 3.9-3.14B, E**). Additionally, between 14hpf and 24hpf, Egfp is weakly expressed anterior to the midbrain in the eye and forebrain, and strongly expressed in the notochord (**Figure 3.9-3.11B, E**). Egfp expression in the notochord is strongest posteriorly and is reduced to its lowest level toward the trunk. By 48hpf and onward, Egfp expression is absent in the notochord, eye, and forebrain, but persists in the optic tectum of the midbrain, hindbrain, and dorsal neural tube (**Figure 3.12 – 3.14B, E**).

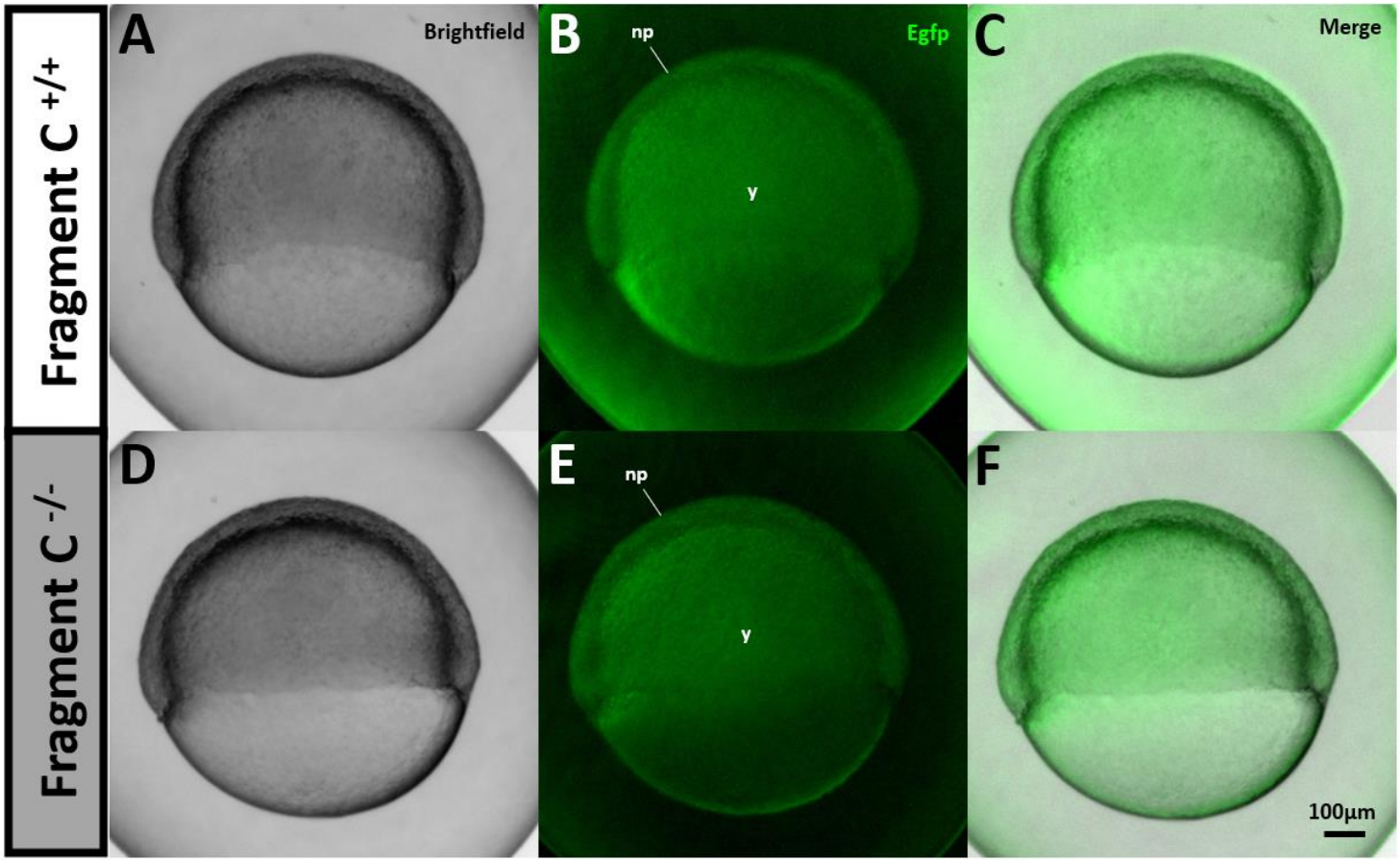

Figure 3.6. Fragment C-driven Egfp expression in zebrafish embryos at 8hpf. Embryos from a cross of *Tg(Fragment C-βG:Egfp)ot1;Fragment* $C^{+/-}$ siblings of were collected within 10 minutes of fertilization and grown in Petri dishes at a density of 60 embryos per dish until 5hpf, after which embryos were grown individually in wells of a 24-well plate. Embryos were imaged at 8hpf, 9.5hpf, 11hpf, 14hpf and 19hpf, dechorionated at 20hpf, and imaged again at 24hpf, 48hpf, 72hpf, and 7dpf with brightfield light and UV light filtered at 488nm. Anterior is left, posterior is right. **A, D.** brightfield images of 14hpf Fragment $C^{+/+}$ (**A**), and Fragment $C^{-/-}$ (**D**) embryos. **B, E.** Epifluorescence images of 14hpf Fragment $C^{+/+}$ (**B**), and Fragment $C^{-/-}$ embryos (**E**). **C.** merge of **A** and **B**. **F.** Merge of **D** and **E**. Scale bar (black line, bottom right) represents a length of 1mm. np = neural plate. y = yolk sac.

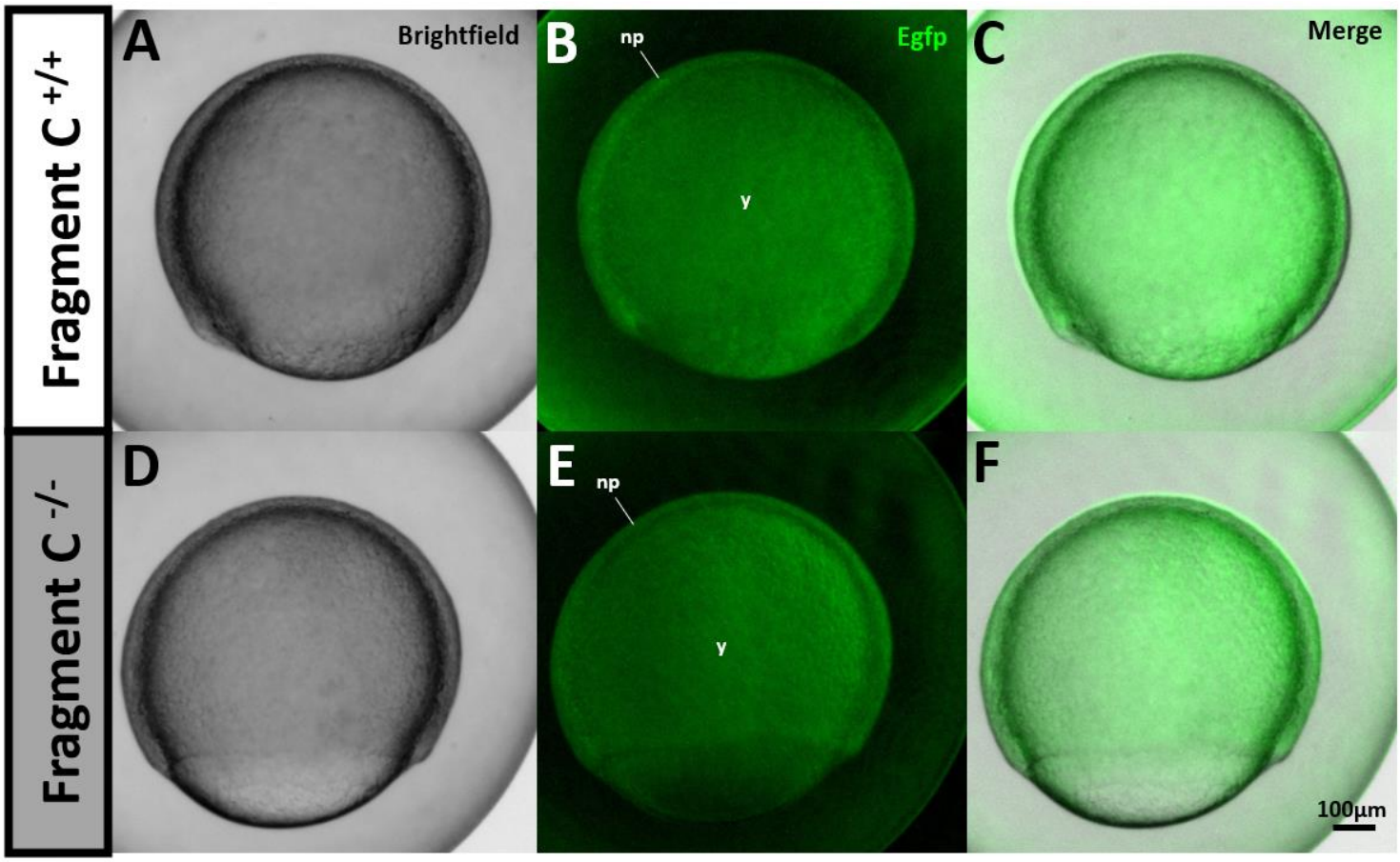

Figure 3.7. Fragment C-driven Egfp expression in zebrafish embryos at 9.5hpf. Embryos from a cross of *Tg(Fragment C-βG:Egfp)ot1;Fragment C*$^{+/-}$ siblings. Anterior is left, posterior is right. **A, D.** brightfield images of 14hpf Fragment C$^{+/+}$ (**A**), and Fragment C$^{-/-}$ (**D**) embryos. **B, E.** Epifluorescence images of 14hpf Fragment C$^{+/+}$ (**B**), and Fragment C$^{-/-}$ embryos (**E**). **C.** merge of **A** and **B**. **F.** Merge of **D** and **E**. Scale bar (black line, bottom right) represents a length of 100µm. np = neural plate. y = yolk sac.

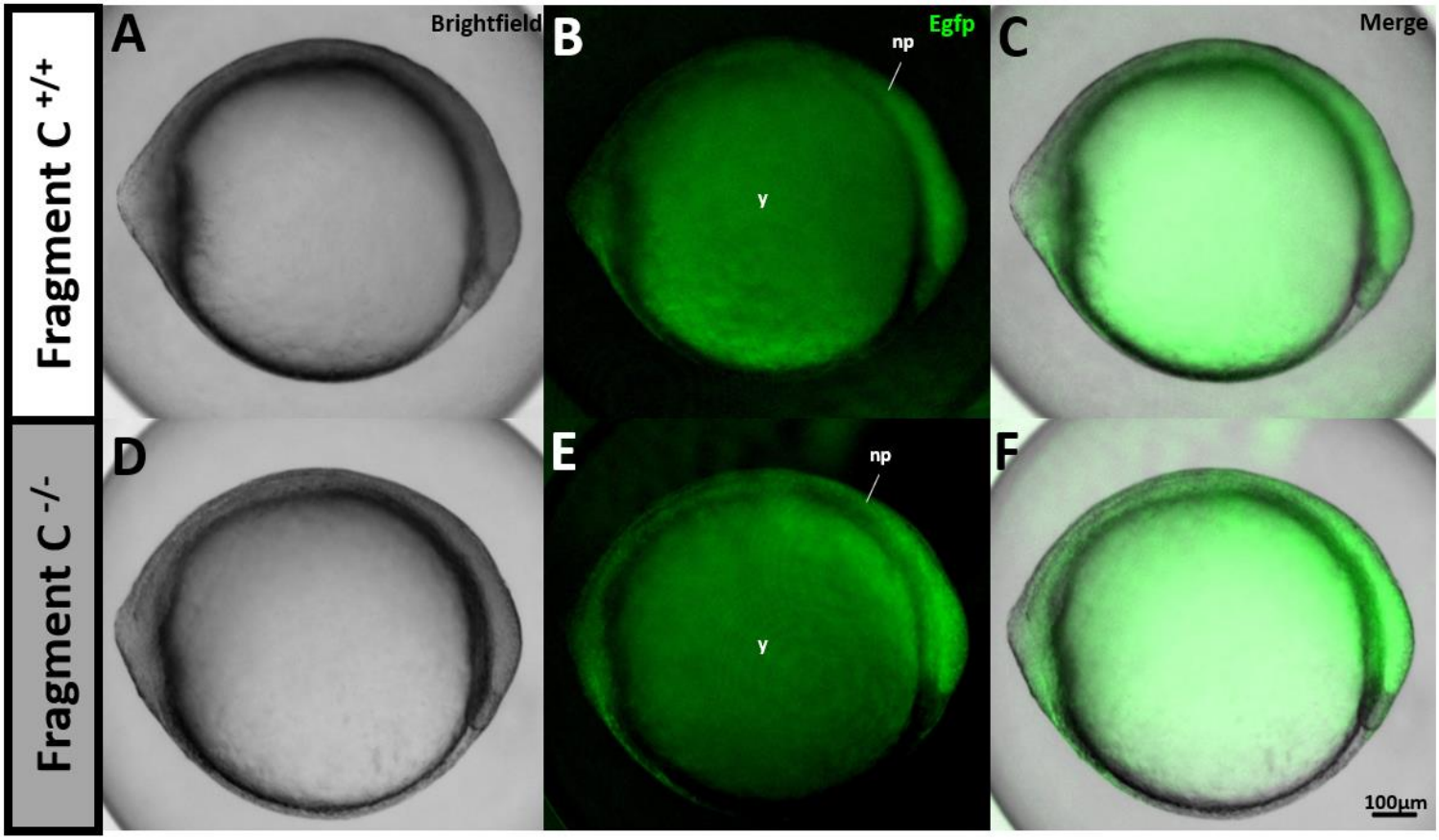

Figure 3.8. Fragment C-driven Egfp expression in zebrafish embryos at 11hpf. Embryos from a cross of *Tg(Fragment C-βG:Egfp)ot1;Fragment C*$^{+/-}$ siblings. Anterior is left, posterior is right. **A, D.** brightfield images of 14hpf Fragment C$^{+/+}$ (**A**), and Fragment C$^{-/-}$ (**D**) embryos. **B, E.** Epifluorescence images of 14hpf Fragment C$^{+/+}$ (**B**), and Fragment C$^{-/-}$ embryos (**E**). **C.** merge of **A** and **B**. **F.** Merge of **D** and **E**. Scale bar (black line, bottom right) represents a length of 100µm. np = neural plate. y = yolk sac.

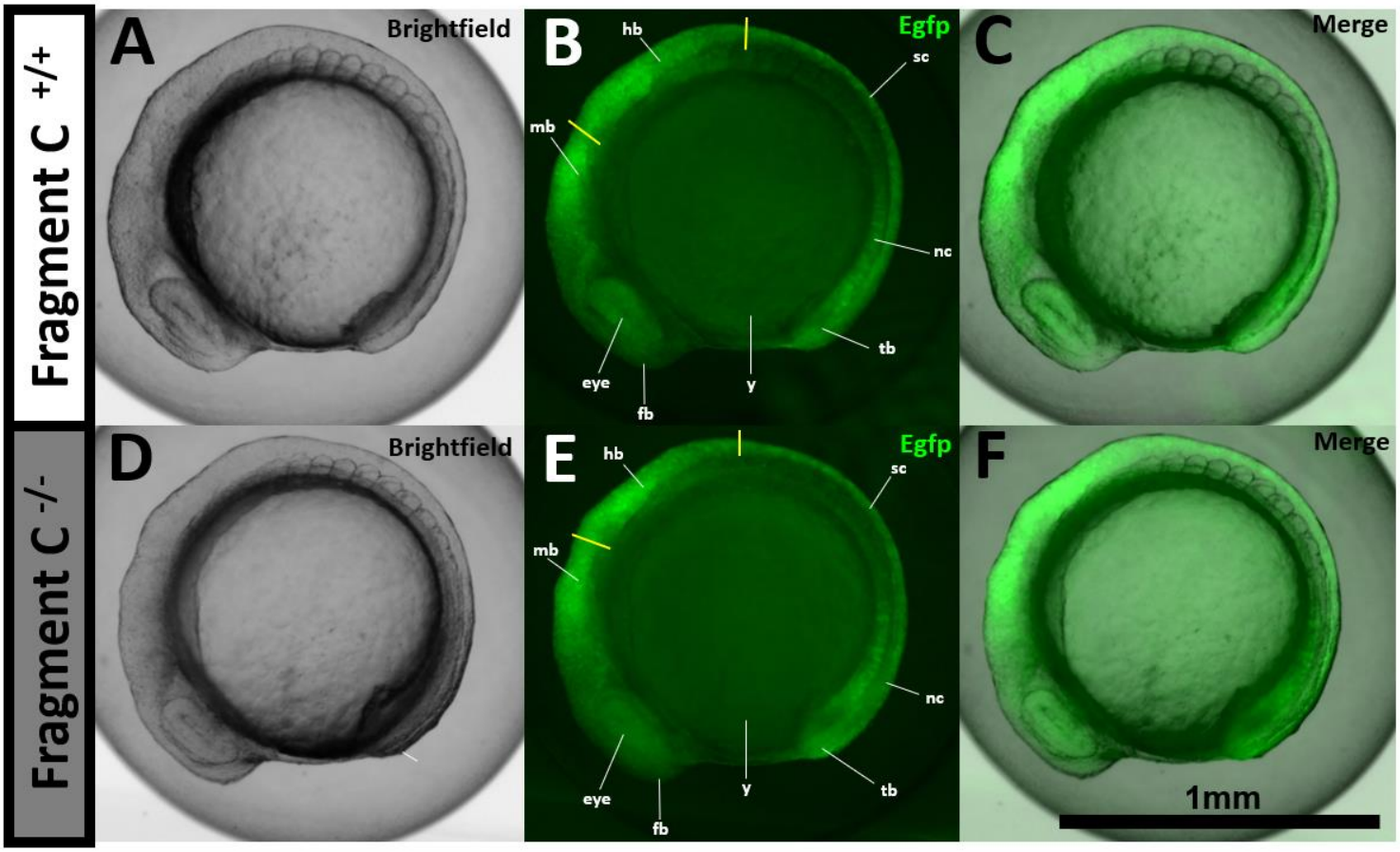

Figure 3.9. Fragment C-driven Egfp expression in zebrafish embryos at 14hpf. Embryos from a cross of *Tg(Fragment C-βG:Egfp)ot1;Fragment C*$^{+/-}$ siblings. Anterior is left, posterior is right. **A, D.** brightfield images of 14hpf Fragment C$^{+/+}$ (**A**), and Fragment C$^{-/-}$ (**D**) embryos. **B, E.** Epifluorescence images of 14hpf Fragment C$^{+/+}$ (**B**), and Fragment C$^{-/-}$ embryos (**E**). **C.** merge of **A** and **B**. **F.** Merge of **D** and **E**. Scale bar (black line, bottom right) represents a length of 1mm. Yellow lines indicate the midbrain-hindbrain boundary and boundary of the hindbrain and presumptive spinal cord. fb = forebrain. mb = midbrain. hb = hindbrain. sc = presumptive spinal cord. nc = notochord. tb = tailbud. y = yolk sac.

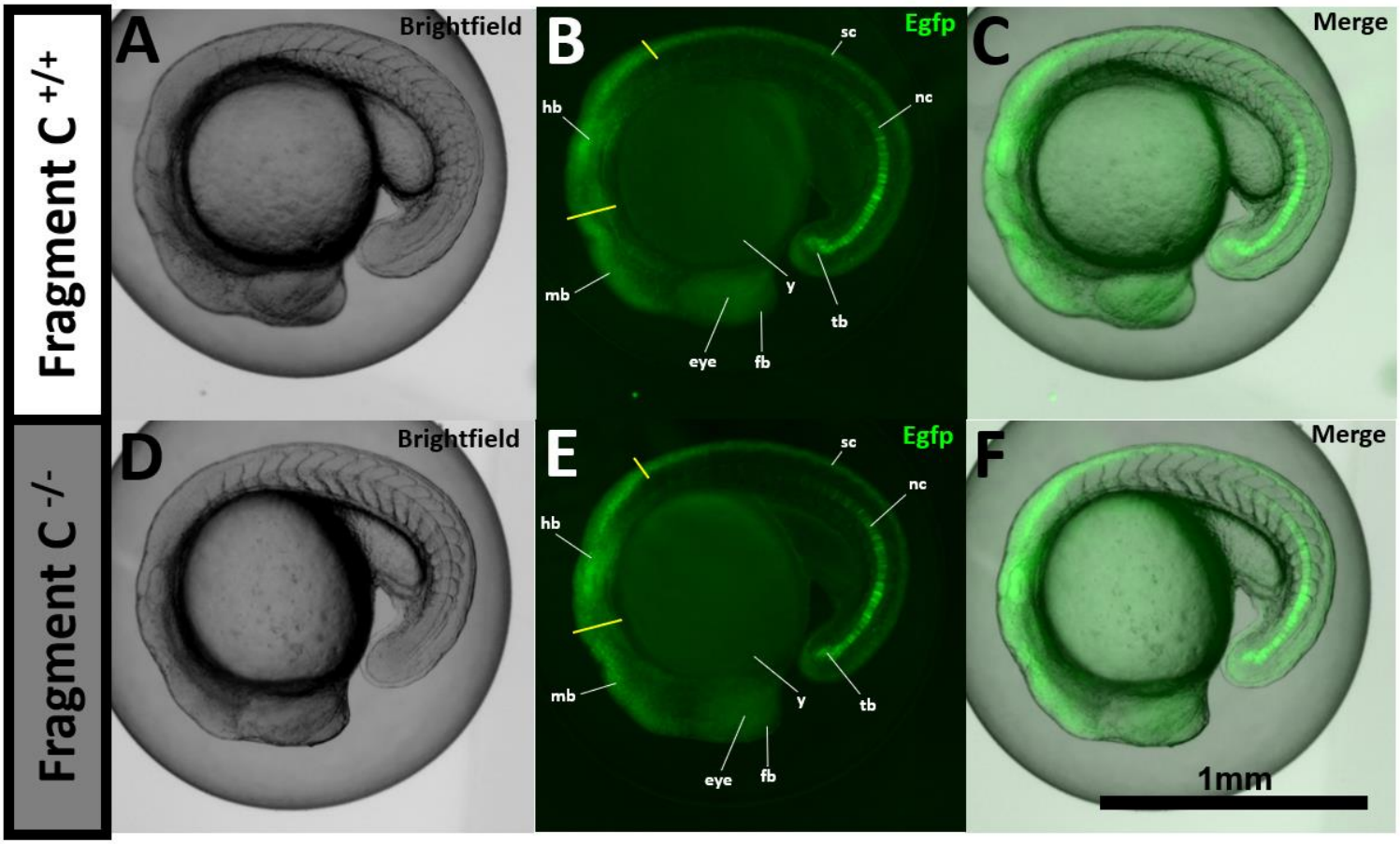

Figure 3.10. Fragment C-driven Egfp expression in zebrafish embryos at 19hpf. Embryos from a cross of *Tg(Fragment C-βG:Egfp)ot1;Fragment C*$^{+/-}$ siblings. Anterior is left, posterior is right. **A, D.** brightfield images of 14hpf Fragment C$^{+/+}$ (**A**), and Fragment C$^{-/-}$ (**D**) embryos. **B, E.** Epifluorescence images of 14hpf Fragment C$^{+/+}$ (**B**), and Fragment C$^{-/-}$ embryos (**E**). **C.** merge of **A** and **B**. **F.** Merge of **D** and **E**. Scale bar (black line, bottom right) represents a length of 1mm. Yellow lines indicate the midbrain-hindbrain boundary and boundary of the hindbrain and presumptive spinal cord. fb = forebrain. mb = midbrain. hb = hindbrain. sc = presumptive spinal cord. nc = notochord. tb = tailbud. y = yolk sac.

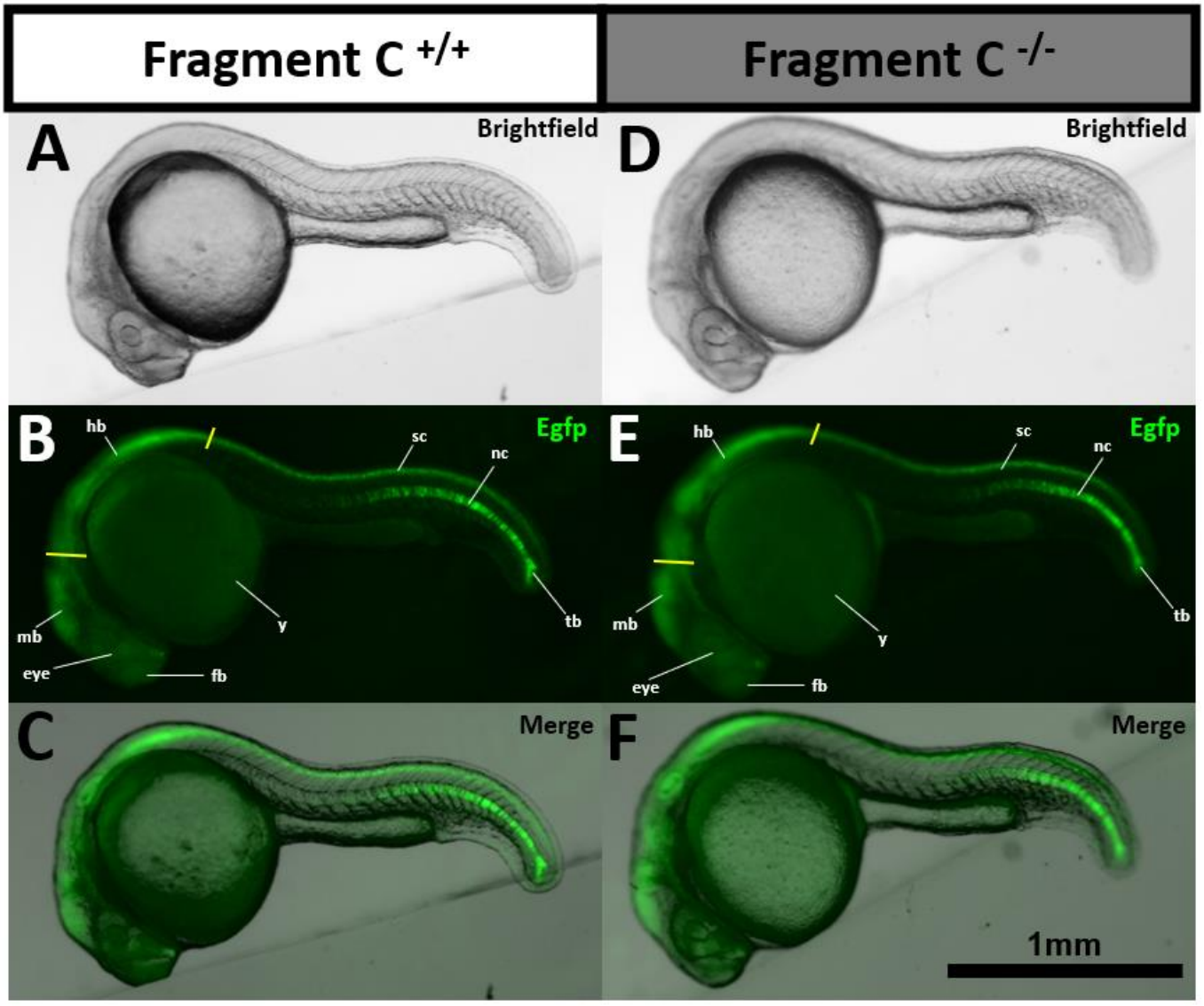

Figure 3.11. Fragment C-driven Egfp expression in zebrafish embryos at 24hpf. Embryos from a cross of *Tg(Fragment C-βG:Egfp)ot1;Fragment C*$^{+/-}$ siblings. Anterior is left, posterior is right. **A, D.** brightfield images of 14hpf Fragment C$^{+/+}$ (**A**), and Fragment C$^{-/-}$ (**D**) embryos. **B, E.** Epifluorescence images of 14hpf Fragment C$^{+/+}$ (**B**), and Fragment C$^{-/-}$ embryos (**E**). **C.** merge of **A** and **B**. **F.** Merge of **D** and **E**. Scale bar (black line, bottom right) represents a length of 1mm. Yellow lines indicate the midbrain-hindbrain boundary and boundary of the hindbrain and presumptive spinal cord. fb = forebrain. mb = midbrain. hb = hindbrain. sc = presumptive spinal cord. nc = notochord. tb = tailbud. y = yolk sac.

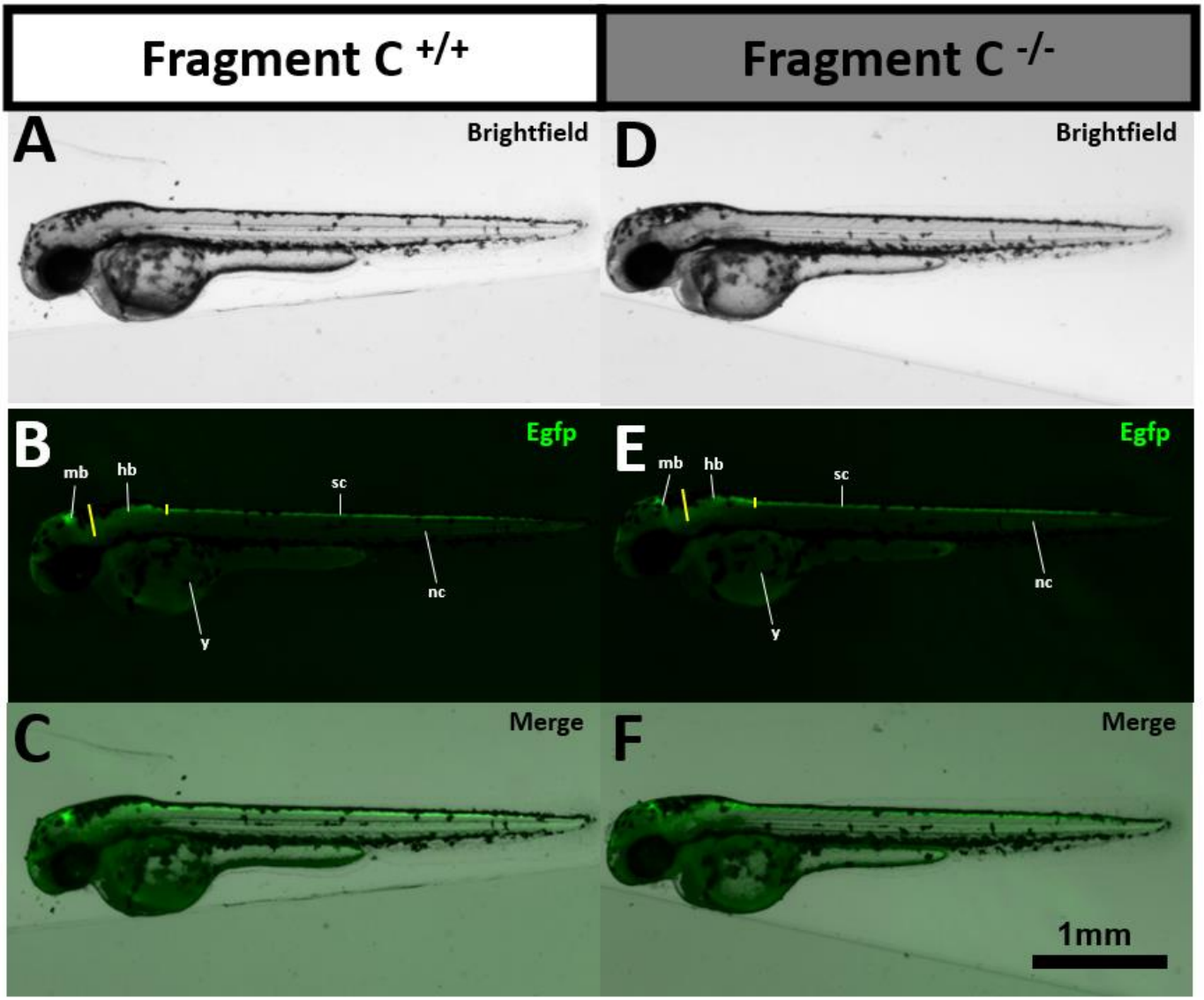

Figure 3.12. Fragment C-driven Egfp expression in zebrafish embryos at 48hpf. Embryos from a cross of *Tg(Fragment C-βG:Egfp)ot1;Fragment C*$^{+/-}$ siblings. Anterior is left, posterior is right. **A, D.** brightfield images of 14hpf Fragment C$^{+/+}$ (**A**), and Fragment C$^{-/-}$ (**D**) embryos. **B, E.** Epifluorescence images of 14hpf Fragment C$^{+/+}$ (**B**), and Fragment C$^{-/-}$ embryos (**E**). **C.** merge of **A** and **B**. **F.** Merge of **D** and **E**. Scale bar (black line, bottom right) represents a length of 1mm. Yellow lines indicate the midbrain-hindbrain boundary and boundary of the hindbrain and presumptive spinal cord. mb = midbrain. hb = hindbrain. sc = presumptive spinal cord. nc = notochord. y = yolk sac.

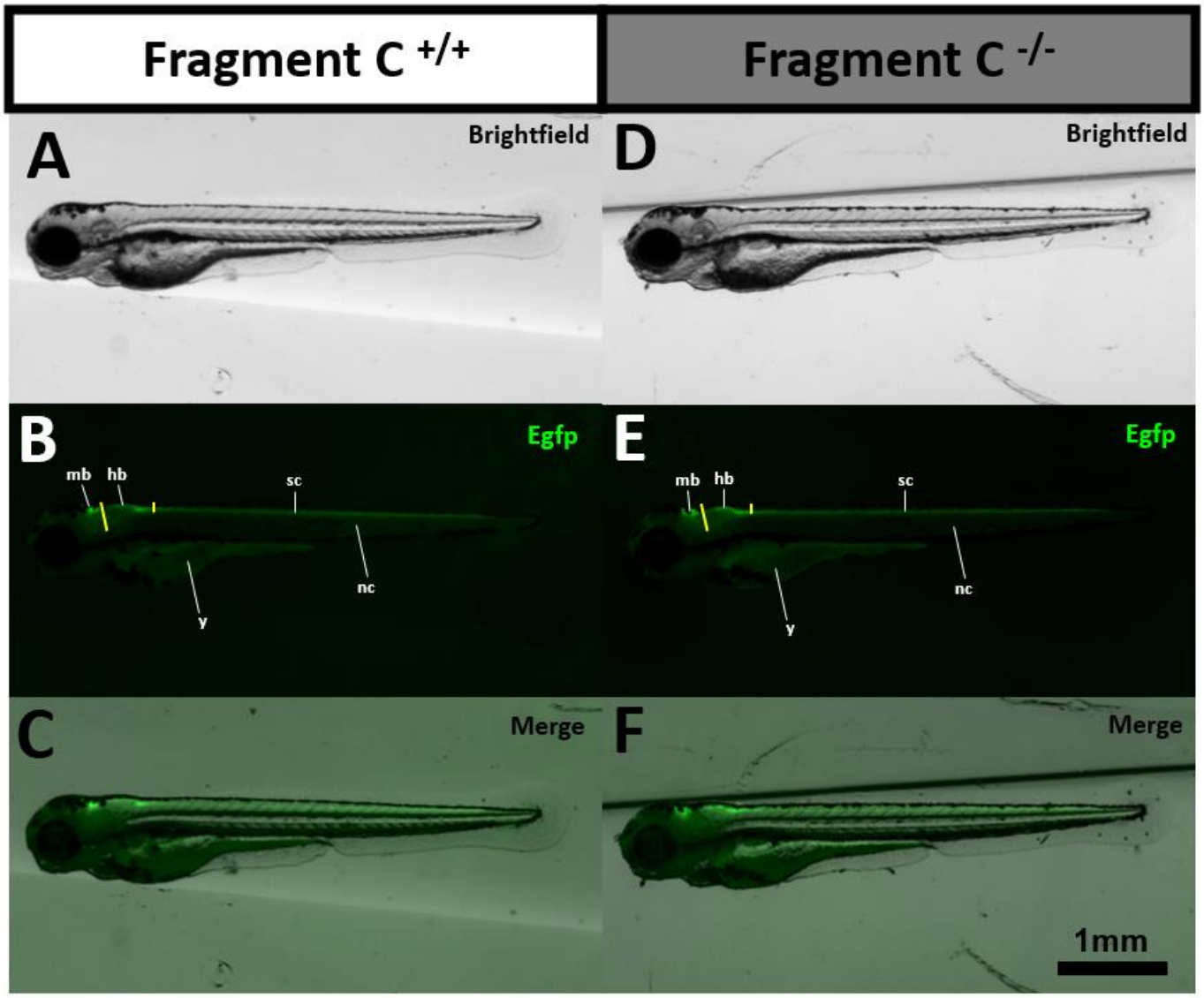

Figure 3.13. Fragment C-driven Egfp expression in zebrafish embryos at 72hpf. Embryos from a cross of *Tg(Fragment C-βG:Egfp)ot1;Fragment C*$^{+/-}$ siblings. Anterior is left, posterior is right. **A, D.** brightfield images of 14hpf Fragment C$^{+/+}$ (**A**), and Fragment C$^{-/-}$ (**D**) embryos. **B, E.** Epifluorescence images of 14hpf Fragment C$^{+/+}$ (**B**), and Fragment C$^{-/-}$ embryos (**E**). **C.** merge of **A** and **B**. **F.** Merge of **D** and **E**. Scale bar (black line, bottom right) represents a length of 1mm. Yellow lines indicate the midbrain-hindbrain boundary and boundary of the hindbrain and presumptive spinal cord. mb = midbrain. hb = hindbrain. sc = presumptive spinal cord. nc = notochord. y = yolk sac.

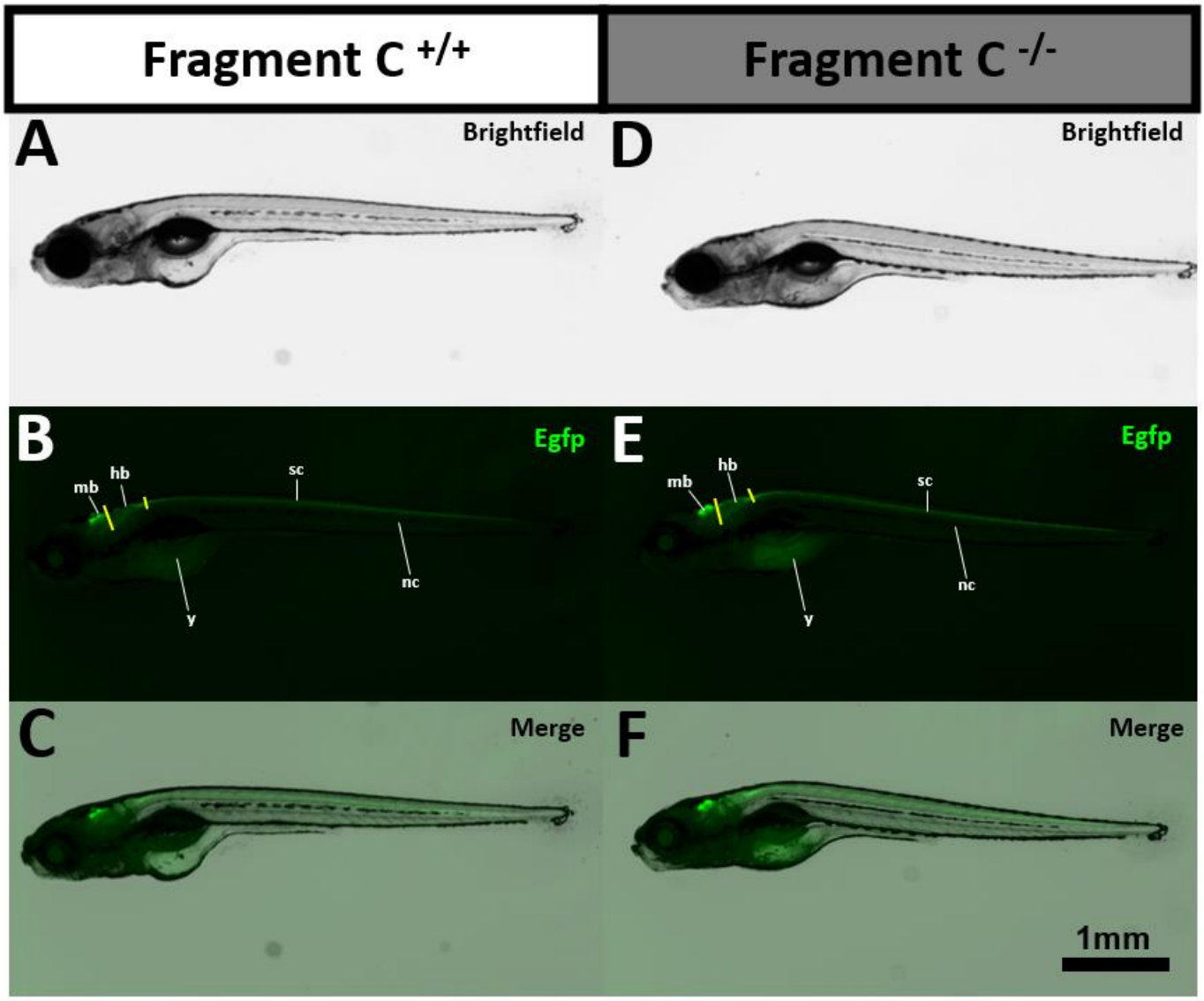

Figure 3.14. Fragment C-driven Egfp expression in zebrafish embryos at 7dpf. Embryos from a cross of *Tg(Fragment C-βG:Egfp)ot1;Fragment C*$^{+/-}$ siblings. Anterior is left, posterior is right. **A, D.** brightfield images of 14hpf Fragment C$^{+/+}$ (**A**), and Fragment C$^{-/-}$ (**D**) embryos. **B, E.** Epifluorescence images of 14hpf Fragment C$^{+/+}$ (**B**), and Fragment C$^{-/-}$ embryos (**E**). **C.** merge of **A** and **B**. **F.** Merge of **D** and **E**. Scale bar (black line, bottom right) represents a length of 1mm. Yellow lines indicate the midbrain-hindbrain boundary and boundary of the hindbrain and presumptive spinal cord. mb = midbrain. hb = hindbrain. sc = presumptive spinal cord. nc = notochord. y = yolk sac.

3.4 Loss of Fragment C results in loss of *msx3* expression in dorsal cells of the neural tube

We hypothesize that Fragment C contains an enhancer of *msx3* due to its upstream proximity to the *msx3* gene (**Figure 1.3**), and its ability to drive reporter Egfp expression (**Figure 3.6 – 3.14**) in the dorsal neural tube similar to that of *msx3* (see **Figure 3.17B,C**). While no overt differences in Egfp fluorescence were observed between Fragment $C^{+/+}$ and Fragment $C^{-/-}$ zebrafish, we tested if the loss of Fragment C results in a loss of *msx3* expression in the dorsal neural tube. Whole mount fluorescent *in situ* hybridization with antisense RNA probes for *msx3* and *egfp* was performed on 24hpf Fragment $C^{-/-}$ embryos and their wild-type siblings (**Figure 3.15**). Consistent with the time course of Egfp fluorescence, there was no difference in the domain of *egfp* expression between Fragment $C^{+/+}$ and Fragment $C^{-/-}$ embryos. Both genotypes showed *egfp* expression in the dorsal third of the neural tube excluding the dorsal-most row of cells, and in the posterior notochord (**Figure. 3.15B, E)**. In both Fragment $C^{+/+}$ and Fragment $C^{-/-}$ embryos, *msx3* expression was observed in the pronephric duct, proctodeum, median fin fold, and enveloping layer around the yolk extension **(Figure 3.15A, D).**

To better visualize the expression domains of *msx3* and *egfp* in the neural tube, higher magnification lateral images were taken of the neural tube at the level of the yolk extension (**Figure 3.16).** Furthermore, to observe both the dorso-ventral and medio-lateral spatial distribution of *msx3* and *egfp* expression in the neural tube, ImageJ was used to orthogonally reslice z-stacks from lateral to transverse sections of the neural tube at the level of the yolk extension (**Figure 3.17**). *msx3* expression is observed in the dorsal-most row of cells of the neural tube (where roof plate cells typically reside) in both Fragment $C^{+/+}$ and Fragment $C^{-/-}$ embryos (**Figure 3.16A,E**, red arrowheads) but in Fragment $C^{-/-}$ embryos, there is a loss of *msx3*

expression in more ventral cells of the dorsal neural tube in comparison with Fragment $C^{+/+}$ embryos (**Figure 3.16A,E**, yellow and green arrowheads to denote both *msx3* and *egfp* expression and *egfp* expression alone, respectively). The dorsal *msx3* expression in the neural tube that persists after loss of the Fragment C enhancer does not colocalize with *egfp* (**Figure 3.17G-J,** *msx3* and *egfp* expression are bounded by a red and green trace, respectively), while the more ventral *msx3* expression observed in Fragment $C^{+/+}$ embryos but not Fragment $C^{-/-}$ embryos colocalizes with *egfp* expression. (**Figure 3.17B-E**). To quantify where *msx3* expression is lost in the Fragment $C^{-/-}$ neural tube, the ventral boundary of *msx3* expression was measured from the resliced z-stacks with transverse orientation for both Fragment C deletion mutants and their wildtype siblings (**Figure 3.18**). The ventral boundary was measured starting from the dorsal-most point of the neural tube, and the entire length of the neural tube was measured along the dorsoventral axis. The fraction of the neural tube from the dorsal-most point that expresses *msx3* relative to the entire neural tube length was calculated from seven Fragment $C^{+/+}$ embryos and six Fragment $C^{-/-}$ embryos, with three sections measured per embryo. For Fragment $C^{+/+}$ embryos, *msx3* is expressed in the dorsal 21.95 ± 2.33% of the neural tube (mean ± sample standard deviation), while for Fragment $C^{-/-}$ embryos, *msx3* is expressed in the dorsal 6.81 ± 1.41% of the neural tube (mean ± sample standard deviation). These results support the conclusion that the Fragment C deletion abolishes m*sx3* expression in the dorsal neural tube except for in the dorsal-most cells.

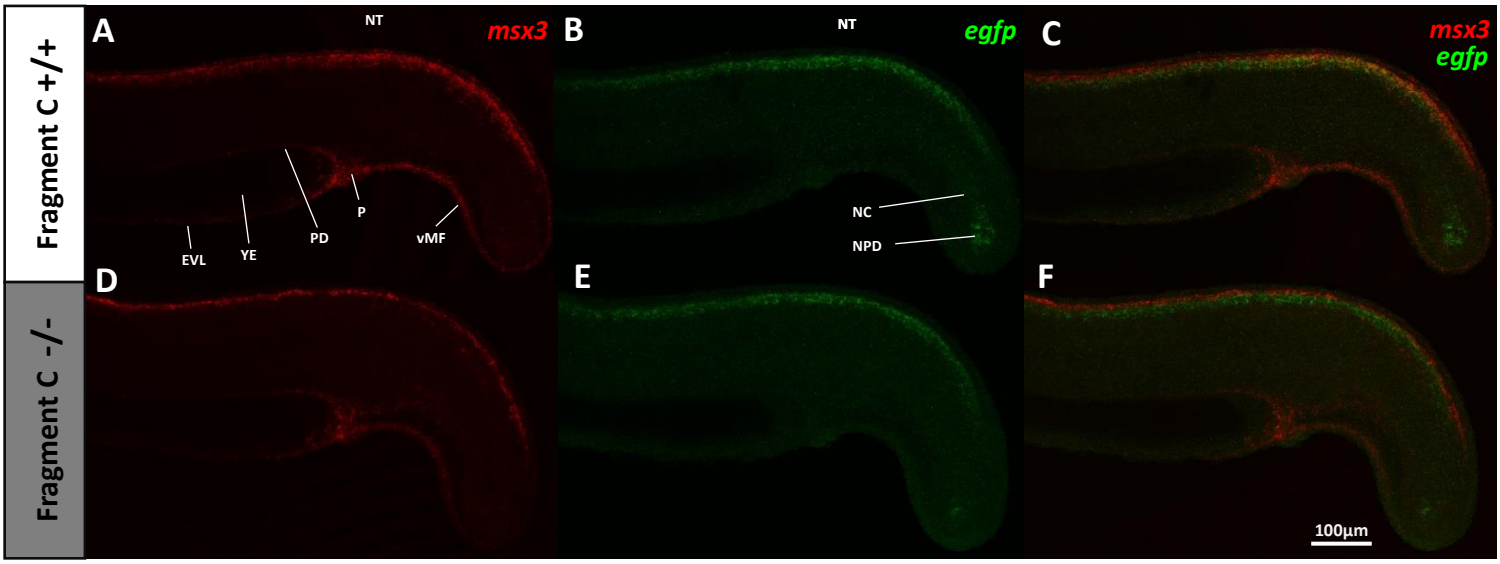

Figure 3.15. *msx3* and *egfp* mRNA expression in trunk and tail of wild-type and Fragment C deletion mutants at 24hpf. Whole-mount double fluorescent *in situ* hybridization with antisense RNA probes for *msx3* and *egfp* was performed on 24hpf offspring of a cross between *Tg(Fragment C-βG:Egfp)ot1;Fragment C*$^{+/-}$ (heterozygous) siblings. 11 Fragment C $^{+/+}$ (wild-type sibling) and 11 Fragment C $^{-/-}$ (homozygous mutant) embryos were imaged. **A-C.** representative image of the Fragment C $^{+/+}$ expression profile of *msx3* and *egfp* in the trunk and tail. **D-F.** representative image of the Fragment C $^{-/-}$ expression profile of *msx3* and *egfp* in the trunk and tail. *msx3* expression in red, *egfp* expression in green. Red arrowheads indicate *msx3* expression in the dorsal-most cells of the neural tube, which is not affect by the deletion of Fragment C. Yellow arrowheads indicate *msx3* expression that overlaps with *egfp* expression and is abolished in mutants. Scale bar (bottom right, white line) represents a length of 100 µm. Anterior toward left of images, dorsal toward top of images. EVL: enveloping layer. YE: yolk extension. PD: pronephric duct. P: proctodeum. dMF and vMF: dorsal and ventral median fin fold, respectively. NT: neural tube. NC: notochord. NPD: notochord progenitor domain.

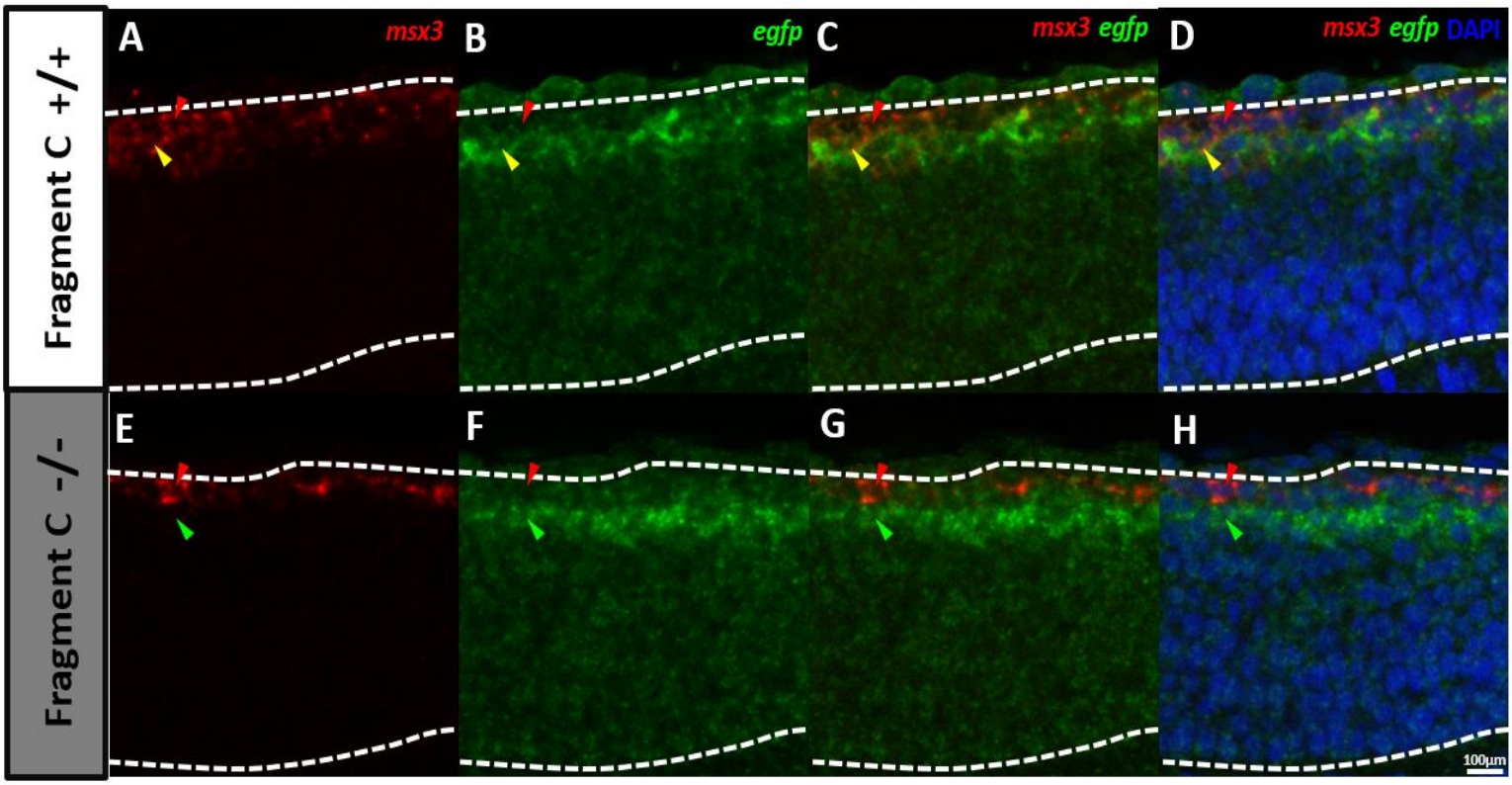

Figure 3.16. Lateral view of *msx3* and *egfp* mRNA expression in the neural tube of wild-type and Fragment C deletion mutants at 24hpf. Whole-mount double fluorescent *in situ* hybridization with antisense probes for *msx3* and *egfp* was performed on 24hpf offspring of a cross between *Tg(Fragment C-βG:Egfp)ot1;Fragment C*$^{+/-}$ siblings. 6 Fragment C $^{+/+}$ (wild-type sibling) and 5 Fragment C $^{-/-}$ (homozygous mutant) embryos were imaged at the level of the yolk extension. **A-D.** representative image of the Fragment C $^{+/+}$ expression profile of *msx3* and *egfp* in the neural tube. **E-H.** representative image of the Fragment C $^{-/-}$ expression profile of *msx3* and *egfp* in the neural tube. *msx3* expression in red, *egfp* expression in green, DAPI stain (which labels cell nuclei) in blue. The dorsal-most row of neural tube cells expresses *msx3* but not *egfp*, regardless of the Fragment C deletion genotype (red arrowheads). Excluding these cells, cells in the dorsal third of the neural tube express both *msx3* and *egfp* in Fragment C$^{+/+}$ embryos (yellow arrowheads), but only *egfp* in Fragment C$^{-/-}$ mutants (green arrowheads). Scale bar (bottom right, white line) represents a length of 100 µm. Anterior toward left of images, dorsal toward top of images. Dorsal and ventral limits of the neural tube are outlined by a white dashed line.

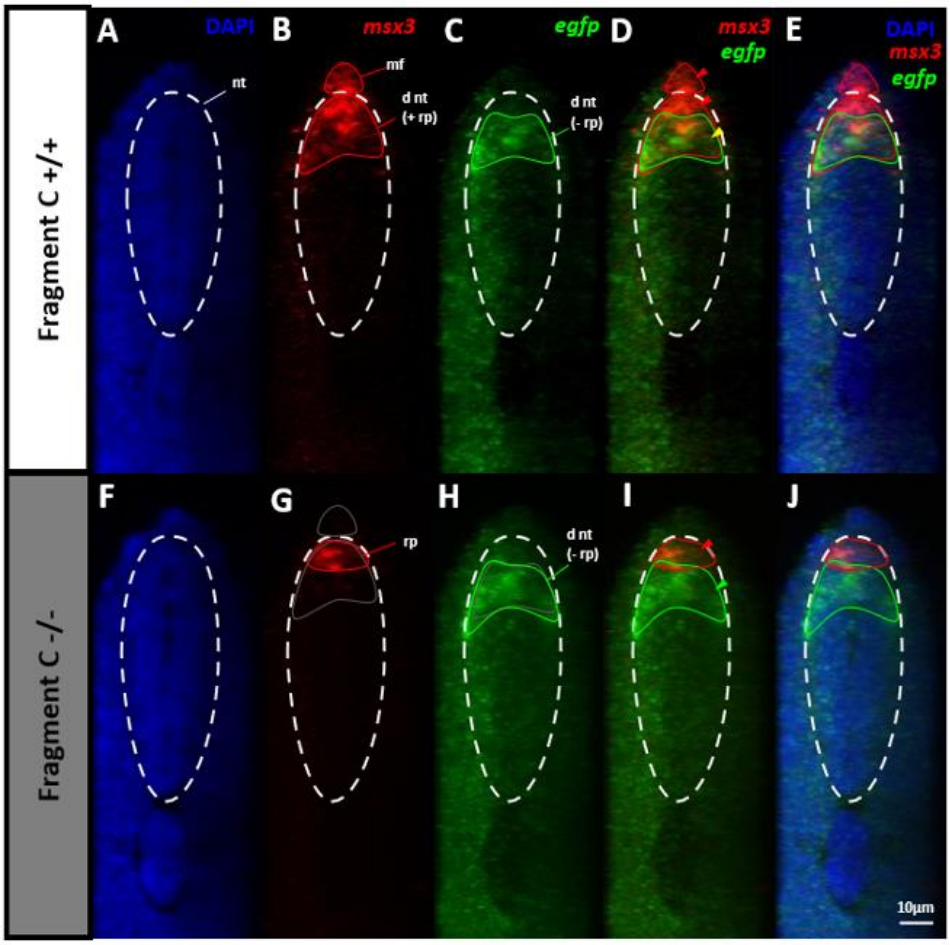

Figure 3.17. transverse view of *msx3* and *egfp* mRNA expression in the neural tube of wild-type and Fragment C deletion mutants at 24hpf. Whole-mount double fluorescent *in situ* hybridization with antisense probes for *msx3* and *egfp* was performed on 24hpf offspring of a cross between *Tg(Fragment C-βG:Egfp)ot1;Fragment C*$^{+/-}$ *siblings.* 11 Fragment C $^{+/+}$ (wild-type sibling) and 11 Fragment C $^{-/-}$ (homozygous mutant) embryos were imaged. ImageJ was used to orthogonally reslice z-stacks from sagittal to transverse, and maximum-intensity projections spanning 20µm along the anterior-posterior axis were created at the level of the yolk extension. **A-E.** Fragment C$^{+/+}$ expression profile of *msx3* and *egfp* in the neural tube with DAPI labelling cell nuclei. **F-J.** Fragment C$^{-/-}$ expression profile of *msx3* and *egfp* in the neural tube with DAPI labelling cell nuclei. Expression domain boundaries are traced (*msx3* traced in red, *egfp* traced in green). Expression boundaries of Fragment C$^{+/+}$ embryos are traced in gray over Fragment C$^{-/-}$ images for comparison. Red, green, and yellow arrowheads point to cells with *msx3* expression only, *egfp* expression only, or both *msx3* and *egfp* expression, respectively. *msx3* expression is lost in the expression domain that overlaps with *egfp* expression (yellow and green arrows in Fragment C$^{+/+}$ and Fragment C$^{-/-}$ embryos, respectively). Scale bar (bottom right, white line) represents a length of 10µm. Dorsal toward top of image, medial toward centre of horizontal axis of image. White dashed line marks the outer border of the neural tube. nt: neural tube. d nt: dorsal neural tube. rp: roof plate. mf: median fin fold.

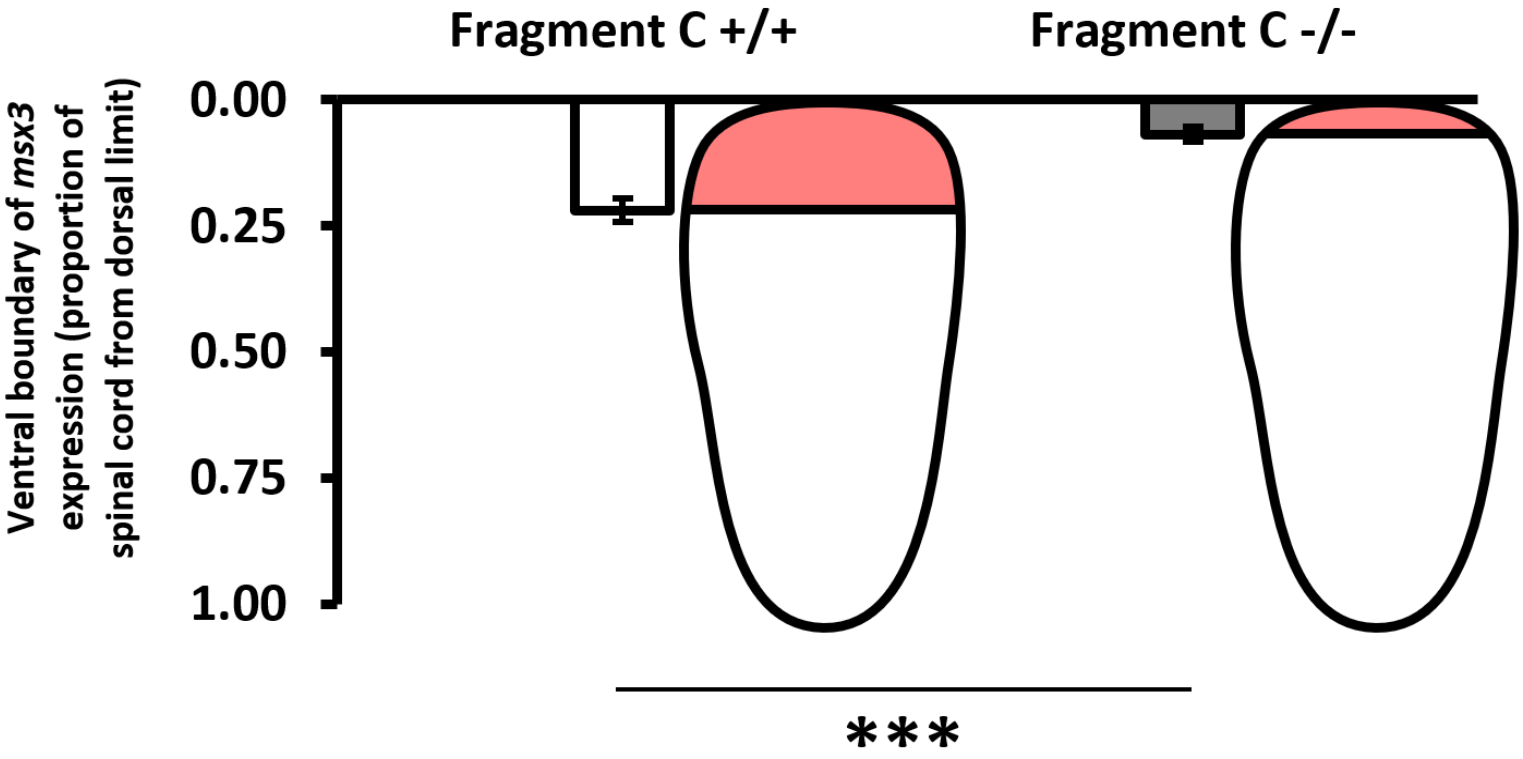

Figure 3.18. Ventral boundary of msx3 expression in 24hpf wildtype and Fragment C deletion mutants. Whole-mount double fluorescent *in situ* hybridization with antisense probes for *msx3* and *egfp* was performed on 24hpf offspring of a cross between *Tg(Fragment C-βG:Egfp)ot1;Fragment C*$^{+/-}$ siblings. ImageJ was used to orthogonally re-slice z-stacks from sagittal to transverse. Transverse z-stacks represent 20µm, and images at the level of the yolk extension were used for measurements. DAPI staining was used to measure the dorso-ventral length of the neural tube, and the ventral boundary of *msx3* expression within the neural tube was measured from the dorsal-most point of the neural tube. the ventral boundary of *msx3* expression is expressed as a proportion of entire dorsoventral length of the spinal cord (from the dorsal-most point). Each value counted toward the number of samples is the mean ventral boundary of *msx3* expression from 3 z-stacks per embryo, with 7 and 6 wildtype and homozygous mutant embryos used for measurements, respectively. Height of bars represent the average ventral boundary of *msx3* expression as a fraction of the entire length of the neural tube. Error bars are ± sample standard deviation. A two-tailed student's t-test was used to compare embryos with no deletion of Fragment C (Fragment C$^{+/+}$) and homozygous deletion of Fragment C (Fragment C$^{-/-}$). *** = $p < 0.0001$

3.5 Loss of the Fragment C enhancer does not alter the size of or number of cells in the neural tube

To examine the morphological effects of the loss of Fragment C on the neural tube, we first assessed if the size of the neural tube or number of cells in the neural tube were altered in Fragment $C^{-/-}$ fish. Embryos (referred to as larvae onwards of hatching from the chorion at around 2.5dpf) were fixed at 1.5dpf and 3dpf and sectioned into 10µm sections at the level of the yolk extension. Immunohistochemistry with antibodies for Gfp (which recognizes the Egfp protein) and either Elavl3/4 or Sox2 (to label nascent neurons and neural progenitors, respectively) was performed, and a DAPI stain (to visualize DNA in the nucleus of cells (Tarnowski et al., 1991)) was applied to the sections. The total number of DAPI-stained nuclei was counted for each section, with three sections counted per embryo/larva. ImageJ was used to create a trace around the neural tube, and the cross-sectional area was calculated from this trace for each section examined.

The mean cross-sectional area of the neural tube ± sample standard deviation was 1382.1 ± 236.7 μm^2 for 1.5dpf Fragment $C^{+/+}$ embryos (N = 11) and 1587.7 ± 288.1 μm^2 for 1.5dpf Fragment $C^{-/-}$ embryos (N = 10), 2305.3 ± 221.5 μm^2 for 3dpf Fragment $C^{+/+}$ embryos (N = 10), and 2296.1 ± 247.6 μm^2 for 3dpf Fragment $C^{-/-}$ embryos (N = 10) **(Figure 3.19)**. At both 1.5dpf and 3dpf, the difference in the cross-sectional area of the neural tube between Fragment $C^{+/+}$ and Fragment $C^{-/-}$ embryos/larvae was not statistically significant (at 1.5dpf, $p = 0.089$, at 3dpf, $p = 0.931$)

The mean number of cells per section of the neural tube ± sample standard deviation was 51.5 ± 5.2 cells for 1.5dpf Fragment $C^{+/+}$ embryos (N = 11) and 54.2 ± 5.8 cells for 1.5dpf Fragment $C^{-/-}$ embryos (N = 10), 64.5 ± 5.0 cells for 3dpf Fragment $C^{+/+}$ embryos (N = 10), and

65.8 ± 4.4 cells for 3dpf Fragment $C^{-/-}$ embryos (N = 10) (**Figure 3.20**). At both 1.5dpf and 3dpf, the difference in the number of cells per section of the neural tube between Fragment $C^{+/+}$ and Fragment $C^{-/-}$ embryos/larvae was not statistically significant (at 1.5dpf, $p = 0.263$, at 3dpf, $p = 0.538$)

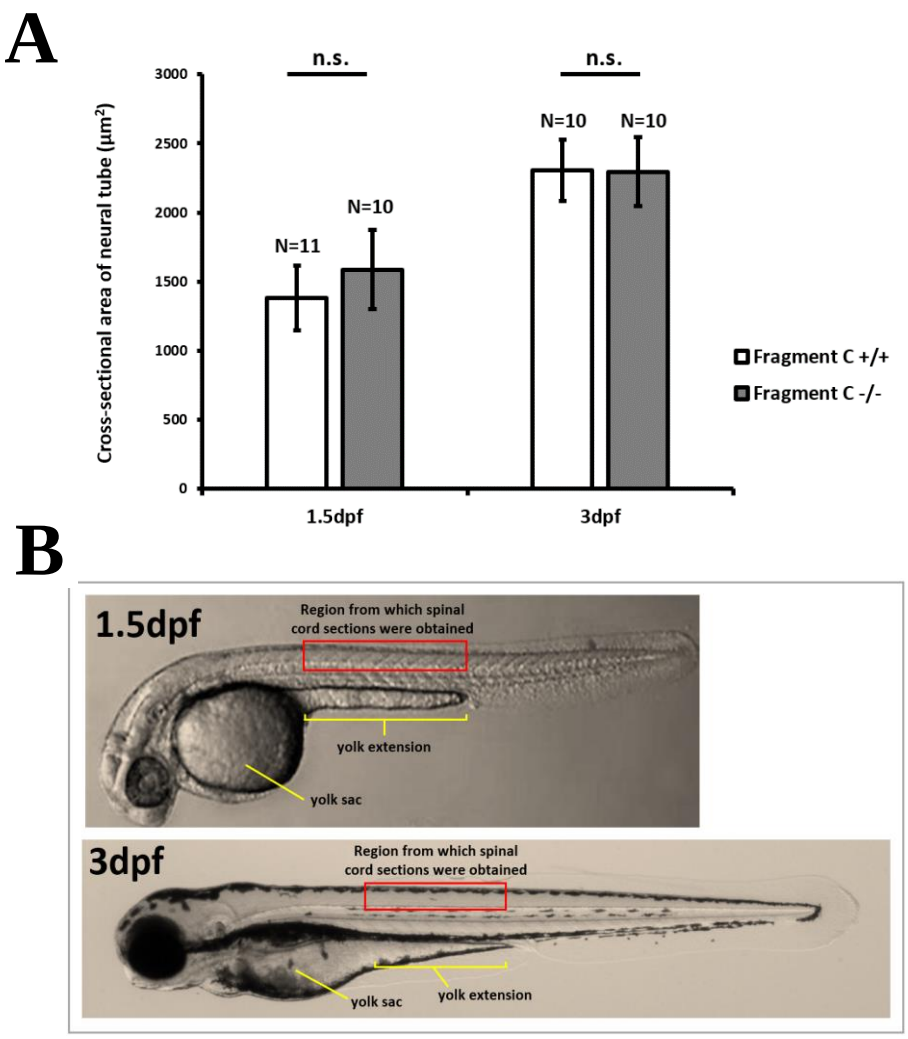

Figure 3.19. Cross-sectional area of the neural tube of wild-type and Fragment C deletion mutants at 1.5df and 3dpf. Immunohistochemistry with antibodies against Gfp (which also labels Egfp) and either Sox2 or Elavl3/4 was performed on 10µm transverse sections at the level of the yolk extension of 1.5dpf and 3dpf offspring of a cross between *Tg(Fragment C-βG:Egfp)ot1;Fragment C*$^{+/-}$ siblings. A combination of images from both Gfp/Elavl3/4 and Gfp/Sox2 immunohistochemistry were used to measure cross-sectional area of the spinal cord for a given genotype and age. The border of the neural tube was demarcated by Gfp antibody staining. Cross-sectional area was measured in ImageJ by tracing a line circling the border of the neural tube. Each value counted toward the number of samples is the mean cross-sectional area from three sections of a single embryo/larvae, with 11 1.5dpf Fragment C$^{+/+}$ embryos and 10 embryos of all other ages/genotypes used for measurements. **A.** Cross-sectional area of the neural tube. Height of bars represent the mean cross-sectional area of the neural tube among all embryos/larvae per genotype and age ± sample standard deviation (error bars). A two-tailed student's t-test was used to compare larvae with no deletion of Fragment C (Fragment C$^{+/+}$) and homozygous deletion of Fragment C (Fragment C$^{-/-}$). Between genotypes at 1.5dpf, p = 0.089, and at 3dpf, p = 0.931. n.s.(not significant) = p > 0.05. **B.** Diagram depicting from where transverse sections of the spinal cord were obtained (red box, corresponding to the anterior-posterior level of the yolk extension).

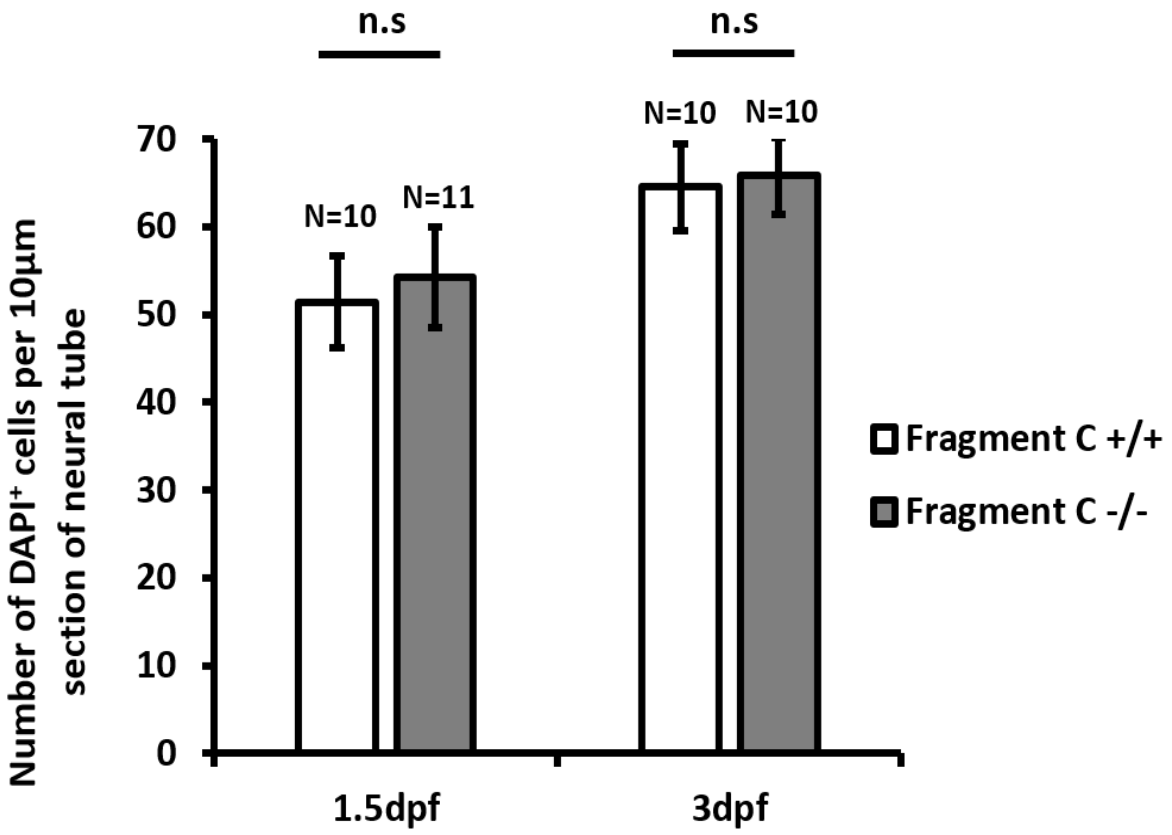

Figure 3.20. Absolute number of cells in the neural tube per 10µm section of wild-type and Fragment C deletion mutants at 1.5dpf and 3dpf. Immunohistochemistry with antibodies against Gfp (which also labels Egfp) and either Elavl3/4 or Sox2 was performed on 10µm transverse sections at the level of the yolk extension of 1.5dpf and 3dpf offspring of a cross between *Tg(Fragment C-βG:Egfp)ot1;Fragment* $C^{+/-}$ siblings. DAPI stain was applied to all sections. Each DAPI-stained nucleus in the neural tube was counted as a cell. Images from both Gfp/Elavl3/4 and Gfp/Sox2 immunohistochemistry were combined toward cell counts. Each value counted toward the number of samples is the mean cell count from 3 sections of a single embryo/larvae, with 11 1.5dpf Fragment $C^{+/+}$ embryos and 10 embryos of all other ages/genotypes used for measurements. Height of bars represent the mean number of DAPI-stained cells among all embryos/larvae per genotype and age ± sample standard deviation (error bars). Two-tailed *Student*'s t-test was used to compare larvae with no deletion of Fragment C (Fragment $C^{+/+}$) and homozygous deletion of Fragment C (Fragment $C^{-/-}$). Between genotypes at 1.5dpf, $p = 0.263$, and at 3dpf, $p = 0.538$. n.s. (not significant) = $p > 0.05$.

3.6 Loss of the Fragment C enhancer slightly reduces the number of Egfp+ cells in the neural tube but does not affect the identity of Egfp+ cells

While no overt changes in Egfp fluorescence were observed in Fragment $C^{-/-}$ embryo/larvae, we wanted to assess if the number and/or identity of $Egfp^{+}$ cells in the neural tube are affected by the loss of Fragment C. To do so, immunohistochemistry with antibodies against Gfp (which recognizes the Egfp protein) and either Elavl3/4 or Sox2 was performed on 10µm transverse sections at the level of the yolk extension of 1.5dpf and 3dpf offspring of a cross between *Tg(Fragment C-βG:Egfp)ot1;Fragment* $C^{+/-}$ siblings. Elavl3/4 labels nascent neurons (Kim et al., 1996), while Sox2 is regarded generally as a marker of neural progenitors (Okuda et al., 2010). In mice, Sox2 has additional roles in several mature neuronal and glial subpopulations of the brain and retina (Kautzman et al., 2018; Bachleda et al., 2016; Cerrato et al., 2018; Cheng et al., 2019; Mercurio et al., 2019; Alqadah et al., 2015) and oligodendrocyte maturation in the spinal cord (Hoffmann et al., 2014; Zhang et al., 2018). However, similar roles for Sox2 have not yet been substantiated in zebrafish. In zebrafish between 24hpf and 72hpf, Sox2 predominantly labels radial glia (and neuroepithelial cells if any remain) in the dorsal neural tube. (Johnson et al., 2016), though not all radial glia will be labelled (especially at 3dpf) as there is an increasing number of $Gfap^{+}/Sox2^{-}$ radial glia that are found in the dorsal neural tube (Johnson et al., 2016).

The presence of strong Gfp antibody staining overlapping with a DAPI-stained nucleus was counted as an $Egfp^{+}$ cell. The mean proportion of $Egfp^{+}$ cells out of the total number of cells per section ± sample standard deviation was 0.221 ± 0.035 for 1.5dpf Fragment $C^{+/+}$ embryos (N

= 11) and 0.188 ± 0.014 for 1.5dpf Fragment $C^{-/-}$ embryos (N = 10), 0.215 ± 0.032 for 3dpf Fragment $C^{+/+}$ embryos (N = 10), and 0.200 ± 0.037 for 3dpf Fragment $C^{-/-}$ embryos (N = 10). (**Figure 3.21**). There was a slight reduction in proportion of $Egfp^{+}$ cells in Fragment $C^{-/-}$ fish compared to Fragment $C^{+/+}$ fish at 1.5dpf (p = 0.013), but there was no statistically significant difference in this proportion at 3dpf (p = 0.322). When comparing the 1.5dpf and 3dpf proportions of $Egfp^{+}$ cells within a given genotype, there was no statistically significant difference (p = 0.7295 between 1.5dpf and 3dpf Fragment $C^{+/+}$ embryos, p = 0.3488 between 1.5dpf and 3dpf Fragment $C^{-/-}$ embryos), implying the number of $Egfp^{+}$ cells remains stable throughout early development.

Images of immunohistochemistry with antibodies against Gfp/Elavl3/4 and Gfp/Sox2 on 10µm sections of the neural tube at the level of the yolk extension are shown in **Figure 3.22** and **Figure 3.23**, respectively. At both 1.5dpf and 3dpf for both Fragment $C^{+/+}$ and Fragment $C^{-/-}$ embryos, there exist $Egfp^{+}$ stain that are positive for Elavl3/4 or Sox2 (examples **Figure 3.22 and 3.23, yellow arrows**) and $Egfp^{+}$ cells that are negative for Sox2 or Elavl3/4 (examples in **Figure 3.22 and 3.23, green arrows**). $Egfp^{+}$ cells are located within approximately the dorsal third of the neural tube, though not all cells within the dorsal third were $Egfp^{+}$(examples in **Figure 3.22 and 3.23, E-I, red arrows**). The $Egfp^{+}$ cells that are also $Elavl3/4^{+}$ represent nascent neurons, while the $Egfp^{+}$ cells that are $Sox2^{+}$ most likely represent neural progenitors. Thus, the $Egfp^{+}$ population of cells contains both nascent neurons and neural progenitors, possibly in addition to mature neurons, $Gfap^{+}/Sox2^{-}$ radial glia, or dorsal oligodendrocytes and their progenitors (which may not be labelled by Sox2 or Elavl3/4).

We next investigated if the proportion of nascent neurons and $Sox2^{+}$ neural progenitors amongst the $Egfp^{+}$ population of cells are affected by the loss of Fragment C. The mean

proportion of Elavl3/4^{+}/Egfp^{+} cells out of total number of Egfp^{+} cells per section ± sample standard deviation was 0.227 ± 0.034 for 1.5dpf Fragment C$^{+/+}$ embryos (N = 5) and 0.255 ± 0.063 for 1.5dpf Fragment C$^{-/-}$ embryos (N = 5), 0.458 ± 0.152 for 3dpf Fragment C$^{+/+}$ embryos (N = 5), and 0.448 ± 0.176 for 3dpf Fragment C$^{-/-}$ embryos (N = 5) (**Figure 3.24**). At both 1.5dpf and 3dpf there was no statistically significant difference in the mean proportion of Elavl3/4^{+}/Egfp^{+} cells out of total number of Egfp^{+} cells (at 1.5dpf, p = 0.415, at 3dpf, p = 0.927). The mean proportion of Sox2^{+}/Egfp^{+} cells out of total number of Egfp^{+} cells per section ± sample standard deviation was 0.756 ± 0.075 for 1.5dpf Fragment C$^{+/+}$ embryos (N = 6) and 0.782 ± 0.079 for 1.5dpf Fragment C$^{-/-}$ embryos (N = 5), 0.339 ± 0.086 for 3dpf Fragment C$^{+/+}$ embryos (N = 5), and 0.298 ± 0.026 for 3dpf Fragment C$^{-/-}$ embryos (N = 5) (**Figure 3.25**). At both 1.5dpf and 3dpf there was no statistically significant difference in the mean proportion of Sox2^{+}/Egfp^{+} cells out of total number of Egfp^{+} cells (at 1.5dpf, p = 0.589, at 3dpf, p = 0.339). Based on these proportions we conclude that the loss of Fragment C does not affect the proportion of nascent neurons nor Sox2^{+} neural progenitors within the population of cells with Fragment C-driven expression.

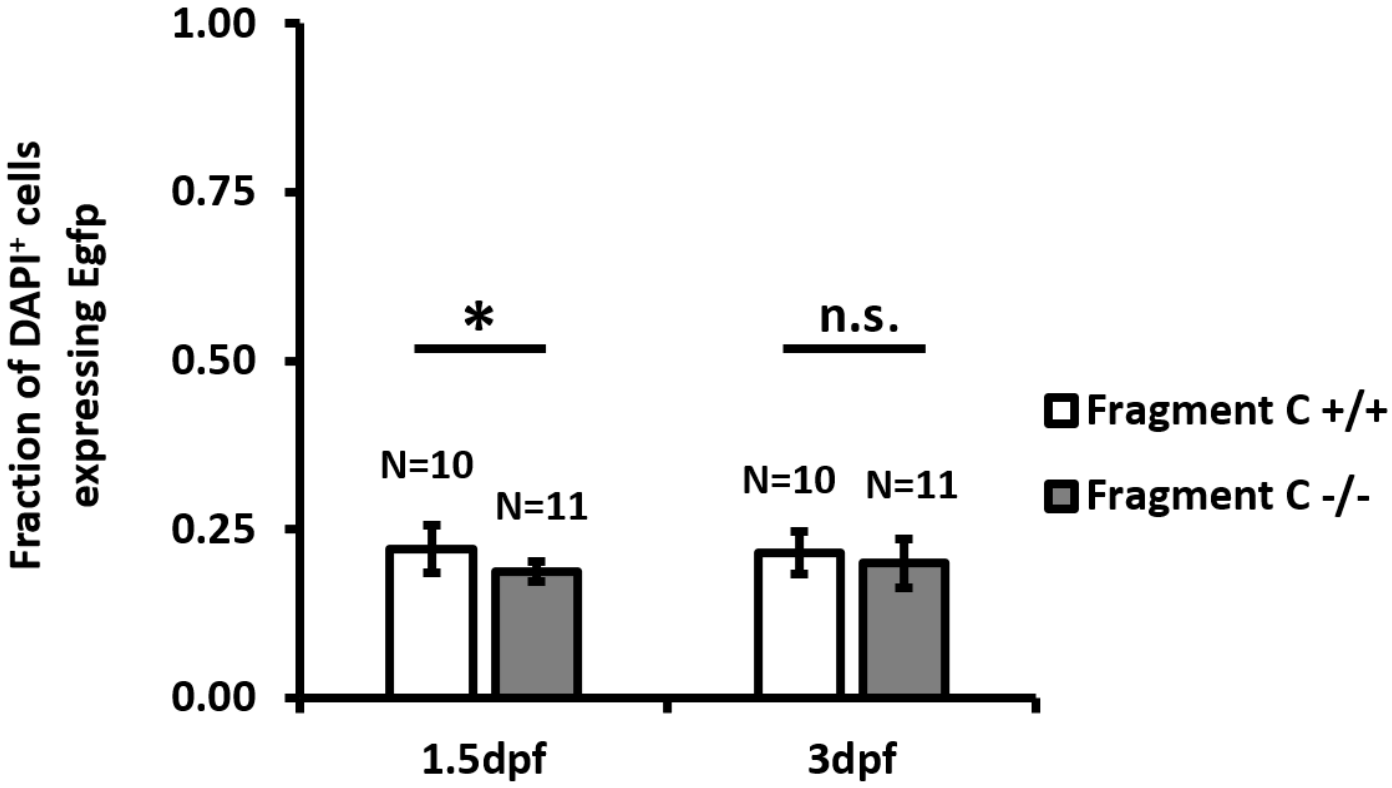

Figure 3.21. Fraction of DAPI^{+} cells expressing Egfp. Immunohistochemistry with antibodies against Gfp (which also recognizes Egfp) and either Elavl3/4 or Sox2 was performed on 10µm transverse sections at the level of the yolk extension of 1.5dpf and 3dpf offspring of a cross between *Tg(Fragment C-βG:Egfp)ot1;Fragment C*$^{+/-}$ siblings. Cells with Alexa-488 labelling within their cell body were counted as Egfp^{+}. Images from both Gfp/Elavl3/4 and Gfp/Sox2 immunohistochemistry were combined toward counts of Egfp^{+} cells. Each value counted toward the number of samples is the mean of cell counts from 3 sections of a single embryo/larvae. Height of bars represent the mean number of Egfp^{+} cells among all embryos/larvae per genotype and age ± sample standard deviation (error bars). Two-tailed *Student*'s t-test was used to compare larvae with no deletion of Fragment C (Fragment C$^{+/+}$) and homozygous deletion of Fragment C (Fragment C$^{-/-}$). Between genotypes at 1.5dpf, $p = 0.013$, and at 3dpf, $p = 0.322$. *n.s.*(not significant) = $p > 0.05$. * = $p < 0.05$

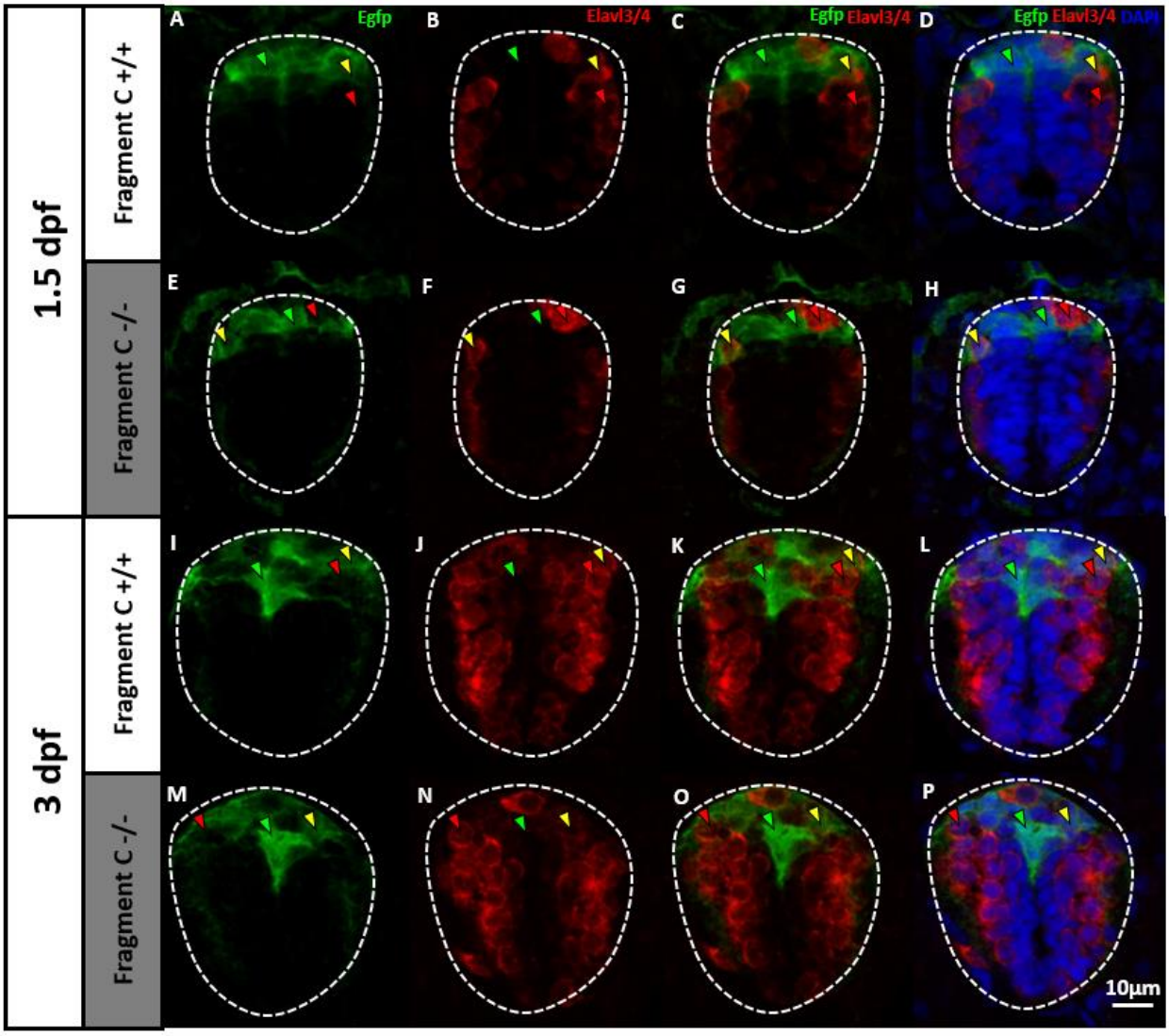

Figure 3.22. Immunohistochemistry for Egfp and Elavl3/4 in embryonic and larval zebrafish neural tube. Immunohistochemistry with antibodies against Gfp (which also labels Egfp) and Elavl3/4 was performed on 10µm transverse sections at the level of the yolk extension of 1.5dpf and 3dpf offspring of a cross between *Tg(Fragment C-βG:Egfp)ot1;Fragment C*$^{+/-}$ siblings. **A-D.** 1.5dpf Fragment C $^{+/+}$. **E-H.** 1.5dpf Fragment C $^{-/-}$. **J-M.** 3dpf Fragment C$^{+/+}$. **N-Q.** 3dpf Fragment C$^{-/-}$. Cells with Alexa-488 labelling within their cell body were counted as Egfp^{+}. Cells with Alexa-588 labelling around DAPI-stained nuclei were counted as Elavl3/4^{+}. White segmented line delineates the neural tube from surrounding tissue. Top of image is dorsal. Green, red, and yellow arrows indicate an example of a Egfp^{+}/Elavl3/4^{-} cell, Egfp^{-}/Elavl3/4^{+} cell, and Egfp^{+}/Elavl3/4^{+} cell, respectively. Scale bar (white line, bottom right) represents a length of 10µm.

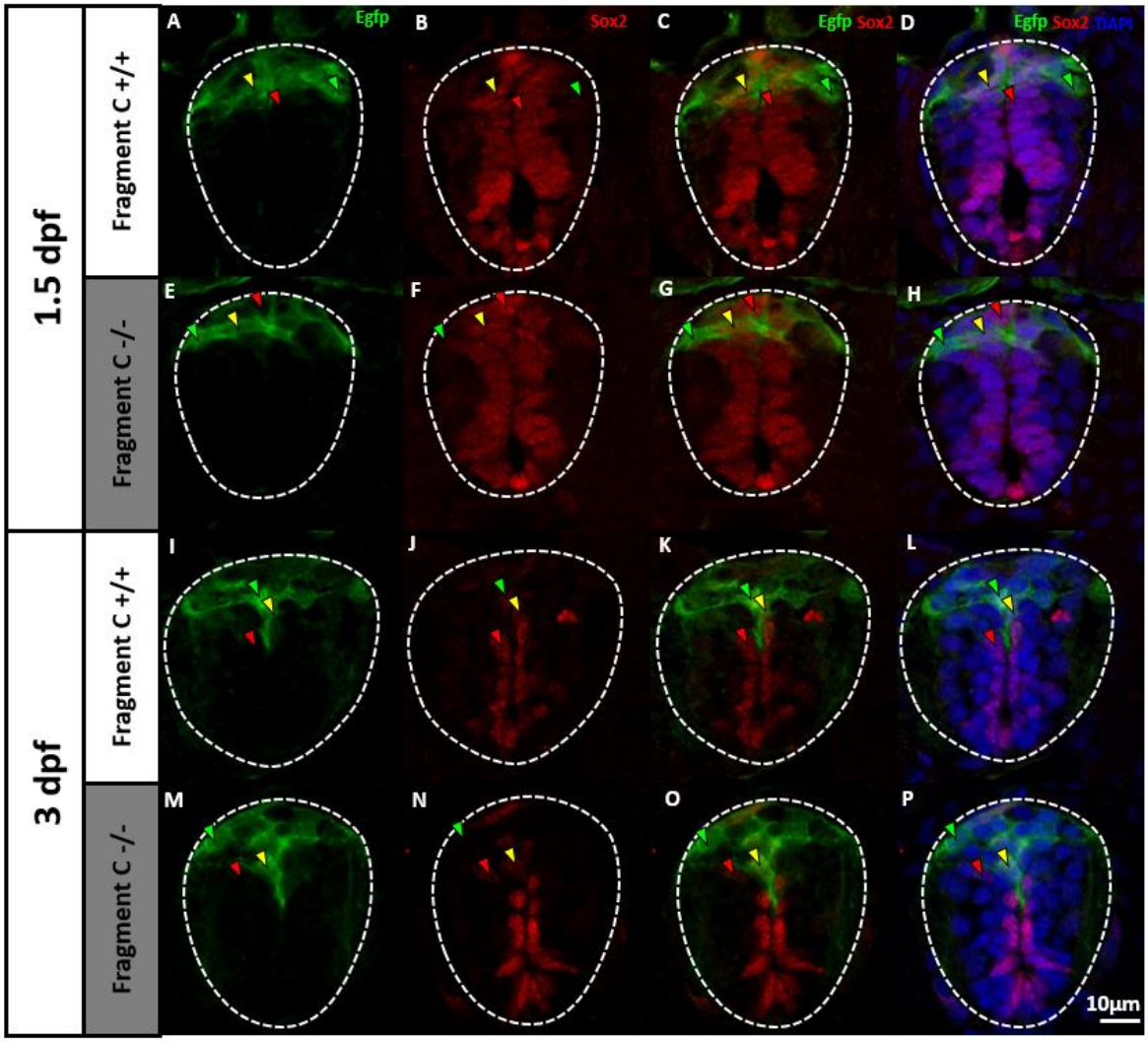

Figure 3.23. Immunohistochemistry for Egfp and Sox2 in embryonic and larval zebrafish neural tube. Immunohistochemistry with antibodies against Gfp (which also labels Egfp) and Sox2 was performed on 10µm transverse sections at the level of the yolk extension of 1.5dpf and 3dpf offspring of a cross between *Tg(Fragment C-βG:Egfp)ot1;Fragment C*$^{+/-}$ siblings. **A-D.** 1.5dpf Fragment C $^{+/+}$. **E-H.** 1.5dpf Fragment C $^{-/-}$. **J-M.** 3dpf Fragment C$^{+/+}$. **N-Q.** 3dpf Fragment C$^{-/-}$. Cells with Alexa-488 labelling within their cell body were counted as Egfp^{+}. Cells with Alexa-588 labelling overlapping with DAPI-stained nuclei were counted as Sox2^{+}.White segmented line delineates the neural tube from surrounding tissue. Top of image is dorsal. Green, red, and yellow arrows indicate an example of a Egfp^{+}/Sox2^{-} cell, Egfp^{-}/Sox2^{+} cell, and Egfp^{+}/Sox2^{+} cell, respectively. Scale bar (white line, bottom right) represents a length of 10µm.

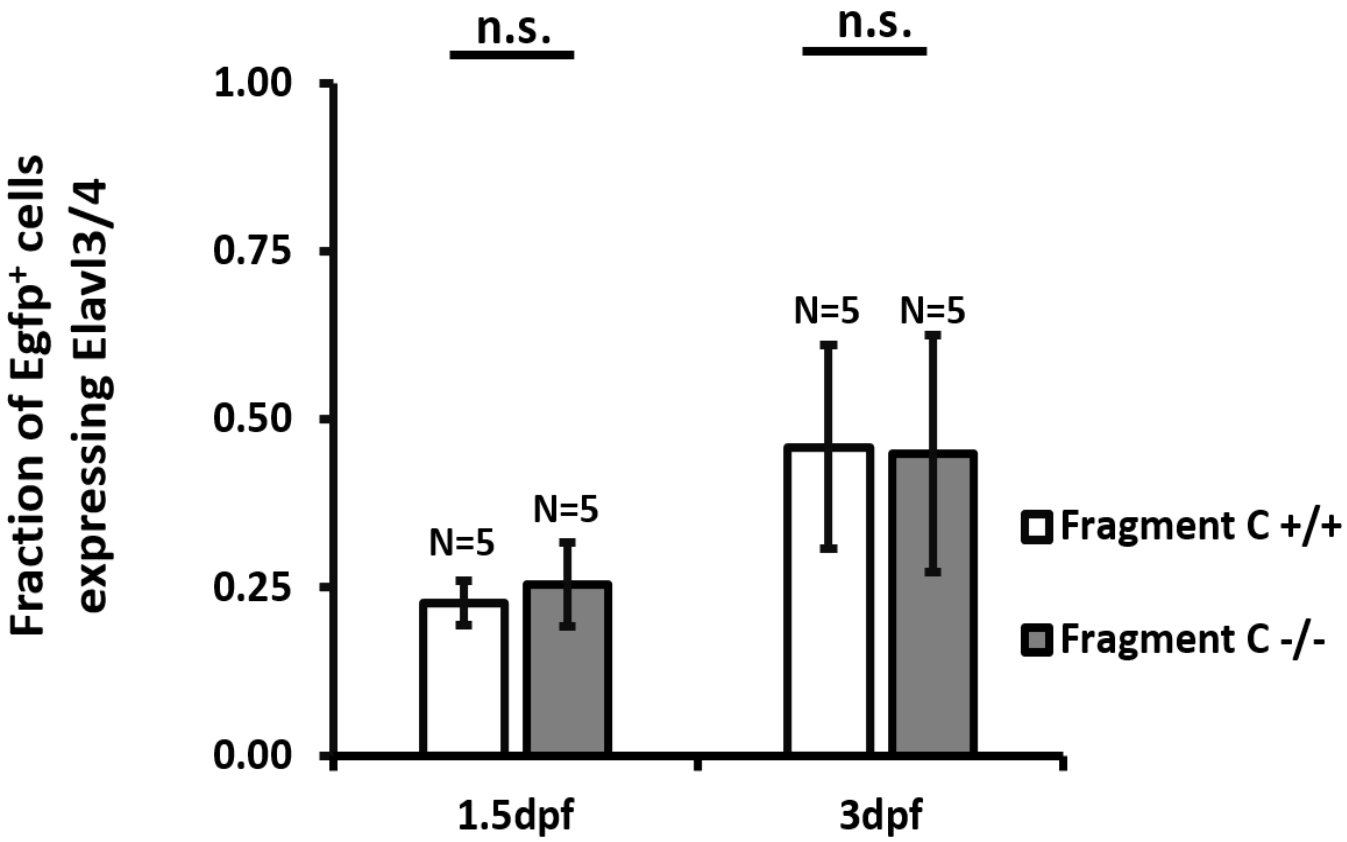

Figure 3.24. Fraction of Egfp^{+} cells expressing Elavl3/4 in wildtype and Fragment C deletion mutants. Immunohistochemistry with antibodies against Gfp (which also labels Egfp) and Elavl3/4 was performed on 10µm transverse sections at the level of the yolk extension of 1.5dpf and 3dpf offspring of a cross between *Tg(Fragment C-βG:Egfp)ot1;Fragment C*$^{+/-}$ siblings. Cells with Alexa-488 labelling within their cell body were counted as Egfp^{+}. Cells with Alexa-588 labelling around DAPI-stained nuclei were counted as Elavl3/4^{+}. Fractions are the number of Egfp^{+}/Elavl3/4^{+} cells as a fraction of the total number of Egfp^{+} cells. Each value counted toward the number of samples is the mean of cell counts from 3 sections of a single embryo/larvae. Height of bars represent the mean number of Egfp^{+}/Elavl3/4^{+} cells as a fraction of the total number of Egfp^{+} cells among all embryos/larvae per genotype and age ± sample standard deviation (error bars). A two-tailed student's t-test was used to compare larvae with no deletion of Fragment C (Fragment C$^{+/+}$) and homozygous deletion of Fragment C (Fragment C$^{-/-}$). Between genotypes at 1.5dpf, $p = 0.415$, and at 3dpf, $p = 0.927$. n.s. (not significant) = $p > 0.05$.

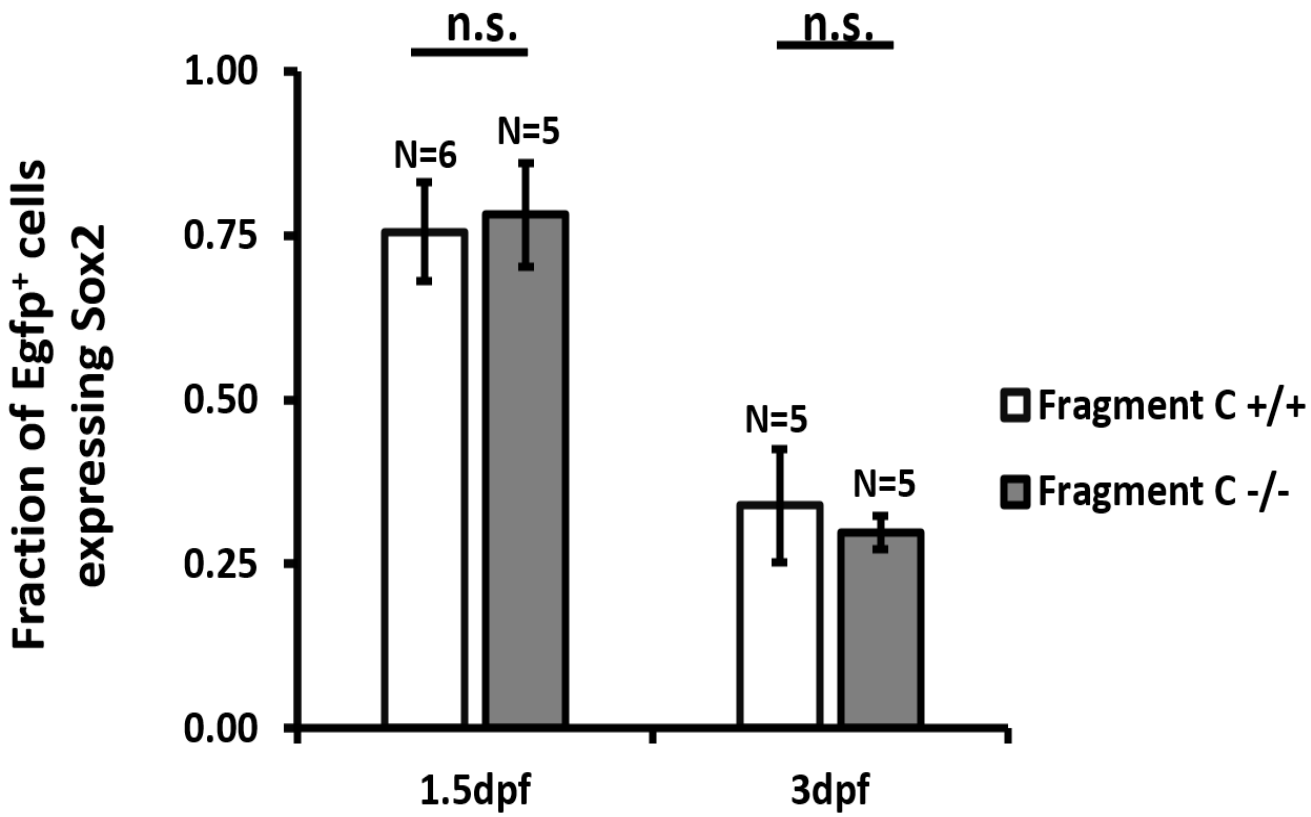

Figure 3.25. Fraction of Egfp$^+$ cells expressing Sox2 in wildtype and Fragment C deletion mutants. Immunohistochemistry with antibodies against Gfp (which also labels Egfp) and Sox2 was performed on 10µm transverse sections at the level of the yolk extension of 1.5dpf and 3dpf offspring of a cross between *Tg(Fragment C-βG:Egfp)ot1;Fragment C*$^{+/-}$ siblings. Cells with Alexa-488 labelling within their cell body were counted as Egfp$^+$. Cells with Alexa-588 labelling overlapping with DAPI-stained nuclei were counted as Sox2$^+$. Fractions are the number of Egfp$^+$/Sox2$^+$ cells as a fraction of the total number of Egfp$^+$ cells. Each value counted toward the number of samples is the mean of cell counts from 3 sections of a single embryo/larvae. Height of bars represent the mean number of Egfp$^+$/Sox2$^+$ cells as a fraction of the total number of Egfp$^+$ cells among all embryos/larvae per genotype and age ± sample standard deviation (error bars). A two-tailed student's t-test was used to compare larvae with no deletion of Fragment C (Fragment C$^{+/+}$) and homozygous deletion of Fragment C (Fragment C$^{-/-}$). Between genotypes at 1.5dpf, $p = 0.589$, and at 3dpf, $p = 0.339$. n.s. (not significant) = $p > 0.05$.

3.7 Loss of the Fragment C enhancer does not affect the spatial domain of Egfp+ cells in the neural tube

As *msx3* is involved in dorsoventral patterning in zebrafish and other vertebrates, we tested if the dorso-ventral domain in which $Egfp^{+}$ cells of the neural tube are found was affected by the loss of Fragment C. In almost all sections examined, the dorsal boundary of Egfp expression in the neural tube was the dorsal limit of the neural tube, and thus the ventral boundary of the $Egfp^{+}$ cell was primarily considered. The distance along the dorso-ventral axis from the dorsal limit of the neural tube to the ventral-most $Egfp^{+}$ cell was measured from sections on which immunohistochemistry was performed with antibodies against Gfp/Sox2 or Gfp/Elavl3/4. This distance was divided by the total dorso-ventral length of the neural tube, and the resulting value represents the proportion of the neural tube where $Egfp^{+}$ cells are found (from the dorsal boundary of the neural tube).

The mean percent coverage of the neural tube by $Egfp^{+}$ cells from the dorsal limit of the neural tube ± sample standard deviation was 0.317 ± 0.027 for 1.5dpf Fragment $C^{+/+}$ embryos (N = 11) and 0.295 ± 0.033 for 1.5dpf Fragment $C^{-/-}$ embryos (N = 10), 0.381 ± 0.077 for 3dpf Fragment $C^{+/+}$ embryos (N = 10), and 0.399 ± 0.071 for 3dpf Fragment $C^{-/-}$ embryos (N = 10) (**Figure 3.26**). At both 1.5dpf and 3dpf there was no statistically significant difference in the mean percent coverage of the neural tube by $Egfp^{+}$ cells from the dorsal limit of the neural tube (at 1.5dpf, $p = 0.106$, at 3dpf, $p = 0.587$). Thus, the spatial domain in which $Egfp^{+}$ cells reside in the neural tube was not affected by the loss of Fragment C (at 1.5dpf, $p = 0.106$, at 3dpf, $p = 0.587$).

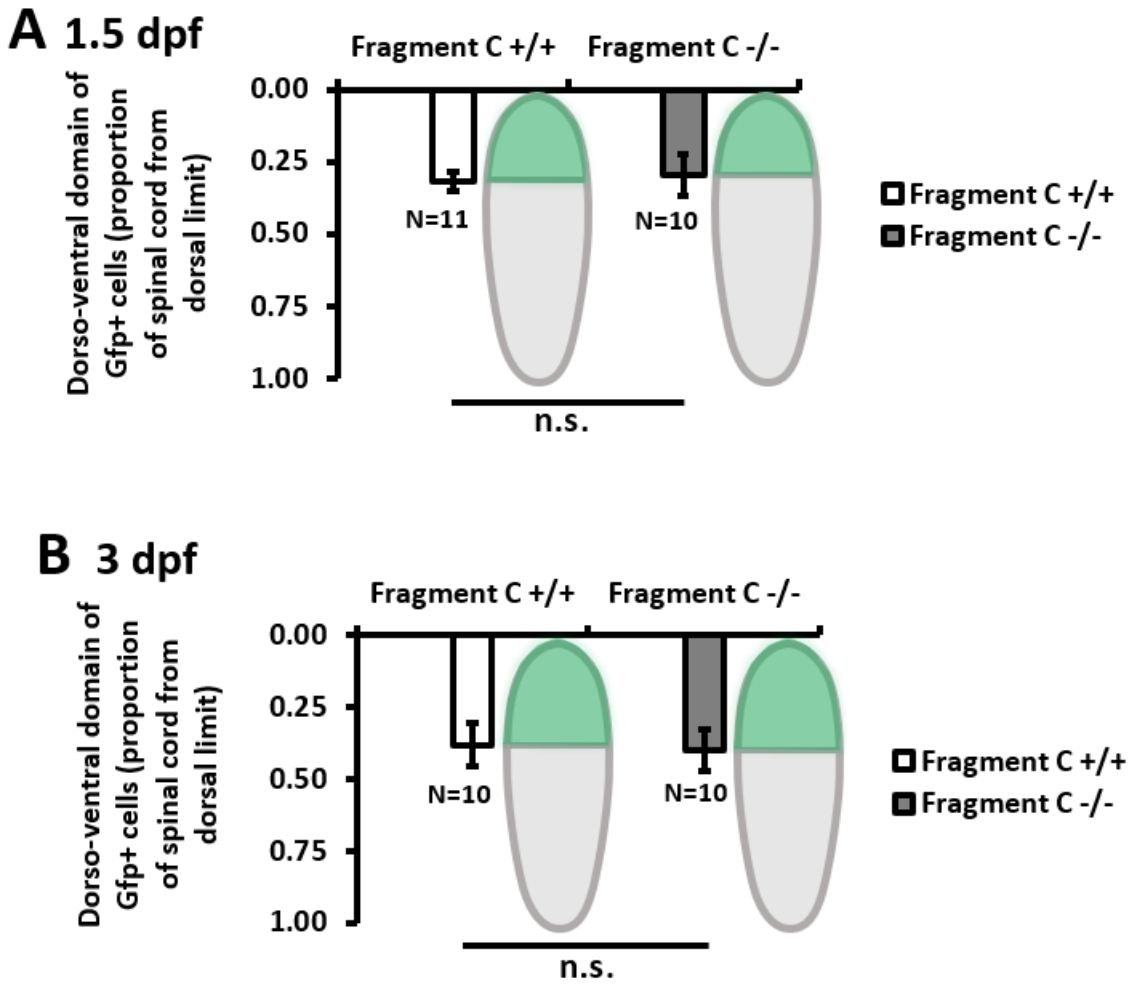

Figure 3.26. The ventral boundary of cells with Fragment C-driven Egfp expression in wildtype and Fragment C deletion mutants. Immunohistochemistry with antibodies against Gfp (which also labels Egfp) and either Elavl3/4 or Sox2 was performed on 10µm transverse sections at the level of the yolk extension of 1.5dpf (**A**) and 3dpf (**B**) offspring of a cross between *Tg(Fragment C-βG:Egfp)ot1;Fragment C*$^{+/-}$ siblings. Cells with Alexa-488 labelling within their cell body were counted as Egfp^{+}. Ventral limit of Egfp expression was set at the bottom of the DAPI-stained nuclei of the ventral-most Egfp^{+} cell. Images from both Gfp/Elavl3/4 and Gfp/Sox2 immunohistochemistry were combined toward cell counts. Each value counted toward the number of samples is the mean of cell counts from 3 sections of a single embryo/larvae. Height of bars represent the average ratio of the position of the ventral-most Egfp^{+} cell (measured from the dorsal limit of the spinal cord) to the entire length along the dorso-ventral axis of the spinal cord. Error bars are ± sample standard deviation. A two-tailed student's t-test was used to compare embryos/larvae with no deletion of Fragment C (Fragment C$^{+/+}$) and homozygous deletion of Fragment C (Fragment C$^{-/-}$). Between genotypes at 1.5dpf, $p = 0.106$, and at 3dpf, $p = 0.587$. n.s. (not significant) = $p > 0.05$.

3.8 *msx1b* does not compensate for the loss of Fragment C-driven *msx3* expression

There were no changes in the dorso-ventral position of $Egfp^{+}$ cells, nor changes in the balance of neurons and neural progenitors in the neural tube during embryonic or larval development. One explanation for the lack of functional consequence on neural tube development after the loss of Fragment C-driven *msx3* expression is that a related gene may compensate for the loss of *msx3* expression. Within the *msx* gene family in zebrafish, only *msx3, msx1b,* and *msx1a* are expressed in the neural tube (Ekker et al., 1997; Phillips et al., 2006). Both the protein-binding and DNA-binding domains of the *msx* genes are highly conserved, and thus represent good candidates for genetic compensation for the loss of *msx3* expression following the deletion of Fragment C. As a preliminary test for gene compensation following the deletion of Fragment C and loss of *msx3* in the dorsal neural tube, I examined only the expression of *msx1b,* though it will be necessary to also examine *msx1a* expression in the neural tube following the deletion of Fragment C (Takahashi et al., 2018). I performed a fluorescent *in situ* hybridization with probes against *egfp* and *msx1b* in Fragment $C^{+/+}$ and Fragment $C^{-/-}$ embryos with a *Tg(Fragment C-βG:Egfp)* genetic background and used ImageJ to generate images of transverse slices through the embryo at the level of the yolk extension. Since *egfp* expression was previously shown to recapitulate *msx3* expression in the neural tube (excluding in the dorsal-most cells where *egfp* is not expressed), we were able to compare *msx3* expression with *msx1b* expression in the neural tube. In both Fragment $C^{+/+}$ and Fragment $C^{-/-}$ embryos at 24hpf, *msx1b* is strongly expressed in the dorsal-most cells of the neural tube, mesenchyme dorsal to the neural tube, and epidermis dorsal to the neural tube. *msx1b* expression progressively decreases ventrally

from the roof plate (**Figure 3.27 B, G**). Thus, *msx1b* colocalizes with *egfp* expression in the dorsal region of the *egfp* expression domain, and only weakly or not in the ventral region of the *egfp* expression domain (**Figure 3.27 D, I**). The deletion of Fragment C had no effect on the spatial domain of *msx1b* expression in the neural tube at 24hpf, though a quantitative analysis of gene expression would be necessary to rule out genetic compensation by *msx1b*.

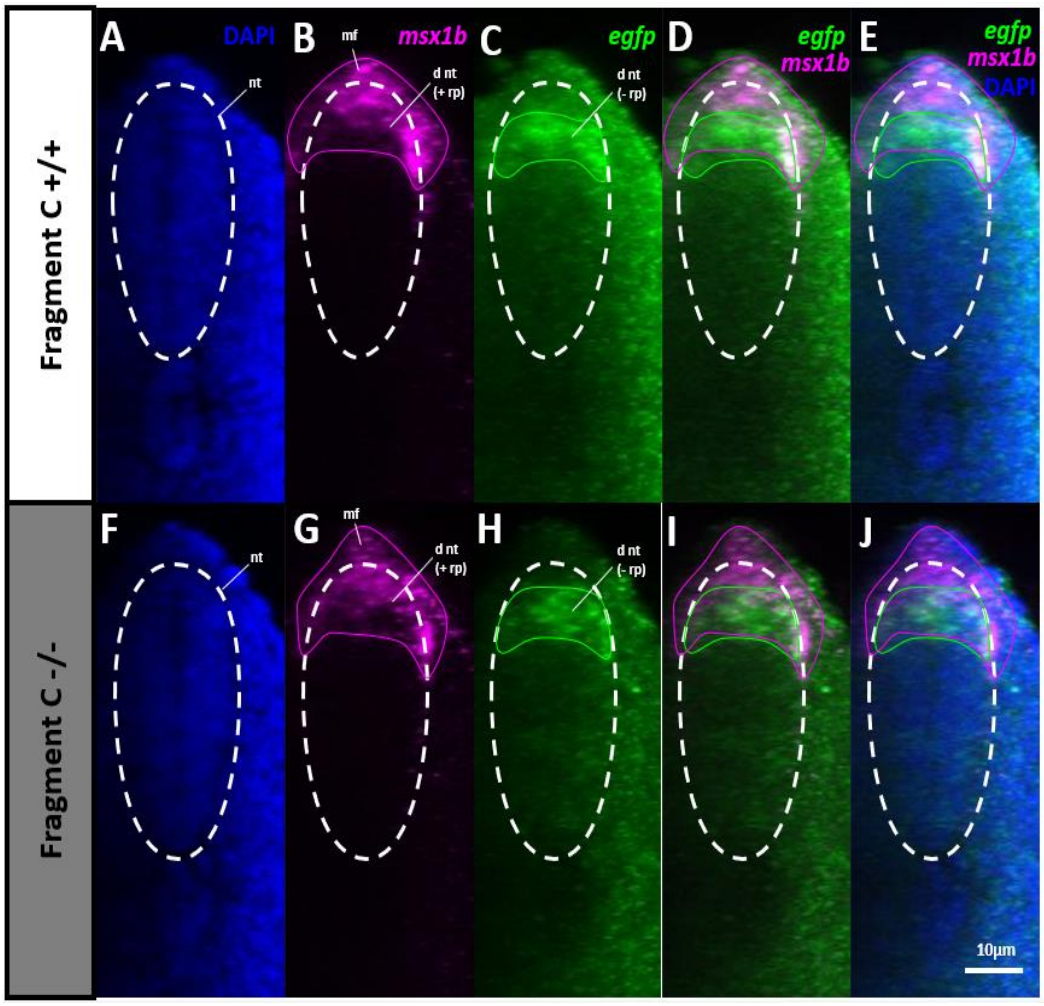

Figure 3.27. *msx1b* and *egfp* mRNA expression in the neural tube of wild-type and Fragment C deletion mutants at 24hpf. Whole-mount double fluorescent *in situ* hybridization with antisense probes for *msx1b* and *egfp* was performed on 24hpf offspring of a cross between *Tg(Fragment C-βG:Egfp)ot1;Fragment C*$^{+/-}$ siblings. 3 Fragment C $^{+/+}$ (wild-type sibling) and 3 Fragment C $^{-/-}$ (homozygous mutant) embryos were imaged. ImageJ was used to orthogonally reslice z-stacks from lateral to transverse, and maximum-intensity projections spanning 20µm along the anterior-posterior axis were created at the level of the yolk extension. **A-E.** Fragment C$^{+/+}$ expression profile of *msx1b* and *egfp* in the neural tube with DAPI labeling cell nuclei. **F-J.** Fragment C$^{-/-}$ expression profile of *msx1b* and *egfp* in the neural tube with DAPI labeling cell nuclei. Expression domain boundaries are traced (*msx1b* traced in magenta, *egfp* traced in green). Scale bar (bottom right, white line) represents a length of 10µm. Dorsal toward top of image, medial toward centre of horizontal axis of image. White dashed line marks the outer border of the neural tube. nt: neural tube. d nt: dorsal neural tube. rp: roof plate. mf: median fin fold.

4 Discussion

4.1 The relationship between the Fragment C enhancer and *msx3*

4.1.1 The onset of Fragment C-driven expression recapitulates the onset of *msx3* expression in the zebrafish embryo

The *Tg(Fragment C-βG:Egfp)ot1* transgenic line has detectable Egfp fluorescence beginning around 8hpf (**Figure 3.6**), with clear Egfp expression occurring between 9.5hpf and 11hpf (**Figure 3.7** and **Figure 3.8**). The onset of *msx3* expression occurs around late gastrulation, or approximately 8hpf at the lateral edges of the neural plate (Ekker et al., 1997; Phillips et al., 2006). Thus, the zebrafish Fragment C enhancer may drive the earliest *msx3* expression in the late gastrula. The onset of Egfp was not affected by the deletion of the endogenous Fragment C enhancer.

4.1.2 The Fragment C enhancer drives *msx3* expression in neural progenitors and neurons of the dorsal neural tube

In situ hybridization with antisense probes for *msx3* and *egfp* show that Fragment $C^{+/+}$ embryos express *msx3* in the dorsal third of the neural tube at 24hpf, whereas 24hpf Fragment $C^{-/-}$ embryos only express *msx3* in the dorsal-most cells of the neural tube (**Figure 3.17, B,G**, see **Figure 3.18** for quantitative support of the loss of ventral *msx3* expression in Fragment $C^{-/-}$ embryos). The domain in which *msx3* expression is lost coincides with where Fragment C-driven *egfp* expression is observed (**Figure 3.17, D,I**). We have shown that $Egfp^{+}$ cells represent nascent neurons and neural progenitors of the dorsal neural tube at both 1.5dpf and 3dpf (**Figure 3.21, A-I, Figure 3.22, A-I**). Thus, *msx3* expression is lost in dorsal neural progenitors and

neurons of the developing neural tube in Fragment $C^{-/-}$ embryos, though *msx3* expression may be lost in other cell types that were not analyzed (such as $Sox2^{-}$ radial glia, for example).

We previously speculated that Fragment C contains an enhancer of *msx3* based on proximity to *msx3*, its conservation with sequences in the mouse genome that are upstream of the mouse *Msx3*, and the similar expression pattern of Fragment C-driven *egfp* expression to *msx3* expression at embryonic and larval stages. Here, we have shown that *msx3* expression is lost in the domain overlapping with Fragment C expression after the deletion of Fragment C from the zebrafish genome, providing compelling evidence that Fragment C contains a *bona fide* enhancer of *msx3.* An alternative hypothesis to explain the loss of *msx3* expression after the deletion of Fragment C is that the loss of Fragment C only indirectly reduces *msx3* expression. By this mechanism, signaling pathways downstream of a different gene target of the Fragment C enhancer would indirectly affect the expression of *msx3* by a different enhancer. However, this hypothesis is a more complicated interpretation of these results and remains to be further substantiated beyond speculation.

Fragment $C^{-/-}$ embryos retain strong *msx3* expression in the dorsal-most cells of the neural tube but lose more ventral *msx3* expression compared to Fragment $C^{+/+}$ embryos (**Figure 3.17, B, I)**. The dorso-medial position of where *msx3* expression is retained coincides with where roof plate cells reside in the neural tube. Thus, roof plate cells are a compelling candidate for the dorsal cell type expressing *msx3* in both wild-type and Fragment $C^{-/-}$ embryos. In mouse, *Msx1* and *Msx2* are expressed in the roof plate, while *Msx3* is not (Liu et al., 2004). *msx3* in zebrafish has been reported to be expressed in the roof plate, though its expression in the roof plate was based solely on position in the neural tube rather than colocalization with known roof plate markers (Phillips et al., 2006; Bonner et al., 2008). As the dorsal progenitor domains also give

rise to Rohon-Beard sensory neurons and neural crest cells, the dorsal cells that retain *msx3* expression may also represent these cells. Thus, we cannot say with certainty whether the cells that retain *msx3* expression in Fragment $C^{-/-}$ embryos are roof plate cells, Rohon-Beard sensory neurons, pre-migratory neural crest cells, or a combination of these cell types. Double in *situ* hybridization with *msx3* and roof plate markers such as *lmx1b* (Elsen et al., 2008), neural crest markers such as *snai1b* (Rocha et al., 2020), and Rohon-Beard sensory neuron markers such as *islet1* (Moreno & Ribera, 2014) can further identify the dorsal cells that retain *msx3* expression and potentially differentiate them from the more ventral cells that lose *msx3* expression after the Fragment C deletion.

While a clear loss of *msx3* expression was observed in Fragment C deletion embryos, some aspects of this loss of expression remain unclear. Firstly, using fluorescent *in situ* hybridization on sections proves difficult to conclude whether *egfp* and *msx3* are expressed in the same cells, or differing cells in the same region of the neural tube. Additionally, we cannot conclude if the apparent loss of *msx3* in Fragment C deletions embryos represents a severe reduction of *msx3* expression or complete loss of *msx3* expression. Quantitative gene expression analysis by quantitative PCR (qPCR) could delineate these possibilities. By crossing the Fragment *Tg(Fragment C-βG:Egfp)ot1* line with transgenic reporter lines labelling specific neural cell types by a different color of fluorescent protein, fluorescent activated cell sorting (FACS) could be used to isolate neural cells with and without Fragment C-driven expression (cells with both fluorescent proteins and cells only with the non-Egfp fluorescent protein, respectively) (Rougeot et al., 2014), and qPCR could subsequently be used to determine if $egfp^{+}msx3^{-}$ or $egfp^{-}msx3^{+}$cells exist in the neural tube and quantify the degree of *msx3* loss in Fragment C deletion embryos relative to wild-type siblings.

The molecular underpinnings responsible for the loss of *msx3* expression from all but the dorsal-most cells of the neural tube after the deletion of Fragment C remain unknown. However, a previous study demonstrated that *msx3* expression can be completely abolished within and dorsal to the neural tube if the *wnt* inhibitor *dkk1* is ectopically expressed at 12hpf, and can be abolished exclusively in the ventral *msx3* expression domain of the neural tube if *dkk1* is ectopically expressed at 18hpf (similar to what is seen in Fragment $C^{-/-}$ embryos) (Bonner et al., 2008). Fragment C drives expression as early as 9.5hpf. While early *wnt* inhibition has more drastic effects than the loss of Fragment C, the similarity in the effect on *msx3* expression between later *wnt* inhibition and the deletion of Fragment C raises the possibility that Fragment C may bind downstream effectors of *wnt* signaling. If true, these effectors of *wnt* signaling may act in parallel on enhancers of *msx3* to drive *msx3* expression in the neural tube, or a single *wnt*-mediated mechanism may permit any transcription of *msx3*, such as changes to chromatin structure at the *msx3* gene itself. The mouse/human transcription factor binding site database TRANSFAC was previously used to determine potential transcription factors that may bind Fragment C and potentially regulate *msx3* expression (Matys et al., 2003). Of note, potential binding sites for the mouse Lef-1, β-catenin, Ascl2, and NeuroD were all found within Fragment C, within or immediately upstream of Fragment C1 (**Supplementary Figure 6.3**, see **Figure 1.3C** for the location of Fragment C1 in Fragment C). Each of the listed transcription factors have been shown to be activated by upstream Wnt signaling in various tissues of mice (Krishnamurthy & Kurzrock, 2018; Santiago et al., 2017; Kuwabara et al., 2009; Schuijers et al., 2015; Lopez-Nunez et al., 2021), with β-catenin, Ascl2, and NeuroD being expressed in neural progenitors (Kuwabara et al., 2009; Liu et al., 2019; Mutch et al., 2009). Chromatin

immunoprecipitation (ChIP) on embryonic zebrafish can be used to confirm these interactions (Lindeman et al., 2009). Using primers to isolate the potential transcription factor binding sites of interest and tagged versions of these transcription factors that can be recognized by a general antibody (or antibodies that can directly recognize these specific proteins), the ChIP assay can be used to confirm binding sites for Wnt signaling mediators preliminarily curated by TRANSFAC. To understand if these transcription factors bind specifically in neural tissue, the neural tissue could be first isolated before conducting the ChIP procedure (Perna & Alberi, 2019).

4.1.3 The Fragment C enhancer drives expression in the posterior notochord that does not recapitulate endogenous *msx3* expression

In the *Tg(Fragment C-βG:Egfp)* transgenic line, Egfp fluorescence is observed strongly in the posterior notochord during the first 2 days of development. This expression is increasingly restricted to the posterior notochord until it is absent from the notochord by 2dpf. We suspect that Fragment C contains an enhancer of *msx3*, and thus Egfp protein expression in notochord was unexpected based on the lack of *msx3* expression in the notochord at 24hpf. An explanation for Fragment C-driven notochord expression is that the insertion site of the *Tg(Fragment C-βG:Egfp*) enhancer/gene transgenic DNA may be in proximity to another enhancer that drives expression in the posterior notochord. Currently the *Tg(Fragment C-βG:Egfp)ot1* line derives from a single embryo injected with the *Tg(Fragment C-βG:Egfp*) construct that was raised and outcrossed with a wildtype zebrafish. Thus, to test the hypothesis that the position of the *Tg(Fragment C-βG:Egfp*) insertion site is driving the ectopic Egfp expression in the notochord, we could be reinject the *Tg(Fragment C-βG:Egfp*) construct into more wildtype embryos at the one cell stage and generate new *Tg(Fragment C-βG:Egfp)* transgenic lines. If these new transgenic lines do not have Egfp fluorescence in the notochord, it is likely that this expression is

caused by the position of the insertion site of the Fragment C enhancer. Alternatively, the Fragment C enhancer may modulate expression of other genes in addition to *msx3*. Two scenarios where multiple genes share an enhancer have been observed: one in which only one gene out of several that can have expression driven by a particular enhancer are enhanced (Khan et al., 2011; Krijger & de Laat, 2016) and one in which all genes are somewhat activated by the enhancer, resulting in differential expression of each gene by the enhancer (Lower et al., 2009; Krijger & de Laat, 2016). However, to my knowledge there are no examples where two genes with expression driven by the same enhancer are spatially defined into subsets of the expression domain of the enhancer and thus this scenario is not likely.

4.1.4 The loss of Fragment C reduces expression of *msx3* in the median fin fold.

The loss of *msx3* expression within the dorsal neural tube corresponds to where *egfp* expression is driven by the Fragment C enhancer. Surprisingly, *msx3* expression was also reduced or absent in the median fin fold after deletion of the Fragment C enhancer (**Supplementary Figure 6.4**). In 9/11 Fragment $C^{+/+}$ embryos, *msx3* expression was detectable in the median fin fold along the entire anterior-posterior axis of the median fin fold. In 11/11 Fragment $C^{-/-}$ embryos, there was no *msx3* expression in the anterior/dorsal median fin fold, and reduced expression in the posterior/ventral median fin fold surrounding the tailbud. The remaining 2/11 Fragment $C^{+/+}$ embryos had reduced *msx3* expression more comparable to that of the Fragment $C^{-/-}$ embryos. This result was unexpected since Egfp fluorescence was not detected in the median fin fold throughout development. It is possible that median fin fold cells that lose *msx3* expression after the loss of Fragment C have Fragment C-driven *msx3* expression earlier in their development. In this scenario, an effector downstream of Fragment C-driven *msx3* expression may in turn activate another enhancer of *msx3* to maintain *msx3* in the median fin

fold. Thus, without the initial Fragment C driven expression, maintenance of *msx3* expression in the fin fold would be lost. A potential enhancer that may take over the role of driving *msx3* expression in the neural tube is the Fragment A enhancer identified in the Akimenko lab. The Fragment A enhancer is located immediately upstream of the *msx3* gene and drives reporter expression throughout the entire median fin fold (**Supplementary Figure 6.5**). If transgenic lines driven by the Fragment A and Fragment C enhancers with different fluorescent reporters are crossed, we will be able to test if there is a transition from Fragment C-driven expression to Fragment A-driven expression in individual cells of the median fin fold.

4.2 Characterization of neural tube cells with Fragment C-driven expression

4.2.1 Cells with Fragment C-driven expression in the neural tube contribute to both neural progenitors and neurons

At both 1.5dpf and 3dpf, some $Egfp^+$ cells in the neural tube of *Tg(Fragment C-βG:Egfp)ot1* zebrafish colocalize with the neural progenitor marker Sox2 while others colocalize with the neuronal marker Elavl3/4. At 1.5dpf, the majority of $Egfp^+$ cells are $Sox2^+$ neural progenitor s (approximately 75%, **Figure 3.25**), with the remaining $Egfp^+$ cells being neurons (approximately 25% **Figure 3.24**). By 3dpf, the neural progenitor population of $Egfp^+$ cells decreases drastically to represent only approximately 40% of $Egfp^+$ cells (**Figure 3.25**), while neurons represent approximately 50% of $Egfp^+$ cells (**Figure 3.24**). This decrease in $Egfp^+$ neural progenitor s and increase in $Egfp^+$ neurons between 1.5dpf and 3dpf coincides with when the zebrafish neural tube is undergoing rapid neurogenesis, and thus some $Egfp^+$ neural progenitor s undergo terminal symmetric neurogenic divisions (Johnson et al., 2016). However, preliminary data from the Bui lab has shown that $Egfp^+$ cells are found at all developmental

stages in the neural tube (embryonic and larval stages) and spinal cord (juvenile and adult stages) of zebrafish (**Supplementary Figure 6.6**). Thus, while many $Egfp^+$ cells exit the cell cycle and become neurons during embryonic and larval development, some $Egfp^+$ neural progenitors are likely maintained into adulthood. Neurogenesis occurs throughout all stages of zebrafish development and is especially active after injury to the nervous system (Hui et al., 2015), so it is possible that cells with Fragment C-driven expression contribute towards adult neurogenesis either in a homeostatic or a regenerating context. One method of testing the possibility that cells with Fragment C-driven expression contribute toward adult neurogenesis would be to perform immunohistochemistry with a marker of nascent neurons such as Elavl3/4 on sectioned adult spinal cords of *Tg(Fragment C-βG:Egfp)ot1* transgenic zebrafish. However, this method will only label cells that have recently differentiated from neural progenitor to neuron.

Combined cell counts of $Egfp^+/Elavl3/4^+$ cells and $Egfp^+/Sox2^+$ cells summed to near 100% of all $Egfp^+$ cells at 1.5dpf, but at 3dpf do not total to 100%. However, using these markers alone, delineation of cell type cannot be completely achieved. Between 1.5dpf and 3dpf, an increasing number of $Sox2^-/Gfap^+$ radial glia accumulates in the dorsal neural tube (Johnson et al., 2016). Furthermore, in mammals, while OPCs express Sox2, mature oligodendrocytes do not, though both express Olig2 (Hoffmann et al., 2014; Reiprich & Wegner, 2014; Traiffort et al., 2016). In zebrafish, mature astrocytes express Glast and Gfap (Chen et al., 2020), and likely do not express Sox2 (though it is possible). Thus, using Sox2 and Elavl3/4 markers alone would not delineate $Egfp^+$ cells representing $Sox2^-$ radial glia, mature astrocytes, or oligodendrocytes. These cell types could be labelled as $Sox2^-/Glast^-/Gfap^+$ cells, $Glast^+$ cells, and $Sox2^-/Olig2^+$ cells, respectively. Antibodies for each of these markers exist in zebrafish, and thus immunohistochemistry with these markers in conjunction with an antibody for Gfp/Egfp would

provide a more complete assessment of the cell types with Fragment C-driven expression in the embryonic/larval neural tube.

4.3 Elucidation of the function of the Fragment C enhancer in the neural tube

4.3.1 Fragment C-driven *msx3* expression does not affect the balance between neural progenitors and neurons in the developing neural tube

In this study, we have shown that *msx3* expression was abolished in most cells of the dorsal third of the neural tube. The Fragment $C^{-/-}$ zebrafish line gives us an opportunity to study neural tube development in the absence of *msx3* in neural progenitors. In the Fragment $C^{-/-}$ embryos at both 1.5dpf and 3dpf there was no difference in the fraction of $Egfp^{+}$ cells that are neural progenitors ($Sox2^{+}$) or neurons ($Elavl3/4^{+}$) compared to that of wildtype siblings. As mentioned in section **1.2.3**, *Msx* genes in mice and chick are implicated in the regulation of the cell cycle of neural progenitors. In mouse, *Msx1* and *Msx2* indirectly activate *CyclinD1* expression, a protein that shortens the cell cycle and pushes the cell cycle toward proliferative divisions over neurogenic divisions (Hu et al., 2001). Electroporation of plasmids driving expression of the cDNA of chick *Msx1*, chick *Msx2*, mouse *Msx1* or *Msx2* into the chick spinal cord represses neuronal differentiation (Liu et al., 2004). However, electroporation of a plasmid driving expression of the cDNA of mouse *Msx3* into the chick neural tube has no effect on neuronal differentiation (Liu et al., 2004). Further research on the role of the zebrafish *msx1a* and *msx1b* is needed to confirm if, like in mice and chick, at least some *msx* genes regulate neural differentiation in the developing spinal cord. *msx1b* morphant zebrafish embryos have reduced numbers of commissural neurons, but also showed greater levels of apoptosis in the neural tube, hindering conclusions about the involvement of *msx1b* in regulation of neuronal differentiation

(Phillips et al., 2006). Similar analyses to that performed in this Master's project looking at the numbers of neural progenitors and neurons the developing spinal cord in *msx1b* and *msx1a* knockout mutants would clarify if *msx* genes retain a role in regulating neuronal differentiation at all in zebrafish. Here, we have shown evidence that Fragment C-driven *msx3* expression does not regulate neuronal differentiation nor the number of neural progenitors in the embryonic and early larval neural tube.

While differentiation and proliferation of neural progenitors are linked processes, we have only indirectly observed no changes in these processes by determining that the number of Elavl3/4^{+}/Egfp^{+} and Sox2^{+}/Egfp^{+} cells did not change relative to the total number of Egfp^{+} cells. As previously mentioned, BrdU pulse/chase experiments can be used to label cycling cells, and thus it would be possible to directly test if the number of proliferating Egfp^{+} cells are altered by the Fragment C deletion. Another approach that could more conclusively rule out a role for Fragment C in regulating proliferation and differentiation would be to assess changes in cell cycle dynamics in the neural tube of Fragment C deletion embryos. Changes in the length of cell cycle phases underlie changes in the differentiation/proliferation of neural progenitors (Lobjois et al., 2004). Thus, measuring the length of cell cycle phases of Egfp^{+} cells could more directly test this hypothesis. Transgenic lines of zebrafish that label different cell cycle phases could be crossed with the Fragment C-deletion line to test this hypothesis (Sakaue-Sawano et al., 2008).

4.3.2 Fragment C-driven *msx3* expression does not affect the dorso-ventral position of cells in the neural tube

In this study we have shown that the deletion of the Fragment C and loss of *msx3* expression in the dorsal neural tube did not affect the dorso-ventral position of cells with Fragment C-driven expression in the neural tube. Previous research has indicated that *msx3* may

play a role in dorso-ventral patterning of the neural tube. Indeed, ectopic expression of mouse *Msx3* in the chick neural tube results in an increase in *Cath1*$^{+}$ neural progenitors and di1 and di3 interneurons (Liu et al., 2004). Evidence also suggests that zebrafish *msx3* in the neural tube acts downstream of *wnt* signaling, another pathway involved in dorso-ventral patterning of the neural tube (Bonner et al., 2008; Flowers et al., 2012). It has been shown that cells in the neural plate do not necessarily end up in equivalent dorso-ventral or medio-lateral positions in the neural tube as their neighbors in the neural plate (Xiong et al., 2013). It has been suggested that the dorso-ventral identity of cells in the neural tube are conveyed by cells in the neural plate based on cell adhesion properties such that cells of a particular identity will adhere more to each other than other cells (Xiong et al., 2013). My hypothesis was that Fragment C$^{-/-}$ zebrafish with a loss of *msx3* in the neural tube may have a perturbed cell sorting during neurulation, resulting in a change in the dorso-ventral position of these cells in the neural tube. Indeed, as *msx3* is present in the dorsal third of the neural tube, the loss of *msx3* could have resulted in an upregulation of a more ventral neural marker, and thus sorting of the cells with Fragment C-driven expression to more ventral positions. We did not observe this change in the ventral boundary of Egfp positive cells after the deletion of Fragment C. We can conclude that *msx3* does not affect the dorso-ventral sorting of cells. However, *msx3* may still have a role in assigning a dorso-ventral identity to progenitors and neurons without affecting the initial sorting of cells based on their dorso-ventral identity. If changes to adhesion properties of cells in the neural plate are not downstream of Msx3, we would not expect the cell sorting during neurulation to be affected by the loss of *msx3* expression. To determine if there is a role for *msx3* in dorso-ventral patterning of the neural tube, it is necessary to look at the effect that the loss of *msx3* has on other markers for the dorsoventral identity of neural progenitors and neurons. *Dbx* genes have a known role in

dorsoventral patterning of neural progenitors in the middle of the dorso-ventral axis of the spinal cord, with *Msx* expression domain bordering above. In chick, which lack an orthologue of *Msx3, Msx1* is expressed in the dorsal third of the spinal cord reminiscent of the mouse/zebrafish *Msx3*/*msx3*. Ectopic expression of chick *Msx1* ventrally results in a loss of $Dbx2^{+}$ neural progenitors, though ectopic expression of Dbx2 dorsally had no impact on Msx1 expression (Timmer et al., 2002). Similarly, in zebrafish, knockdown of *dbx1a/1b* does not affect the ventral boundary of *msx3* at 24hpf, indicating a conserved inability of perturbation in *Dbx* gene expression to alter *msx* gene expression (Gribble et al., 2007). The repression of *dbx1a/1b* by *msx3* has not yet been tested, but one could speculate a similar relationship as that seen in chick, where alterations in *msx3* expression would inversely affect *dbx1a/1b* expression. In situ hybridization with probes against known markers of distinct neural progenitor populations such as *dbx1a/1b* can be performed in Fragment C deletion embryos and their wildtype siblings to determine if the loss of Fragment C-driven *msx3* expression affects dorso-ventral identity of neural progenitors. Moreover, markers for the neurons born from distinct progenitor populations should be similarly analyzed in Fragment C deletion embryos.

4.3.3 *msx1b* does not compensate for the loss of Fragment C-driven *msx3* expression

The loss of Fragment C did not result in changes in the balance of neurons and neural progenitors in the neural tube, nor did it affect the dorso-ventral domain in which $Egfp^{+}$ cells were found. We speculated that a gene related to *msx3* may compensate for the loss of *msx3* expression in the neural tube, buffering against phenotypic consequences in Fragment $C^{-/-}$ embryos, as this phenomenon is well known in zebrafish (El-Brolosy & Stainier, 2017). In the zebrafish neural tube, *msx3*, *msx1b* and *msx1a* are all expressed in the dorsal neural tube (Phillips

et al., 2006). Thus, *msx1b* and *msx1a* represent candidates for gene compensation after the loss of *msx3* expression by deletion of the Fragment C enhancer. Single morpholino knockdown of *msx3, msx1a,* or *msx1b* has minor consequences on neural crest and neural tube cells in comparison to a triple morpholino knockdown of all three *msx* genes, which could indicate that genetic compensation is at play (Phillips et al., 2006). However, my research shows that *msx1b* expression was not affected by the loss of Fragment C. In both Fragment $C^{+/+}$ and Fragment $C^{-/-}$ embryos, *msx1b* is strongly expressed in the dorsal-most cells of the neural tube, mesenchyme dorsal to the neural tube, and epidermis dorsal to the neural tube, and weakly expressed in the expression domain overlapping with *egfp* expression. Still, *msx1a* or an unrelated gene could provide gene compensation after the loss of Fragment C-driven *msx3* expression. Alternatively, *msx1b* and *msx1a* could exert a redundant function to that of *msx3* in the neural tube without employing transcriptional adaptation to the loss of *msx3* gene expression. Finally, no compensatory mechanisms may be at play following the loss of Fragment C, and Fragment C-driven *msx3* expression may simply not influence the cellular processes examined. In future experiments it will be necessary to perform a quantitative gene analysis for *msx1a* and *msx1b* by qPCR to determine if either gene contributes to genetic compensation for the loss of msx3.

Interestingly, previous research has shown that a morpholino knockdown of *msx3* lead to severe ventral tail curvature (Phillips et al., 2006). This phenotype was not observed in Fragment $C^{-/-}$ embryos. This phenotype may be caused by a loss of *msx3* expression that is not driven by Fragment C. However, studies using germline knockout mutations can result in less severe phenotypes than gene knockdown studies, and this compensatory mechanism may be at play in our Fragment $C^{-/-}$ mutants (El-Brolosy & Stainier, 2017; Rossi et al., 2015).

5 Conclusion

The Fragment C enhancer is located upstream of the *msx3* gene in the zebrafish genome. The *Tg(Fragment C-βG:Egfp)ot1* reporter line generated in the Akimenko lab drives Egfp reporter expression in the dorsal neural tube throughout embryogenesis that is maintained into adulthood. The work completed in my Master's thesis has shown that the Fragment C enhancer first drives reporter expression at the time point that *msx3* begins to be expressed. Additionally, by analyzing the colocalization of $Egfp^+$ cells with cell markers in the neural tube, we show that cells with Fragment C-driven expression represent both neural progenitors and neurons, possibly in addition to other cell types. We generated a new mutant line of zebrafish in which a deletion of the Fragment C enhancer has successfully been carried out and analyzed the effect of this deletion on *msx3* expression, the fate of $Egfp^+$ cells in the neural tube, and the dorso-ventral positioning of cells in the neural tube. While Fragment C was a suspected enhancer of *msx3* based on its upstream proximity to *msx3* and ability to drive similar spatial expression in the dorsal neural tube to that of *msx3*, this work marks the first time we show that a subset of *msx3* expression in the neural tube is dependent on the presence of the Fragment C enhancer. Surprisingly, the loss of the Fragment C enhancer greatly reduced *msx3* expression in the dorsal median fin fold despite Fragment C not driving reporter expression in this tissue. The loss of the Fragment C enhancer had no effect on the balance of neurons and neural progenitors in the neural tube, nor did it affect the spatial domain in which $Egfp^+$ cells were found. Thus, my work represents the first attempt to analyze the function of the Fragment C enhancer in driving *msx3* expression in the neural tube. More generally, this work contributes to our understanding of the regulation neural development in vertebrates.

6 Supplementary Figures

A mm1489 enhancer sequence

gacaagtccccaaagacggtaaggatgagagagctgatctccccagatatctagtccctggaaccagctaatggttacaggttgggcaatctttcttgtgccctgggactctaactc
ctgtgcaaccaggcctgtgggttcatctgggctcttgggctccagtgtctacttcaggtagcatgagattgtttagcctttgtggggccagttcctgcacacagatgatgcaaatga
gcaggactattctcgggtctgtaagcccaaagagaagaaggtttttgaggcattgcaaaacaaatacattgtgatcagggtttggaaaatggaaacaaggacatacttgtggtcat
aatagatgacagcagtcccacccttaacctctgatgagtaggaggccttggggctagggctagggtaacagggtaagacatccttagagattggtcccaagagaagatcccttgcct
ggctggagtgttgccttccagtgatggggaggaggagcatgcatctcttactgtgatggacagcacagatcctcccattcctggacccccaaagtttccataaccaataggcccc
aggttggttttaactctatccttctcctgactcattgaatctcaagagcagagccatggggactacaaaggaccctctcaaaccctccacccgtgcccagacacagtactgagcgtc
caggtgtgccgggtatcaaaaccttgagtcaggtgggcatgagtgctcccaggatgcaggccaggggaggtggcgctgttcactggaaatgtctgtagcatcctggaagaggttggt
tagtcttgtgggtcttgggtgcttgagatcagaagtgggaatgaaagcgggactcttgagttggagatattccagacagctgattttctaggggctgtaggtccttcccttcccttg
ccaacgtatgggtgagtgatgcccttaggtcagctcacaacagggtgaggaggggtcagaggacgccctttcgattcagccttcttctcactgtcaagggagctccccagctcctcc
agtcctcagaagcctcttccccagtccctccccgccctactacggagcggtaaggggggtgggggtggtggtggtggacagtgcttgtccctcccacaggcagctccatcagcc
agcacgccctaagatccttggctccctttccagccccgttgagagaatccctgtggccgccgcaccctgccacctcgctggcatctgtaacggagtttttgtcgggatgagctgacc
gccgcgcccccagcggcgtccagatgttgtgagcctcgggccctttaatcactgcccggcggctgcgggcgctttgttccgggttcggcaggattctcccaggcggccccgccgcg
cagggcactgttcaaagggcctggataaacaggcggtacactgcgcggacaaagcacggcagtctccggcggggcgggacctggggaatccgcgccgccggccgccaggcgctttgt
gcgccgcttaatgagctggaaaatacaattggcttccctggctgtgaaaatcgtttcaaggaccgcggcgtcacttggctgctgggagaccccggaattgatctcctttgtccccag
ggtcccagcatatccttgctggggaggcgaccaggctttgcctcttgcagaaaaccccccaagcagactcttaagtatgaggggacccaggattccaagcttgaaactcaaactagac
agcggtgcagttctccggccagcttctgggtgtagacacccagaggtggcttctgcttgatcaaccctgaccaaaagccccggaagacactggctactctaactctacttgcacaaa
tacaagcagccttcagctttcagactcagaagcgggtggctttgctgtacagcaagtgtttccaaaccacggccagcttattcagtaggttaacagattgctgagctagggaaaaag
tgtccaatgttcttgtgtccatttttcctcacattttcttaaggttgacccatcgggctgcagatgctaataaagaggccagagcagtcagcactaagcccccaaaaacggtcattgag
gaagtgaacacagggccttcgctctggccattttcattctctgcagagtgggcttccactccttctccatcctgaggaaagagcacattcttccctattagccacctcaagtggata
ttatatgtcaagaaacaaaatctgaaattggggtctgcacagaa

B mm1489 enhancer expression

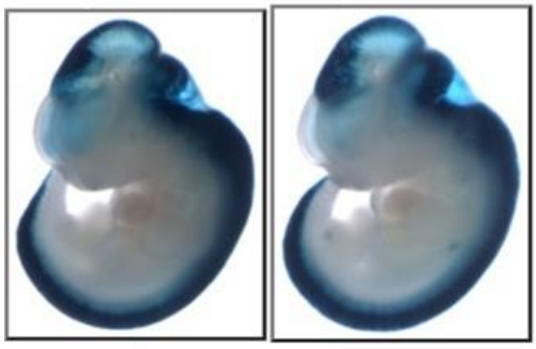

Figure 6.1. The mouse vista enhancer mm1489 contains FragmentC2 and drives a similar reporter expression to that of Fragment C in zebrafish. (A) Sequence in the mouse genome corresponding to the mm1489 enhancer. Red font represents the sequence with sequence similarity to that in Fragment C, and specifically corresponds to Fragment C2. **(B)** mm1489-driven lacZ/Xgal reporter expression in two E11.5 mouse embryos. Expression is found in the neural tube, hindbrain, and midbrain of 5/5 embryos that were injected. Sequences and images obtained from Mouse vista enhancer browser (Visel et al., 2007).

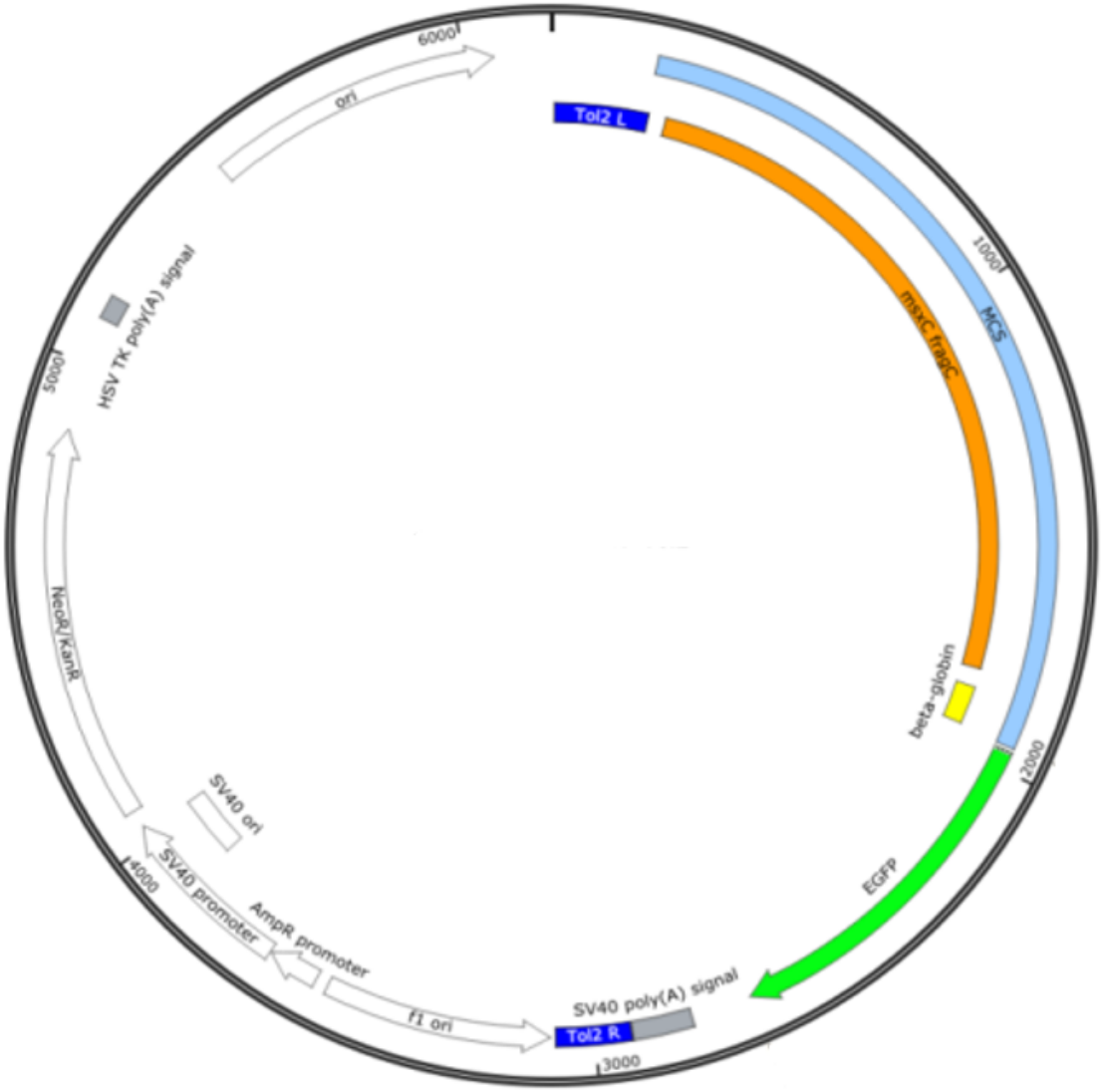

Figure 6.2. Plasmid map of the *Tg(Fragment C-βG:Egfp)* construct. Fragment C (Orange, labelled as msxC FragC) was cloned into the multiple cloning site (MCS) upstream of a β-globin minimal promoter (yellow). The Egfp coding sequence (green), lies upstream of Fragment C:β-globin. The Tol2 arms (blue) flank the Fragment C:β-globin-Egfp sequence. When co-injected with *transposase* mRNA into zebrafish embryos at the one cell stage, Fragment C:β-globin-Egfp is integrated into the zebrafish genome. Length of construct is 8221 base pairs.

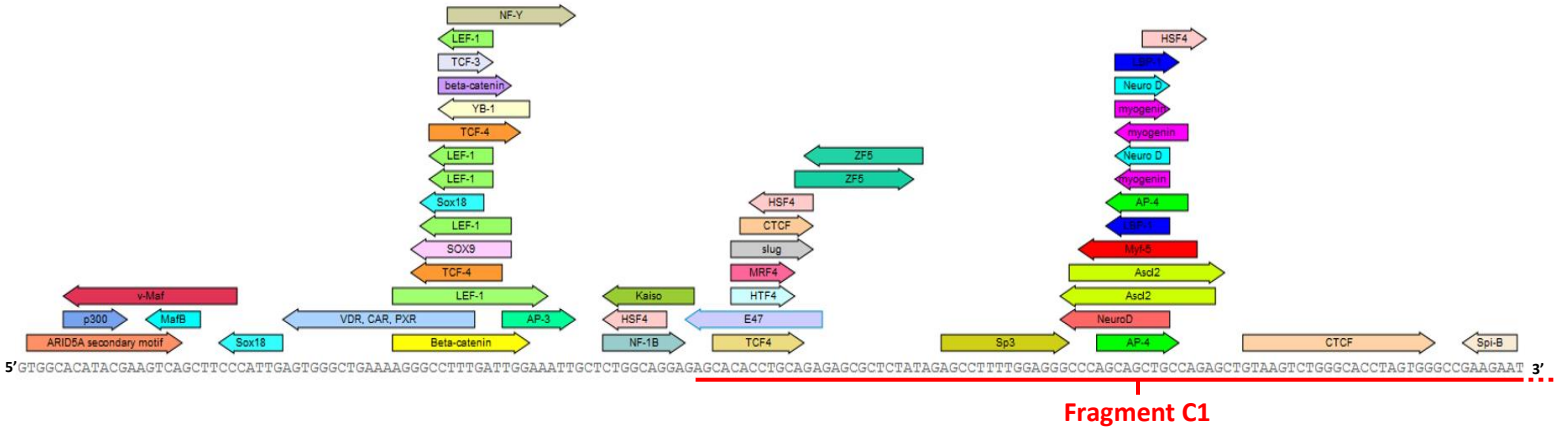

Figure 6.3. TRANSFAC output of putative transcription factor binding sites within part of the Fragment C sequence. The sequence shown is within the Fragment C sequence, including both the beginning of Fragment C1 and some nucleotides upstream of Fragment C1. Arrows are labelled by the transcription factor binding site that they represent, and their position, and length correspond to the position and length of the transcription factor binding site they represent. Orientation of the arrows indicate to which DNA strand they bind (right orientation binds the displayed strand, left orientation binds the complementary DNA strand). Fragment C1 sequence is underlined in red and continues in the 3' direction.

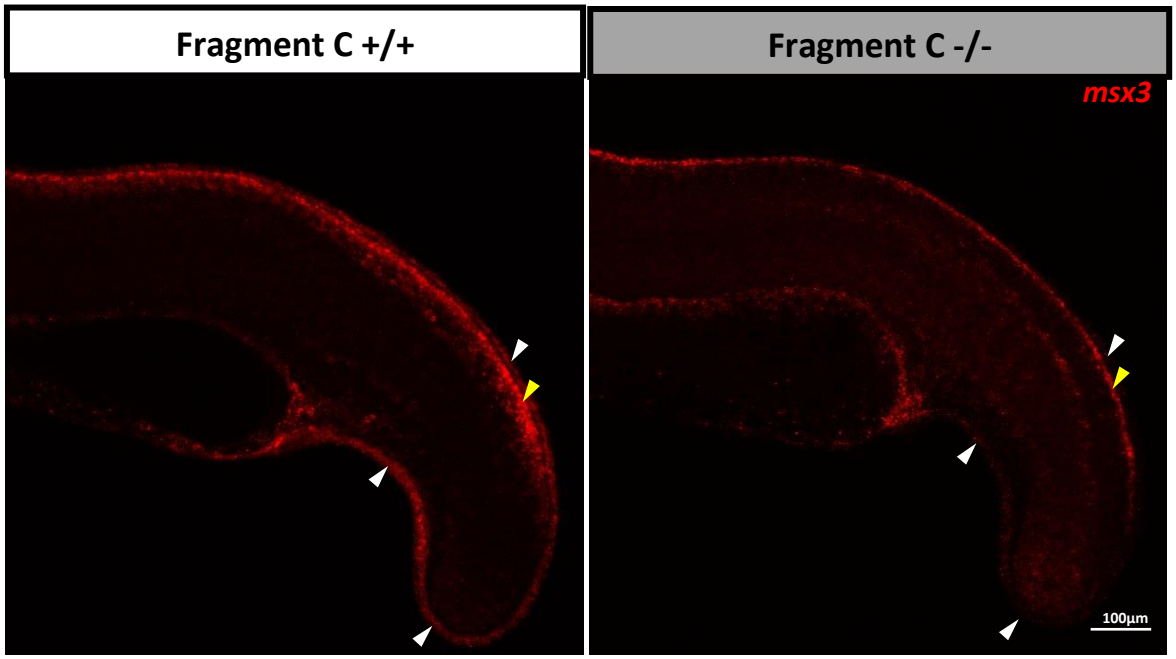

Figure 6.4. The loss of Fragment C-driven expression reduces *msx3* expression along the entire median fin fold. Whole-mount double fluorescent *in situ* hybridization with antisense probes for *msx3* and *egfp* was performed on 24hpf offspring of a cross between *Tg(Fragment C-βG:Egfp)ot1;Fragment C*$^{+/-}$ siblings. 11 Fragment C $^{+/+}$ and 11 Fragment C $^{-/-}$ embryos were imaged. *msx3* expression in red. Scale bar (bottom right, white line) represents a length of 100 µm. Anterior toward left of images, dorsal toward top of images. White arrowheads point to the median fin fold where *msx3* is expressed in Fragment C$^{+/+}$ embryos. Yellow arrowhead points to the strong *msx3* expression in the dorsal-most cells of the neural tube.

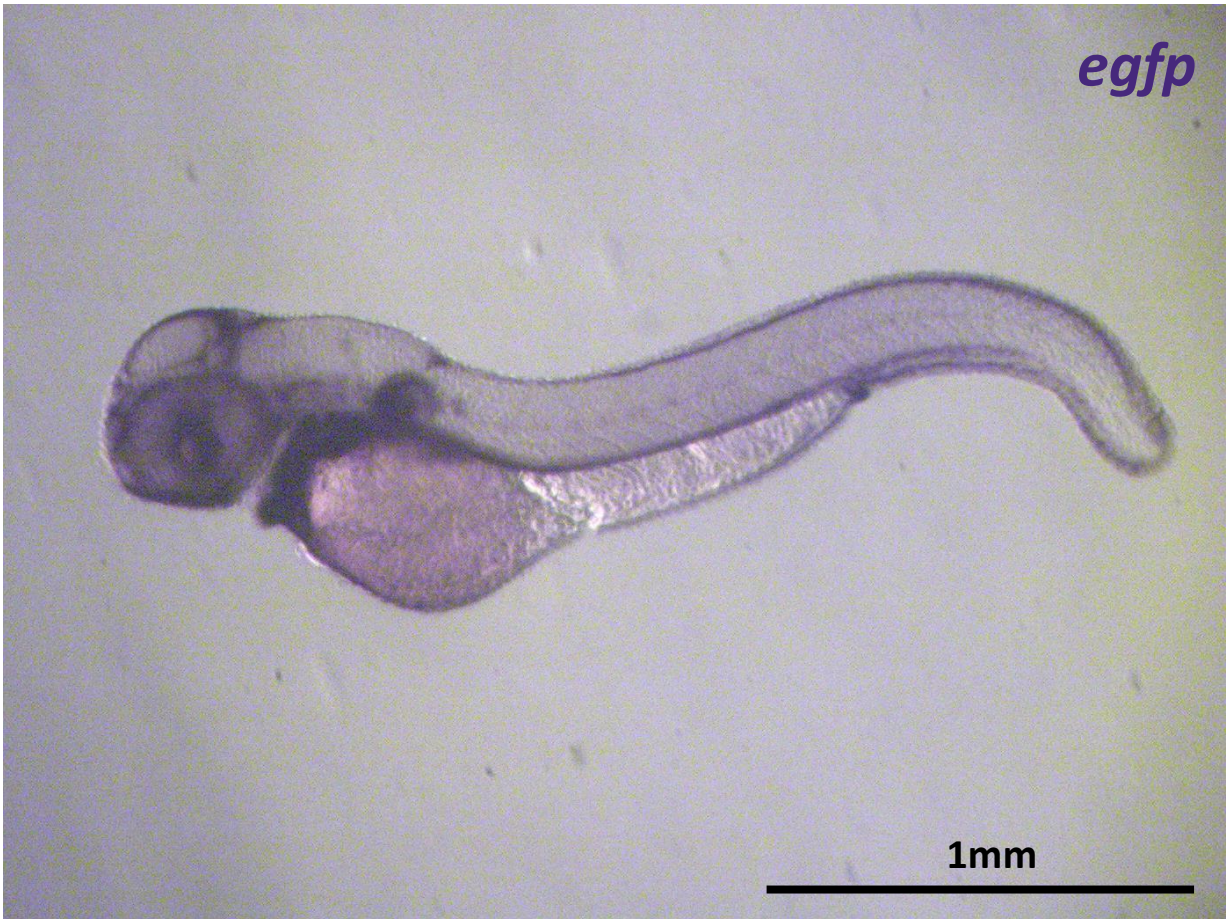

Figure 6.5. *egfp* expression in the *Tg(Fragment A-βG:Egfp)* transgenic line. *In situ* hybridization was performed on 2dpf zebrafish embryos with an antisense probe for *egfp*. *egfp* expression in purple. Scale bar (black line, bottom right) represents 1mm. Image taken by Fatma Legnain of the Akimenko lab.

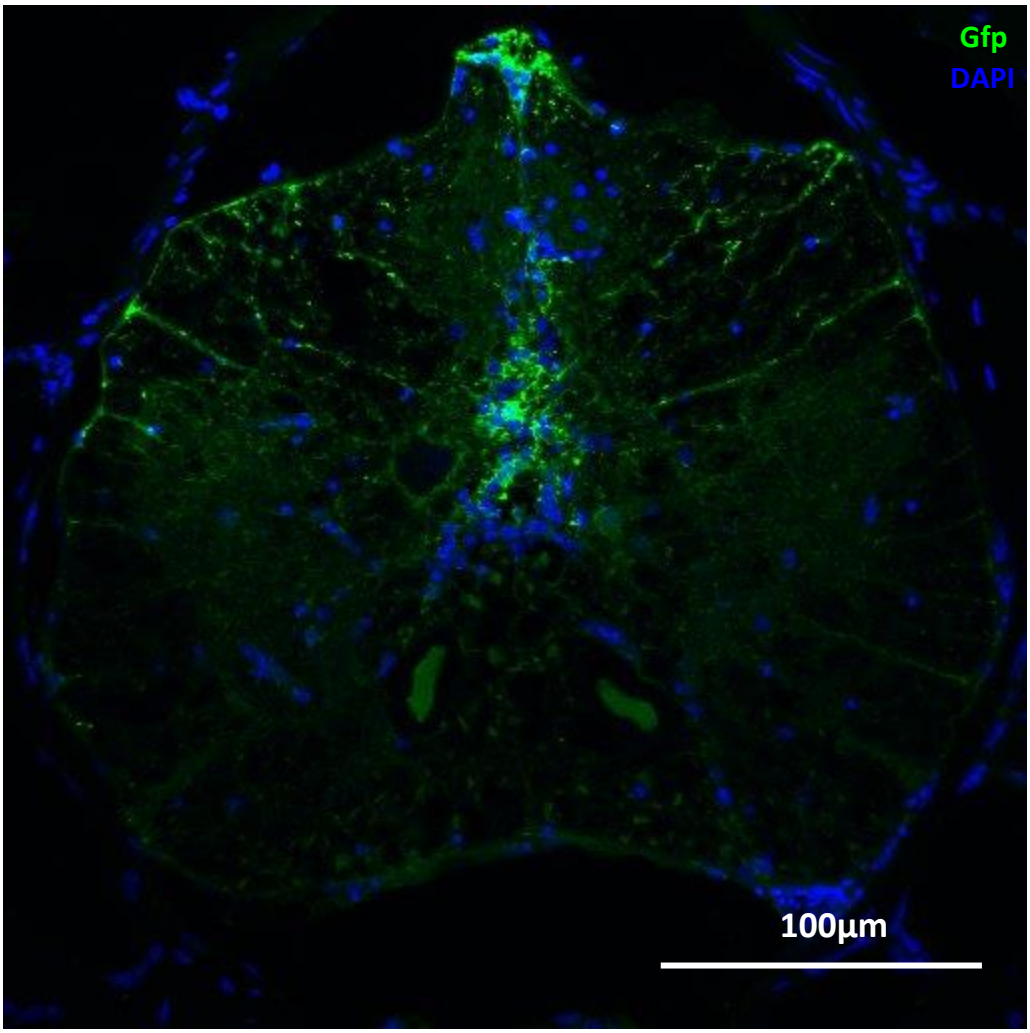

Figure 6.6. Fragment C-driven expression persists in the adult spinal cord. Transverse slice through the spinal cord of a 5-month old *Tg(Fragment C-βG:Egfp)ot1* zebrafish. Scale bar (white line, bottom right) represents 100µm. Dorsal is toward the top, medial toward the centre of the horizontal axis of the image. Image taken by Annabelle Morrissette from the lab of Tuan Bui.

References

Achilleos, A., & Trainor, P. A. (2012). Neural crest stem cells: discovery, properties and potential for therapy. *Cell research*, *22*(2), 288–304. https://doi.org/10.1038/cr.2012.11

Akimenko, M. A., Johnson, S. L., Westerfield, M., & Ekker, M. (1995). Differential induction of four msx homeobox genes during fin development and regeneration in zebrafish. *Development (Cambridge, England)*, *121*(2), 347–357.

Alaynick, W. A., Jessell, T. M., & Pfaff, S. L. (2011). SnapShot: spinal cord development. *Cell*, *146*(1), 178–178.e1. https://doi.org/10.1016/j.cell.2011.06.038

Allende, M. L., & Weinberg, E. S. (1994). The expression pattern of two zebrafish achaete-scute homolog (ash) genes is altered in the embryonic brain of the cyclops mutant. *Developmental biology*, *166*(2), 509–530. https://doi.org/10.1006/dbio.1994.1334

Allende, M. L., & Weinberg, E. S. (1994). The expression pattern of two zebrafish achaete-scute homolog (ash) genes is altered in the embryonic brain of the cyclops mutant. *Developmental biology*, *166*(2), 509–530. https://doi.org/10.1006/dbio.1994.1334

Alqadah, A., Hsieh, Y. W., Vidal, B., Chang, C., Hobert, O., & Chuang, C. F. (2015). Postmitotic diversification of olfactory neuron types is mediated by differential activities of the HMG-box transcription factor SOX-2. *The EMBO journal*, *34*(20), 2574–2589. https://doi.org/10.15252/embj.201592188

Andrews, M. G., Kong, J., Novitch, B. G., & Butler, S. J. (2019). New perspectives on the mechanisms establishing the dorsal-ventral axis of the spinal cord. *Current topics in developmental biology*, *132*, 417–450. https://doi.org/10.1016/bs.ctdb.2018.12.010

Appel, B., Givan, L. A., & Eisen, J. S. (2001). Delta-Notch signaling and lateral inhibition in zebrafish spinal cord development. *BMC developmental biology*, *1*, 13. https://doi.org/10.1186/1471-213x-1-13

Arai, Y., Pulvers, J. N., Haffner, C., Schilling, B., Nüsslein, I., Calegari, F., & Huttner, W. B. (2011). Neural stem and progenitor cells shorten S-phase on commitment to neuron production. *Nature communications*, *2*, 154. https://doi.org/10.1038/ncomms1155

Araya, C., Ward, L. C., Girdler, G. C., & Miranda, M. (2016). Coordinating cell and tissue behavior during zebrafish neural tube morphogenesis. *Developmental dynamics : an official publication of the American Association of Anatomists*, *245*(3), 197–208. https://doi.org/10.1002/dvdy.24304

Azaïs, M., Agius, E., Blanco, S., Molina, A., Pituello, F., Tregan, J. M., Vallet, A., & Gautrais, J. (2019). Timing the spinal cord development with neural progenitor cells losing their proliferative capacity: a theoretical analysis. *Neural development*, *14*(1), 7. https://doi.org/10.1186/s13064-019-0131-3

Bachleda, A. R., Pevny, L. H., & Weiss, E. R. (2016). Sox2-Deficient Müller Glia Disrupt the Structural and Functional Maturation of the Mammalian Retina. *Investigative ophthalmology & visual science*, *57*(3), 1488–1499. https://doi.org/10.1167/iovs.15-17994

Banerji, J., Rusconi, S., & Schaffner, W. (1981). Expression of a beta-globin gene is enhanced by remote SV40 DNA sequences. *Cell*, *27*(2 Pt 1), 299–308. https://doi.org/10.1016/0092-8674(81)90413-x

Barberis, M., Klipp, E., Vanoni, M., & Alberghina, L. (2007). Cell size at S phase initiation: an emergent property of the G1/S network. *PLoS computational biology*, *3*(4), e64. https://doi.org/10.1371/journal.pcbi.0030064

Bendall, A. J., & Abate-Shen, C. (2000). Roles for Msx and Dlx homeoproteins in vertebrate development. *Gene*, *247*(1-2), 17–31. https://doi.org/10.1016/s0378-1119(00)00081-0

Bergeron, S. A., Carrier, N., Li, G. H., Ahn, S., & Burgess, H. A. (2015). Gsx1 expression defines neurons required for prepulse inhibition. *Molecular psychiatry*, *20*(8), 974–985. https://doi.org/10.1038/mp.2014.106

Berman, B. P., Nibu, Y., Pfeiffer, B. D., Tomancak, P., Celniker, S. E., Levine, M., Rubin, G. M., & Eisen, M. B. (2002). Exploiting transcription factor binding site clustering to identify cis-regulatory modules involved in pattern formation in the Drosophila genome. *Proceedings of the National Academy of Sciences of the United States of America*, *99*(2), 757–762. https://doi.org/10.1073/pnas.231608898

Bermingham, N. A., Hassan, B. A., Wang, V. Y., Fernandez, M., Banfi, S., Bellen, H. J., Fritzsch, B., & Zoghbi, H. Y. (2001). Proprioceptor pathway development is dependent on Math1. *Neuron*, *30*(2), 411–422. https://doi.org/10.1016/s0896-6273(01)00305-1

Bertoli, C., Skotheim, J. M., & de Bruin, R. A. (2013). Control of cell cycle transcription during G1 and S phases. *Nature reviews. Molecular cell biology*, *14*(8), 518–528. https://doi.org/10.1038/nrm3629

Blader, P., Fischer, N., Gradwohl, G., Guillemot, F., & Strähle, U. (1997). The activity of neurogenin1 is controlled by local cues in the zebrafish embryo. *Development (Cambridge, England)*, *124*(22), 4557–4569.

Blow, M. J., McCulley, D. J., Li, Z., Zhang, T., Akiyama, J. A., Holt, A., Plajzer-Frick, I., Shoukry, M., Wright, C., Chen, F., Afzal, V., Bristow, J., Ren, B., Black, B. L., Rubin, E. M., Visel, A., & Pennacchio, L. A. (2010). ChIP-Seq identification of weakly conserved heart enhancers. *Nature genetics*, *42*(9), 806–810. https://doi.org/10.1038/ng.650

Bondarenko, V. A., Liu, Y. V., Jiang, Y. I., & Studitsky, V. M. (2003). Communication over a large distance: enhancers and insulators. *Biochemistry and cell biology = Biochimie et biologie cellulaire*, *81*(3), 241–251. https://doi.org/10.1139/o03-051

Bonner, J., Gribble, S. L., Veien, E. S., Nikolaus, O. B., Weidinger, G., & Dorsky, R. I. (2008). Proliferation and patterning are mediated independently in the dorsal spinal cord downstream of canonical Wnt signaling. *Developmental biology*, *313*(1), 398–407. https://doi.org/10.1016/j.ydbio.2007.10.041

Bonnet, F., Molina, A., Roussat, M., Azais, M., Bel-Vialar, S., Gautrais, J., Pituello, F., & Agius, E. (2018). Neurogenic decisions require a cell cycle independent function of the CDC25B phosphatase. *eLife*, *7*, e32937. https://doi.org/10.7554/eLife.32937

Bouzier-Sore, A. K., & Pellerin, L. (2013). Unraveling the complex metabolic nature of astrocytes. *Frontiers in cellular neuroscience*, *7*, 179. https://doi.org/10.3389/fncel.2013.00179

Briscoe, J., Pierani, A., Jessell, T. M., & Ericson, J. (2000). A homeodomain protein code specifies progenitor cell identity and neuronal fate in the ventral neural tube. *Cell*, *101*(4), 435–445. https://doi.org/10.1016/s0092-8674(00)80853-3

Briscoe, J., Sussel, L., Serup, P., Hartigan-O'Connor, D., Jessell, T. M., Rubenstein, J. L., & Ericson, J. (1999). Homeobox gene Nkx2.2 and specification of neuronal identity by graded Sonic hedgehog signalling. *Nature*, *398*(6728), 622–627. https://doi.org/10.1038/19315

Brody, T., Rasband, W., Baler, K., Kuzin, A., Kundu, M., & Odenwald, W. F. (2008). Sequence conservation and combinatorial complexity of Drosophila neural precursor cell enhancers. *BMC genomics*, *9*, 371. https://doi.org/10.1186/1471-2164-9-371

Catron, K. M., Zhang, H., Marshall, S. C., Inostroza, J. A., Wilson, J. M., & Abate, C. (1995). Transcriptional repression by Msx-1 does not require homeodomain DNA-binding sites. *Molecular and cellular biology*, *15*(2), 861–871. https://doi.org/10.1128/MCB.15.2.861

Cau, E., & Blader, P. (2009). Notch activity in the nervous system: to switch or not switch?. *Neural development*, *4*, 36. https://doi.org/10.1186/1749-8104-4-36

Cerrato, V., Mercurio, S., Leto, K., Fucà, E., Hoxha, E., Bottes, S., Pagin, M., Milanese, M., Ngan, C. Y., Concina, G., Ottolenghi, S., Wei, C. L., Bonanno, G., Pavesi, G., Tempia, F., Buffo, A., & Nicolis, S. K. (2018). Sox2 conditional mutation in mouse causes ataxic symptoms, cerebellar vermis hypoplasia, and postnatal defects of Bergmann glia. *Glia*, *66*(9), 1929–1946. https://doi.org/10.1002/glia.23448

Chen, J., Poskanzer, K. E., Freeman, M. R., & Monk, K. R. (2020). Live-imaging of astrocyte morphogenesis and function in zebrafish neural circuits. *Nature neuroscience*, *23*(10), 1297–1306. https://doi.org/10.1038/s41593-020-0703-x

Cheng, A. H., Bouchard-Cannon, P., Hegazi, S., Lowden, C., Fung, S. W., Chiang, C. K., Ness, R. W., & Cheng, H. M. (2019). SOX2-Dependent Transcription in Clock Neurons Promotes the Robustness of the Central Circadian Pacemaker. *Cell reports*, *26*(12), 3191–3202.e8. https://doi.org/10.1016/j.celrep.2019.02.068

Chizhikov, V. V., & Millen, K. J. (2004). Mechanisms of roof plate formation in the vertebrate CNS. *Nature reviews. Neuroscience*, *5*(10), 808–812. https://doi.org/10.1038/nrn1520

Colas, J. F., & Schoenwolf, G. C. (2001). Towards a cellular and molecular understanding of neurulation. *Developmental dynamics : an official publication of the American Association of Anatomists*, *221*(2), 117–145. https://doi.org/10.1002/dvdy.1144

Cong, L., Ran, F. A., Cox, D., Lin, S., Barretto, R., Habib, N., Hsu, P. D., Wu, X., Jiang, W., Marraffini, L. A., & Zhang, F. (2013). Multiplex genome engineering using CRISPR/Cas systems. *Science (New York, N.Y.), 339*(6121), 819–823. https://doi.org/10.1126/science.1231143

Corbo, C. P., Othman, N. A., Gutkin, M. C., Alonso, A., & Fulop, Z. L. (2012). Use of different morphological techniques to analyze the cellular composition of the adult zebrafish optic tectum. *Microscopy research and technique*, *75*(3), 325–333. https://doi.org/10.1002/jemt.21061.

Dallérac, G., Chever, O., & Rouach, N. (2013). How do astrocytes shape synaptic transmission? Insights from electrophysiology. *Frontiers in cellular neuroscience, 7*, 159. https://doi.org/10.3389/fncel.2013.00159

Das, P. M., Ramachandran, K., vanWert, J., & Singal, R. (2004). Chromatin immunoprecipitation assay. *BioTechniques*, *37*(6), 961–969. https://doi.org/10.2144/04376RV01

Dessaud, E., McMahon, A. P., & Briscoe, J. (2008). Pattern formation in the vertebrate neural tube: a sonic hedgehog morphogen-regulated transcriptional network. *Development (Cambridge, England)*, *135*(15), 2489–2503. https://doi.org/10.1242/dev.009324

Duval, N., Daubas, P., Bourcier de Carbon, C., St Cloment, C., Tinevez, J. Y., Lopes, M., Ribes, V., & Robert, B. (2014). Msx1 and Msx2 act as essential activators of Atoh1 expression in the murine spinal cord. *Development (Cambridge, England), 141*(8), 1726–1736. https://doi.org/10.1242/dev.099002

Ekker, M., Akimenko, M. A., Allende, M. L., Smith, R., Drouin, G., Langille, R. M., Weinberg, E. S., & Westerfield, M. (1997). Relationships among msx gene structure and function in zebrafish and other vertebrates. *Molecular biology and evolution*, *14*(10), 1008–1022. https://doi.org/10.1093/oxfordjournals.molbev.a025707

El-Brolosy, M. A., & Stainier, D. (2017). Genetic compensation: A phenomenon in search of mechanisms. *PLoS genetics*, *13*(7), e1006780. https://doi.org/10.1371/journal.pgen.1006780

Elsen, G. E., Choi, L. Y., Millen, K. J., Grinblat, Y., & Prince, V. E. (2008). Zic1 and Zic4 regulate zebrafish roof plate specification and hindbrain ventricle morphogenesis. *Developmental biology*, *314*(2), 376–392. https://doi.org/10.1016/j.ydbio.2007.12.006

England, S., Batista, M. F., Mich, J. K., Chen, J. K., & Lewis, K. E. (2011). Roles of Hedgehog pathway components and retinoic acid signalling in specifying zebrafish ventral spinal cord neurons. *Development (Cambridge, England)*, *138*(23), 5121–5134. https://doi.org/10.1242/dev.066159

Ericson, J., Rashbass, P., Schedl, A., Brenner-Morton, S., Kawakami, A., van Heyningen, V., Jessell, T. M., & Briscoe, J. (1997). Pax6 controls progenitor cell identity and neuronal fate in response to graded Shh signaling. *Cell*, *90*(1), 169–180. https://doi.org/10.1016/s0092-8674(00)80323-2

Ferg, M., Armant, O., Yang, L., Dickmeis, T., Rastegar, S., & Strähle, U. (2014). Gene transcription in the zebrafish embryo: regulators and networks. *Briefings in functional genomics*, *13*(2), 131–143. https://doi.org/10.1093/bfgp/elt044

Ferg, M., Armant, O., Yang, L., Dickmeis, T., Rastegar, S., & Strähle, U. (2014). Gene transcription in the zebrafish embryo: regulators and networks. *Briefings in functional genomics*, *13*(2), 131–143. https://doi.org/10.1093/bfgp/elt044

Ferretti, P., Mackay, M., & Walder, S. (2006). The developing human spinal cord contains distinct populations of neural precursors. *Neuro-degenerative diseases*, *3*(1-2), 38–44. https://doi.org/10.1159/000092091

Filippi, A., Mueller, T., & Driever, W. (2014). vglut2 and gad expression reveal distinct patterns of dual GABAergic versus glutamatergic cotransmitter phenotypes of dopaminergic and noradrenergic

neurons in the zebrafish brain. *The Journal of comparative neurology*, *522*(9), 2019–2037. https://doi.org/10.1002/cne.23524

Filippi, A., Tiso, N., Deflorian, G., Zecchin, E., Bortolussi, M., & Argenton, F. (2005). The basic helix-loop-helix olig3 establishes the neural plate boundary of the trunk and is necessary for development of the dorsal spinal cord. *Proceedings of the National Academy of Sciences of the United States of America*, *102*(12), 4377–4382. https://doi.org/10.1073/pnas.0407284102

Finnerty, J. R., Mazza, M. E., & Jezewski, P. A. (2009). Domain duplication, divergence, and loss events in vertebrate Msx paralogs reveal phylogenomically informed disease markers. *BMC evolutionary biology*, *9*, 18. https://doi.org/10.1186/1471-2148-9-18

Flowers, G. P., Topczewska, J. M., & Topczewski, J. (2012). A zebrafish Notum homolog specifically blocks the Wnt/β-catenin signaling pathway. *Development (Cambridge, England)*, *139*(13), 2416–2425. https://doi.org/10.1242/dev.063206

Forghani, R., Garofalo, L., Foran, D. R., Farhadi, H. F., Lepage, P., Hudson, T. J., Tretjakoff, I., Valera, P., & Peterson, A. (2001). A distal upstream enhancer from the myelin basic protein gene regulates expression in myelin-forming schwann cells. *The Journal of neuroscience : the official journal of the Society for Neuroscience*, *21*(11), 3780–3787. https://doi.org/10.1523/JNEUROSCI.21-11-03780.2001

Fukuhara, S., Zhang, J., Yuge, S., Ando, K., Wakayama, Y., Sakaue-Sawano, A., Miyawaki, A., & Mochizuki, N. (2014). Visualizing the cell-cycle progression of endothelial cells in zebrafish. *Developmental biology*, *393*(1), 10–23. https://doi.org/10.1016/j.ydbio.2014.06.015

Ghosh, S., & Hui, S. P. (2016). Regeneration of Zebrafish CNS: Adult Neurogenesis. *Neural plasticity*, *2016*, 5815439. https://doi.org/10.1155/2016/5815439

Ghosh, S., & Hui, S. P. (2018). Axonal regeneration in zebrafish spinal cord. *Regeneration (Oxford, England)*, *5*(1), 43–60. https://doi.org/10.1002/reg2.99

Giniger, E., Varnum, S. M., & Ptashne, M. (1985). Specific DNA binding of GAL4, a positive regulatory protein of yeast. *Cell*, *40*(4), 767–774. https://doi.org/10.1016/0092-8674(85)90336-8

Glasgow, S. M., Henke, R. M., Macdonald, R. J., Wright, C. V., & Johnson, J. E. (2005). Ptf1a determines GABAergic over glutamatergic neuronal cell fate in the spinal cord dorsal horn. *Development (Cambridge, England)*, *132*(24), 5461–5469. https://doi.org/10.1242/dev.02167

Götz, M., & Barde, Y. A. (2005). Radial glial cells defined and major intermediates between embryonic stem cells and CNS neurons. *Neuron*, *46*(3), 369–372. https://doi.org/10.1016/j.neuron.2005.04.012

Götz, M., & Huttner, W. B. (2005). The cell biology of neurogenesis. *Nature reviews. Molecular cell biology*, *6*(10), 777–788. https://doi.org/10.1038/nrm1739

Götz, M., & Huttner, W. B. (2005). The cell biology of neurogenesis. *Nature reviews. Molecular cell biology*, *6*(10), 777–788. https://doi.org/10.1038/nrm1739

Goulding M. (2009). Circuits controlling vertebrate locomotion: moving in a new direction. *Nature reviews. Neuroscience*, *10*(7), 507–518. https://doi.org/10.1038/nrn2608

Goulding, M. D., Lumsden, A., & Gruss, P. (1993). Signals from the notochord and floor plate regulate the region-specific expression of two Pax genes in the developing spinal cord. *Development (Cambridge, England)*, *117*(3), 1001–1016.

Gowan, K., Helms, A. W., Hunsaker, T. L., Collisson, T., Ebert, P. J., Odom, R., & Johnson, J. E. (2001). Crossinhibitory activities of Ngn1 and Math1 allow specification of distinct dorsal interneurons. *Neuron*, *31*(2), 219–232. https://doi.org/10.1016/s0896-6273(01)00367-1

Gribble, S. L., Nikolaus, O. B., & Dorsky, R. I. (2007). Regulation and function of Dbx genes in the zebrafish spinal cord. *Developmental dynamics : an official publication of the American Association of Anatomists*, *236*(12), 3472–3483. https://doi.org/10.1002/dvdy.21367

Grillner, S., & Jessell, T. M. (2009). Measured motion: searching for simplicity in spinal locomotor networks. *Current opinion in neurobiology*, *19*(6), 572–586. https://doi.org/10.1016/j.conb.2009.10.011

Guo S. (2009). Using zebrafish to assess the impact of drugs on neural development and function. *Expert opinion on drug discovery*, *4*(7), 715–726. https://doi.org/10.1517/17460440902988464

Hardwick, L. J., Ali, F. R., Azzarelli, R., & Philpott, A. (2015). Cell cycle regulation of proliferation versus differentiation in the central nervous system. *Cell and tissue research*, *359*(1), 187–200. https://doi.org/10.1007/s00441-014-1895-8

Haushalter, C., Asselin, L., Fraulob, V., Dollé, P., & Rhinn, M. (2017). Retinoic acid controls early neurogenesis in the developing mouse cerebral cortex. *Developmental biology*, *430*(1), 129–141. https://doi.org/10.1016/j.ydbio.2017.08.006

Helms, A. W., Battiste, J., Henke, R. M., Nakada, Y., Simplicio, N., Guillemot, F., & Johnson, J. E. (2005). Sequential roles for Mash1 and Ngn2 in the generation of dorsal spinal cord interneurons. *Development (Cambridge, England)*, *132*(12), 2709–2719. https://doi.org/10.1242/dev.01859

Hoffmann, S. A., Hos, D., Küspert, M., Lang, R. A., Lovell-Badge, R., Wegner, M., & Reiprich, S. (2014). Stem cell factor Sox2 and its close relative Sox3 have differentiation functions in oligodendrocytes. *Development (Cambridge, England)*, *141*(1), 39–50. https://doi.org/10.1242/dev.098418

Hollyday M. (2001). Neurogenesis in the vertebrate neural tube. *International journal of developmental neuroscience : the official journal of the International Society for Developmental Neuroscience*, *19*(2), 161–173. https://doi.org/10.1016/s0736-5748(00)00093-9

Hornig, J., Fröb, F., Vogl, M. R., Hermans-Borgmeyer, I., Tamm, E. R., & Wegner, M. (2013). The transcription factors Sox10 and Myrf define an essential regulatory network module in differentiating oligodendrocytes. *PLoS genetics*, *9*(10), e1003907. https://doi.org/10.1371/journal.pgen.1003907

Hu, G., Lee, H., Price, S. M., Shen, M. M., & Abate-Shen, C. (2001). Msx homeobox genes inhibit differentiation through upregulation of cyclin D1. *Development (Cambridge, England)*, *128*(12), 2373–2384.

Hudish, L. I., Blasky, A. J., & Appel, B. (2013). miR-219 regulates neural precursor differentiation by direct inhibition of apical par polarity proteins. *Developmental cell*, *27*(4), 387–398. https://doi.org/10.1016/j.devcel.2013.10.015

Hui, S. P., Nag, T. C., & Ghosh, S. (2015). Characterization of Proliferating Neural Progenitors after Spinal Cord Injury in Adult Zebrafish. *PloS one*, *10*(12), e0143595. https://doi.org/10.1371/journal.pone.0143595

Hwang, W. Y., Fu, Y., Reyon, D., Maeder, M. L., Tsai, S. Q., Sander, J. D., Peterson, R. T., Yeh, J. R., & Joung, J. K. (2013). Efficient genome editing in zebrafish using a CRISPR-Cas system. *Nature biotechnology*, *31*(3), 227–229. https://doi.org/10.1038/nbt.2501

Ijaz, S., & Hoffman, E. J. (2016). Zebrafish: A Translational Model System for Studying Neuropsychiatric Disorders. *Journal of the American Academy of Child and Adolescent Psychiatry*, *55*(9), 746–748. https://doi.org/10.1016/j.jaac.2016.06.008

Jessell, T. M., & Dodd, J. (1990). Floor plate-derived signals and the control of neural cell pattern in vertebrates. *Harvey lectures*, *86*, 87–128.

Jimenez, L., Wang, J., Morrison, M. A., Whatcott, C., Soh, K. K., Warner, S., Bearss, D., Jette, C. A., & Stewart, R. A. (2016). Phenotypic chemical screening using a zebrafish neural crest EMT reporter identifies retinoic acid as an inhibitor of epithelial morphogenesis. *Disease models & mechanisms*, *9*(4), 389–400. https://doi.org/10.1242/dmm.021790

Jinek, M., Chylinski, K., Fonfara, I., Hauer, M., Doudna, J. A., & Charpentier, E. (2012). A programmable dual-RNA-guided DNA endonuclease in adaptive bacterial immunity. *Science (New York, N.Y.)*, *337*(6096), 816–821. https://doi.org/10.1126/science.1225829

Johnson, K., Barragan, J., Bashiruddin, S., Smith, C. J., Tyrrell, C., Parsons, M. J., Doris, R., Kucenas, S., Downes, G. B., Velez, C. M., Schneider, C., Sakai, C., Pathak, N., Anderson, K., Stein, R., Devoto, S. H., Mumm, J. S., & Barresi, M. J. (2016). *Glia*, *64*(7), 1170–1189. https://doi.org/10.1002/glia.22990

Kaaij, L., van der Weide, R. H., Ketting, R. F., & de Wit, E. (2018). Systemic Loss and Gain of Chromatin Architecture throughout Zebrafish Development. *Cell reports*, *24*(1), 1–10.e4. https://doi.org/10.1016/j.celrep.2018.06.003

Kautzman, A. G., Keeley, P. W., Nahmou, M. M., Luna, G., Fisher, S. K., & Reese, B. E. (2018). Sox2 regulates astrocytic and vascular development in the retina. *Glia*, *66*(3), 623–636. https://doi.org/10.1002/glia.23269

Khan, M., Vaes, E., & Mombaerts, P. (2011). Regulation of the probability of mouse odorant receptor gene choice. *Cell*, *147*(4), 907–921. https://doi.org/10.1016/j.cell.2011.09.049

Kheradpour, P., Stark, A., Roy, S., & Kellis, M. (2007). Reliable prediction of regulator targets using 12 Drosophila genomes. *Genome research*, *17*(12), 1919–1931. https://doi.org/10.1101/gr.7090407

Kim, C. H., Ueshima, E., Muraoka, O., Tanaka, H., Yeo, S. Y., Huh, T. L., & Miki, N. (1996). Zebrafish elav/HuC homologue as a very early neuronal marker. *Neuroscience letters*, *216*(2), 109–112. https://doi.org/10.1016/0304-3940(96)13021-4

Kim, H., Shin, J., Kim, S., Poling, J., Park, H. C., & Appel, B. (2008). Notch-regulated oligodendrocyte specification from radial glia in the spinal cord of zebrafish embryos. *Developmental dynamics : an official publication of the American Association of Anatomists*, *237*(8), 2081–2089. https://doi.org/10.1002/dvdy.21620

Kimmel, C. B., Ballard, W. W., Kimmel, S. R., Ullmann, B., & Schilling, T. F. (1995). Stages of embryonic development of the zebrafish. *Developmental dynamics : an official publication of the American Association of Anatomists*, *203*(3), 253–310. https://doi.org/10.1002/aja.1002030302

Konno, D., Shioi, G., Shitamukai, A., Mori, A., Kiyonari, H., Miyata, T., & Matsuzaki, F. (2008). Neuroepithelial progenitors undergo LGN-dependent planar divisions to maintain self-renewability during mammalian neurogenesis. *Nature cell biology*, *10*(1), 93–101. https://doi.org/10.1038/ncb1673

Kosodo, Y., Toida, K., Dubreuil, V., Alexandre, P., Schenk, J., Kiyokage, E., Attardo, A., Mora-Bermúdez, F., Arii, T., Clarke, J. D., & Huttner, W. B. (2008). Cytokinesis of neuroepithelial cells can divide their basal process before anaphase. *The EMBO journal*, *27*(23), 3151–3163. https://doi.org/10.1038/emboj.2008.227

Kriegstein, A., & Alvarez-Buylla, A. (2009). The glial nature of embryonic and adult neural stem cells. *Annual review of neuroscience*, *32*, 149–184. https://doi.org/10.1146/annurev.neuro.051508.135600

Krijger, P. H., & de Laat, W. (2016). Regulation of disease-associated gene expression in the 3D genome. *Nature reviews. Molecular cell biology*, *17*(12), 771–782. https://doi.org/10.1038/nrm.2016.138

Kriks, S., Lanuza, G. M., Mizuguchi, R., Nakafuku, M., & Goulding, M. (2005). Gsh2 is required for the repression of Ngn1 and specification of dorsal interneuron fate in the spinal cord. *Development (Cambridge, England)*, *132*(13), 2991–3002. https://doi.org/10.1242/dev.01878

Krishnamurthy, N., & Kurzrock, R. (2018). Targeting the Wnt/beta-catenin pathway in cancer: Update on effectors and inhibitors. *Cancer treatment reviews*, *62*, 50–60. https://doi.org/10.1016/j.ctrv.2017.11.002

Krivega, I., & Dean, A. (2012). Enhancer and promoter interactions-long distance calls. *Current opinion in genetics & development*, *22*(2), 79–85. https://doi.org/10.1016/j.gde.2011.11.001

Kuwabara, T., Hsieh, J., Muotri, A., Yeo, G., Warashina, M., Lie, D. C., Moore, L., Nakashima, K., Asashima, M., & Gage, F. H. (2009). Wnt-mediated activation of NeuroD1 and retro-elements during adult neurogenesis. *Nature neuroscience*, *12*(9), 1097–1105. https://doi.org/10.1038/nn.2360

Kvon E. Z. (2015). Using transgenic reporter assays to functionally characterize enhancers in animals. *Genomics*, *106*(3), 185–192. https://doi.org/10.1016/j.ygeno.2015.06.007

Labun, K., Montague, T. G., Gagnon, J. A., Thyme, S. B., & Valen, E. (2016). CHOPCHOP v2: a web tool for the next generation of CRISPR genome engineering. *Nucleic acids research*, *44*(W1), W272–W276. https://doi.org/10.1093/nar/gkw398

Lai, H. C., Seal, R. P., & Johnson, J. E. (2016). Making sense out of spinal cord somatosensory development. *Development (Cambridge, England)*, *143*(19), 3434–3448. https://doi.org/10.1242/dev.139592

Lanctot, A. A., Guo, Y., Le, Y., Edens, B. M., Nowakowski, R. S., & Feng, Y. (2017). Loss of Brap Results in Premature G1/S Phase Transition and Impeded Neural Progenitor Differentiation. *Cell reports*, *20*(5), 1148–1160. https://doi.org/10.1016/j.celrep.2017.07.018

Lange, C., Huttner, W. B., & Calegari, F. (2009). Cdk4/cyclinD1 overexpression in neural stem cells shortens G1, delays neurogenesis, and promotes the generation and expansion of basal progenitors. *Cell stem cell*, *5*(3), 320–331. https://doi.org/10.1016/j.stem.2009.05.026

Lee, H. J., Hou, Y., Chen, Y., Dailey, Z. Z., Riddihough, A., Jang, H. S., Wang, T., & Johnson, S. L. (2020). Regenerating zebrafish fin epigenome is characterized by stable lineage-specific DNA methylation and dynamic chromatin accessibility. *Genome biology*, *21*(1), 52. https://doi.org/10.1186/s13059-020-1948-0

Lee, K. J., & Jessell, T. M. (1999). The specification of dorsal cell fates in the vertebrate central nervous system. *Annual review of neuroscience*, *22*, 261–294. https://doi.org/10.1146/annurev.neuro.22.1.261

Lewis, K. E., Bates, J., & Eisen, J. S. (2005). Regulation of iro3 expression in the zebrafish spinal cord. *Developmental dynamics : an official publication of the American Association of Anatomists*, *232*(1), 140–148. https://doi.org/10.1002/dvdy.20215

Liem, K. F., Jr, Tremml, G., Roelink, H., & Jessell, T. M. (1995). Dorsal differentiation of neural plate cells induced by BMP-mediated signals from epidermal ectoderm. *Cell*, *82*(6), 969–979. https://doi.org/10.1016/0092-8674(95)90276-7

Lindeman, L. C., Vogt-Kielland, L. T., Aleström, P., & Collas, P. (2009). Fish'n ChIPs: chromatin immunoprecipitation in the zebrafish embryo. *Methods in molecular biology (Clifton, N.J.), 567*, 75–86. https://doi.org/10.1007/978-1-60327-414-2_5

Liu, Y., Helms, A. W., & Johnson, J. E. (2004). Distinct activities of Msx1 and Msx3 in dorsal neural tube development. *Development (Cambridge, England), 131*(5), 1017–1028. https://doi.org/10.1242/dev.00994

Liu, Z., Wang, X., Jiang, K., Ji, X., Zhang, Y. A., & Chen, Z. (2019). TNFα-induced Up-regulation of *Ascl2* Affects the Differentiation and Proliferation of Neural Stem Cells. *Aging and disease, 10*(6), 1207–1220. https://doi.org/10.14336/AD.2018.1028

Lobjois, V., Bel-Vialar, S., Trousse, F., & Pituello, F. (2008). Forcing neural progenitor cells to cycle is insufficient to alter cell-fate decision and timing of neuronal differentiation in the spinal cord. *Neural development, 3*, 4. https://doi.org/10.1186/1749-8104-3-4

Lobjois, V., Benazeraf, B., Bertrand, N., Medevielle, F., & Pituello, F. (2004). Specific regulation of cyclins D1 and D2 by FGF and Shh signaling coordinates cell cycle progression, patterning, and differentiation during early steps of spinal cord development. *Developmental biology, 273*(2), 195–209. https://doi.org/10.1016/j.ydbio.2004.05.031

Lopez-Nunez, O., Alaggio, R., John, I., Ciolfi, A., Pedace, L., Mastronuzzi, A., Gianno, F., Giangaspero, F., Rossi, S., Donofrio, V., Cinalli, G., Surrey, L. F., Tartaglia, M., Locatelli, F., & Miele, E. (2021). Melanotic Neuroectodermal Tumor of Infancy (MNTI) and Pineal Anlage Tumor (PAT) Harbor A Medulloblastoma Signature by DNA Methylation Profiling. *Cancers, 13*(4), 706. https://doi.org/10.3390/cancers13040706

Lower, K. M., Hughes, J. R., De Gobbi, M., Henderson, S., Viprakasit, V., Fisher, C., Goriely, A., Ayyub, H., Sloane-Stanley, J., Vernimmen, D., Langford, C., Garrick, D., Gibbons, R. J., &

Higgs, D. R. (2009). Adventitious changes in long-range gene expression caused by polymorphic structural variation and promoter competition. *Proceedings of the National Academy of Sciences of the United States of America*, *106*(51), 21771–21776. https://doi.org/10.1073/pnas.0909331106

Lyons, D. A., & Talbot, W. S. (2014). Glial cell development and function in zebrafish. *Cold Spring Harbor perspectives in biology*, *7*(2), a020586. https://doi.org/10.1101/cshperspect.a020586

Mali, P., Yang, L., Esvelt, K. M., Aach, J., Guell, M., DiCarlo, J. E., Norville, J. E., & Church, G. M. (2013). RNA-guided human genome engineering via Cas9. *Science (New York, N.Y.)*, *339*(6121), 823–826. https://doi.org/10.1126/science.1232033

Marina, R. J., Brannan, K. W., Dong, K. D., Yee, B. A., & Yeo, G. W. (2020). Evaluation of Engineered CRISPR-Cas-Mediated Systems for Site-Specific RNA Editing. *Cell reports*, *33*(5), 108350. https://doi.org/10.1016/j.celrep.2020.108350

März, M., Chapouton, P., Diotel, N., Vaillant, C., Hesl, B., Takamiya, M., Lam, C. S., Kah, O., Bally-Cuif, L., & Strähle, U. (2010). Heterogeneity in progenitor cell subtypes in the ventricular zone of the zebrafish adult telencephalon. *Glia*, *58*(7), 870–888. https://doi.org/10.1002/glia.20971

Matys, V., Fricke, E., Geffers, R., Gössling, E., Haubrock, M., Hehl, R., Hornischer, K., Karas, D., Kel, A. E., Kel-Margoulis, O. V., Kloos, D. U., Land, S., Lewicki-Potapov, B., Michael, H., Münch, R., Reuter, I., Rotert, S., Saxel, H., Scheer, M., Thiele, S., … Wingender, E. (2003). TRANSFAC: transcriptional regulation, from patterns to profiles. *Nucleic acids research*, *31*(1), 374–378. https://doi.org/10.1093/nar/gkg108

McDermott, K. W., Barry, D. S., & McMahon, S. S. (2005). Role of radial glia in cytogenesis, patterning and boundary formation in the developing spinal cord. *Journal of anatomy*, *207*(3), 241–250. https://doi.org/10.1111/j.1469-7580.2005.00462.x

McGaughey, D. M., & McCallion, A. S. (2010). Efficient discovery of ASCL1 regulatory sequences through transgene pooling. *Genomics*, *95*(6), 363–369. https://doi.org/10.1016/j.ygeno.2010.02.011

Megason, S. G., & McMahon, A. P. (2002). A mitogen gradient of dorsal midline Wnts organizes growth in the CNS. *Development (Cambridge, England)*, *129*(9), 2087–2098.

Mercurio, S., Serra, L., Motta, A., Gesuita, L., Sanchez-Arrones, L., Inverardi, F., Foglio, B., Barone, C., Kaimakis, P., Martynoga, B., Ottolenghi, S., Studer, M., Guillemot, F., Frassoni, C., Bovolenta, P., & Nicolis, S. K. (2019). Sox2 Acts in Thalamic Neurons to Control the Development of Retina-Thalamus-Cortex Connectivity. *iScience*, *15*, 257–273. https://doi.org/10.1016/j.isci.2019.04.030

Misumi, S., Kim, T. S., Jung, C. G., Masuda, T., Urakawa, S., Isobe, Y., Furuyama, F., Nishino, H., & Hida, H. (2008). Enhanced neurogenesis from neural progenitor cells with G1/S-phase cell cycle arrest is mediated by transforming growth factor beta1. *The European journal of neuroscience*, *28*(6), 1049–1059. https://doi.org/10.1111/j.1460-9568.2008.06420.x

Mizuguchi, R., Kriks, S., Cordes, R., Gossler, A., Ma, Q., & Goulding, M. (2006). Ascl1 and Gsh1/2 control inhibitory and excitatory cell fate in spinal sensory interneurons. *Nature neuroscience*, *9*(6), 770–778. https://doi.org/10.1038/nn1706

Mo, C., Li, W., Jia, K., Liu, W., & Yi, M. (2021). Proper Balance of Small GTPase *rab10* Is Critical for PGC Migration in Zebrafish. *International journal of molecular sciences*, *22*(21), 11962. https://doi.org/10.3390/ijms222111962

Molina, A., & Pituello, F. (2017). Playing with the cell cycle to build the spinal cord. *Developmental biology*, *432*(1), 14–23. https://doi.org/10.1016/j.ydbio.2016.12.022

Moore, S., Ribes, V., Terriente, J., Wilkinson, D., Relaix, F., & Briscoe, J. (2013). Distinct regulatory mechanisms act to establish and maintain Pax3 expression in the developing neural tube. *PLoS genetics*, *9*(10), e1003811. https://doi.org/10.1371/journal.pgen.1003811

Moreno, R. L., & Ribera, A. B. (2014). Spinal neurons require Islet1 for subtype-specific differentiation of electrical excitability. *Neural development*, *9*, 19. https://doi.org/10.1186/1749-8104-9-19

Moreno-Mateos, M. A., Vejnar, C. E., Beaudoin, J. D., Fernandez, J. P., Mis, E. K., Khokha, M. K., & Giraldez, A. J. (2015). CRISPRscan: designing highly efficient sgRNAs for CRISPR-Cas9 targeting in vivo. *Nature methods*, *12*(10), 982–988. https://doi.org/10.1038/nmeth.3543

Mutch, C. A., Funatsu, N., Monuki, E. S., & Chenn, A. (2009). Beta-catenin signaling levels in progenitors influence the laminar cell fates of projection neurons. *The Journal of neuroscience : the official journal of the Society for Neuroscience*, *29*(43), 13710–13719. https://doi.org/10.1523/JNEUROSCI.3022-09.2009

Nguyen, V. H., Trout, J., Connors, S. A., Andermann, P., Weinberg, E., & Mullins, M. C. (2000). Dorsal and intermediate neuronal cell types of the spinal cord are established by a BMP signaling pathway. *Development (Cambridge, England)*, *127*(6), 1209–1220.

Nguyen, V. H., Trout, J., Connors, S. A., Andermann, P., Weinberg, E., & Mullins, M. C. (2000). Dorsal and intermediate neuronal cell types of the spinal cord are established by a BMP signaling pathway. *Development (Cambridge, England)*, *127*(6), 1209–1220.

Nurse P. M. (2002). Nobel Lecture. Cyclin dependent kinases and cell cycle control. *Bioscience reports*, *22*(5-6), 487–499. https://doi.org/10.1023/a:1022017701871

Odenwald, W. F., Rasband, W., Kuzin, A., & Brody, T. (2005). EVOPRINTER, a multigenomic comparative tool for rapid identification of functionally important DNA. *Proceedings of the*

National Academy of Sciences of the United States of America, *102*(41), 14700–14705. https://doi.org/10.1073/pnas.0506915102

Okuda, Y., Ogura, E., Kondoh, H., & Kamachi, Y. (2010). B1 SOX coordinate cell specification with patterning and morphogenesis in the early zebrafish embryo. *PLoS genetics*, *6*(5), e1000936. https://doi.org/10.1371/journal.pgen.1000936

Parichy, D. M., Elizondo, M. R., Mills, M. G., Gordon, T. N., & Engeszer, R. E. (2009). Normal table of postembryonic zebrafish development: staging by externally visible anatomy of the living fish. *Developmental dynamics : an official publication of the American Association of Anatomists*, *238*(12), 2975–3015. https://doi.org/10.1002/dvdy.22113

Patthey, C., & Gunhaga, L. (2014). Signaling pathways regulating ectodermal cell fate choices. *Experimental cell research*, *321*(1), 11–16. https://doi.org/10.1016/j.yexcr.2013.08.002

Pei, Z., Wang, B., Chen, G., Nagao, M., Nakafuku, M., & Campbell, K. (2011). Homeobox genes Gsx1 and Gsx2 differentially regulate telencephalic progenitor maturation. *Proceedings of the National Academy of Sciences of the United States of America*, *108*(4), 1675–1680. https://doi.org/10.1073/pnas.1008824108

Pennacchio, L. A., Bickmore, W., Dean, A., Nobrega, M. A., & Bejerano, G. (2013). Enhancers: five essential questions. *Nature reviews. Genetics*, *14*(4), 288–295. https://doi.org/10.1038/nrg3458

Perna, A., & Alberi, L. A. (2019). TF-ChIP Method for Tissue-Specific Gene Targets. *Frontiers in cellular neuroscience*, *13*, 95. https://doi.org/10.3389/fncel.2019.00095

Peukert, D., Weber, S., Lumsden, A., & Scholpp, S. (2011). Lhx2 and Lhx9 determine neuronal differentiation and compartition in the caudal forebrain by regulating Wnt signaling. *PLoS biology*, *9*(12), e1001218. https://doi.org/10.1371/journal.pbio.1001218

Phillips, B. T., Kwon, H. J., Melton, C., Houghtaling, P., Fritz, A., & Riley, B. B. (2006). Zebrafish msxB, msxC and msxE function together to refine the neural-nonneural border and regulate cranial placodes and neural crest development. *Developmental biology*, *294*(2), 376–390. https://doi.org/10.1016/j.ydbio.2006.03.001

Pierani, A., Brenner-Morton, S., Chiang, C., & Jessell, T. M. (1999). A sonic hedgehog-independent, retinoid-activated pathway of neurogenesis in the ventral spinal cord. *Cell*, *97*(7), 903–915. https://doi.org/10.1016/s0092-8674(00)80802-8

Raible, D. W., & Ungos, J. M. (2006). Specification of sensory neuron cell fate from the neural crest. *Advances in experimental medicine and biology*, *589*, 170–180. https://doi.org/10.1007/978-0-387-46954-6_10

Raj, B., Wagner, D. E., McKenna, A., Pandey, S., Klein, A. M., Shendure, J., Gagnon, J. A., & Schier, A. F. (2018). Simultaneous single-cell profiling of lineages and cell types in the vertebrate brain. *Nature biotechnology*, *36*(5), 442–450. https://doi.org/10.1038/nbt.4103

Rakic P. (2003). Elusive radial glial cells: historical and evolutionary perspective. *Glia*, *43*(1), 19–32. https://doi.org/10.1002/glia.10244

Ramos, C., & Robert, B. (2005). msh/Msx gene family in neural development. *Trends in genetics : TIG*, *21*(11), 624–632. https://doi.org/10.1016/j.tig.2005.09.001

Reiprich, S., & Wegner, M. (2014). Sox2: A multitasking networker. *Neurogenesis (Austin, Tex.)*, *1*(1), e962391. https://doi.org/10.4161/23262125.2014.962391

Reiter, F., Wienerroither, S., & Stark, A. (2017). Combinatorial function of transcription factors and cofactors. *Current opinion in genetics & development*, *43*, 73–81. https://doi.org/10.1016/j.gde.2016.12.007

Rocha M, Singh N, Ahsan K, Beiriger A, Prince VE. Neural crest development: insights from the zebrafish. *Dev Dyn*. 2020;249(1):88-111. doi:10.1002/dvdy.122

Roeder R. G. (1996). The role of general initiation factors in transcription by RNA polymerase II. *Trends in biochemical sciences*, *21*(9), 327–335.

Roeder R. G. (2005). Transcriptional regulation and the role of diverse coactivators in animal cells. *FEBS letters*, *579*(4), 909–915. https://doi.org/10.1016/j.febslet.2004.12.007

Rossi, A., Kontarakis, Z., Gerri, C., Nolte, H., Hölper, S., Krüger, M., & Stainier, D. Y. (2015). Genetic compensation induced by deleterious mutations but not gene knockdowns. *Nature*, *524*(7564), 230–233. https://doi.org/10.1038/nature14580

Rougeot, J., Zakrzewska, A., Kanwal, Z., Jansen, H. J., Spaink, H. P., & Meijer, A. H. (2014). RNA sequencing of FACS-sorted immune cell populations from zebrafish infection models to identify cell specific responses to intracellular pathogens. *Methods in molecular biology (Clifton, N.J.)*, *1197*, 261–274. https://doi.org/10.1007/978-1-4939-1261-2_15

Ruvinsky, I., & Ruvkun, G. (2003). Functional tests of enhancer conservation between distantly related species. *Development (Cambridge, England)*, *130*(21), 5133–5142. https://doi.org/10.1242/dev.00711

Sakai, C., Ijaz, S., & Hoffman, E. J. (2018). Zebrafish Models of Neurodevelopmental Disorders: Past, Present, and Future. *Frontiers in molecular neuroscience*, *11*, 294. https://doi.org/10.3389/fnmol.2018.00294

Sakaue-Sawano, A., Kurokawa, H., Morimura, T., Hanyu, A., Hama, H., Osawa, H., Kashiwagi, S., Fukami, K., Miyata, T., Miyoshi, H., Imamura, T., Ogawa, M., Masai, H., & Miyawaki, A. (2008). Visualizing spatiotemporal dynamics of multicellular cell-cycle progression. *Cell*, *132*(3), 487–498. https://doi.org/10.1016/j.cell.2007.12.033

Santiago, L., Daniels, G., Wang, D., Deng, F. M., & Lee, P. (2017). Wnt signaling pathway protein LEF1 in cancer, as a biomarker for prognosis and a target for treatment. *American journal of cancer research, 7*(6), 1389–1406.

Sasai Y. (1998). Identifying the missing links: genes that connect neural induction and primary neurogenesis in pvertebrate embryos. *Neuron, 21*(3), 455–458. https://doi.org/10.1016/s0896-6273(00)80554-1

Satou, C., Kimura, Y., Hirata, H., Suster, M. L., Kawakami, K., & Higashijima, S. (2013). Transgenic tools to characterize neuronal properties of discrete populations of zebrafish neurons. *Development (Cambridge, England), 140*(18), 3927–3931. https://doi.org/10.1242/dev.099531

Schmidt, R., Strähle, U., & Scholpp, S. (2013). Neurogenesis in zebrafish - from embryo to adult. *Neural development, 8*, 3. https://doi.org/10.1186/1749-8104-8-3

Schmidt, R., Strähle, U., & Scholpp, S. (2013). Neurogenesis in zebrafish - from embryo to adult. *Neural development, 8*, 3. https://doi.org/10.1186/1749-8104-8-3

Schröder, S., Herker, E., Itzen, F., He, D., Thomas, S., Gilchrist, D. A., Kaehlcke, K., Cho, S., Pollard, K. S., Capra, J. A., Schnölzer, M., Cole, P. A., Geyer, M., Bruneau, B. G., Adelman, K., & Ott, M. (2013). Acetylation of RNA polymerase II regulates growth-factor-induced gene transcription in mammalian cells. *Molecular cell, 52*(3), 314–324. https://doi.org/10.1016/j.molcel.2013.10.009

Schuijers, J., Junker, J. P., Mokry, M., Hatzis, P., Koo, B. K., Sasselli, V., van der Flier, L. G., Cuppen, E., van Oudenaarden, A., & Clevers, H. (2015). Ascl2 acts as an R-spondin/Wnt-responsive switch to control stemness in intestinal crypts. *Cell stem cell, 16*(2), 158–170. https://doi.org/10.1016/j.stem.2014.12.006

Shlyueva, D., Stampfel, G., & Stark, A. (2014). Transcriptional enhancers: from properties to genome-wide predictions. *Nature reviews. Genetics*, *15*(4), 272–286. https://doi.org/10.1038/nrg3682

Sin, A. T., & Harrison, R. E. (2016). Growth of the Mammalian Golgi Apparatus during Interphase. *Molecular and cellular biology*, *36*(18), 2344–2359. https://doi.org/10.1128/MCB.00046-16

Singleman, C., & Holtzman, N. G. (2014). Growth and maturation in the zebrafish, Danio rerio: a staging tool for teaching and research. *Zebrafish*, *11*(4), 396–406. https://doi.org/10.1089/zeb.2014.0976

Spitz, F., & Furlong, E. E. (2012). Transcription factors: from enhancer binding to developmental control. *Nature reviews. Genetics*, *13*(9), 613–626. https://doi.org/10.1038/nrg3207

Sun, Y., Zhang, B., Luo, L., Shi, D. L., Wang, H., Cui, Z., Huang, H., Cao, Y., Shu, X., Zhang, W., Zhou, J., Li, Y., Du, J., Zhao, Q., Chen, J., Zhong, H., Zhong, T. P., Li, L., Xiong, J. W., Peng, J., … ZAKOC Consortium (2019). Systematic genome editing of the genes on zebrafish Chromosome 1 by CRISPR/Cas9. *Genome research*, *30*(1), 118–126. Advance online publication. https://doi.org/10.1101/gr.248559.119

Suster, M. L., Kikuta, H., Urasaki, A., Asakawa, K., & Kawakami, K. (2009). Transgenesis in zebrafish with the tol2 transposon system. *Methods in molecular biology (Clifton, N.J.)*, *561*, 41–63. https://doi.org/10.1007/978-1-60327-019-9_3

Takahashi, H., Kamiya, A., Ishiguro, A., Suzuki, A. C., Saitou, N., Toyoda, A., & Aruga, J. (2008). Conservation and diversification of Msx protein in metazoan evolution. *Molecular biology and evolution*, *25*(1), 69–82. https://doi.org/10.1093/molbev/msm228

Takezaki N. (2018). Global Rate Variation in Bony Vertebrates. *Genome biology and evolution*, *10*(7), 1803–1815. https://doi.org/10.1093/gbe/evy125

Tambalo, M., Mitter, R., & Wilkinson, D. G. (2020). A single cell transcriptome atlas of the developing zebrafish hindbrain. *Development (Cambridge, England)*, *147*(6), dev184143. https://doi.org/10.1242/dev.184143

Tarnowski, B. I., Spinale, F. G., & Nicholson, J. H. (1991). DAPI as a useful stain for nuclear quantitation. *Biotechnic & histochemistry : official publication of the Biological Stain Commission*, *66*(6), 297–302.

Taverna, E., & Huttner, W. B. (2010). Neural progenitor nuclei IN motion. *Neuron*, *67*(6), 906–914. https://doi.org/10.1016/j.neuron.2010.08.027

Tawk, M., Araya, C., Lyons, D. A., Reugels, A. M., Girdler, G. C., Bayley, P. R., Hyde, D. R., Tada, M., & Clarke, J. D. (2007). A mirror-symmetric cell division that orchestrates neuroepithelial morphogenesis. *Nature*, *446*(7137), 797–800. https://doi.org/10.1038/nature05722

Thisse, B., Pflumio, S., Fürthauer, M., Loppin, B., Heyer, V., Degrave, A., Woehl, R., Lux, A., Steffan, T., Charbonnier, X.Q. and Thisse, C. (2001) Expression of the zebrafish genome during embryogenesis (NIH R01 RR15402). ZFIN Direct Data Submission. . (http://zfin.org).

Tozer, S., Baek, C., Fischer, E., Goiame, R., & Morin, X. (2017). Differential Routing of Mindbomb1 via Centriolar Satellites Regulates Asymmetric Divisions of Neural Progenitors. Neuron, 93(3), 542–551.e4. https://doi.org/10.1016/j.neuron.2016.12.042

Traiffort, E., Zakaria, M., Laouarem, Y., & Ferent, J. (2016). Hedgehog: A Key Signaling in the Development of the Oligodendrocyte Lineage. *Journal of developmental biology*, *4*(3), 28. https://doi.org/10.3390/jdb4030028

Umeda, K., & Shoji, W. (2017). From neuron to behavior: Sensory-motor coordination of zebrafish turning behavior. *Development, growth & differentiation*, *59*(3), 107–114. https://doi.org/10.1111/dgd.12345

van Straaten, H. W., Hekking, J. W., Wiertz-Hoessels, E. J., Thors, F., & Drukker, J. (1988). Effect of the notochord on the differentiation of a floor plate area in the neural tube of the chick embryo. *Anatomy and embryology*, *177*(4), 317–324. https://doi.org/10.1007/BF00315839

Visel, A., Minovitsky, S., Dubchak, I., & Pennacchio, L. A. (2007). VISTA Enhancer Browser--a database of tissue-specific human enhancers. *Nucleic acids research*, *35*(Database issue), D88–D92. https://doi.org/10.1093/nar/gkl822

Visel, A., Blow, M. J., Li, Z., Zhang, T., Akiyama, J. A., Holt, A., Plajzer-Frick, I., Shoukry, M., Wright, C., Chen, F., Afzal, V., Ren, B., Rubin, E. M., & Pennacchio, L. A. (2009). ChIP-seq accurately predicts tissue-specific activity of enhancers. *Nature*, *457*(7231), 854–858. https://doi.org/10.1038/nature07730

Visel, A., Rubin, E. M., & Pennacchio, L. A. (2009). Genomic views of distant-acting enhancers. *Nature*, *461*(7261), 199–205. https://doi.org/10.1038/nature08451

Wang, W., Chen, X., Xu, H., & Lufkin, T. (1996). Msx3: a novel murine homologue of the Drosophila msh homeobox gene restricted to the dorsal embryonic central nervous system. *Mechanisms of development*, *58*(1-2), 203–215. https://doi.org/10.1016/s0925-4773(96)00562-x

Werner, T., Hammer, A., Wahlbuhl, M., Bösl, M. R., & Wegner, M. (2007). Multiple conserved regulatory elements with overlapping functions determine Sox10 expression in mouse embryogenesis. *Nucleic acids research*, *35*(19), 6526–6538. https://doi.org/10.1093/nar/gkm727

Xiong, F., Tentner, A. R., Huang, P., Gelas, A., Mosaliganti, K. R., Souhait, L., Rannou, N., Swinburne, I. A., Obholzer, N. D., Cowgill, P. D., Schier, A. F., & Megason, S. G. (2013). Specified neural progenitors sort to form sharp domains after noisy Shh signaling. *Cell*, *153*(3), 550–561. https://doi.org/10.1016/j.cell.2013.03.023

Yáñez-Cuna, J. O., Dinh, H. Q., Kvon, E. Z., Shlyueva, D., & Stark, A. (2012). Uncovering cis-regulatory sequence requirements for context-specific transcription factor binding. *Genome research*, *22*(10), 2018–2030. https://doi.org/10.1101/gr.132811.111

Yang, S., Oksenberg, N., Takayama, S., Heo, S. J., Poliakov, A., Ahituv, N., Dubchak, I., & Boffelli, D. (2015). Functionally conserved enhancers with divergent sequences in distant vertebrates. *BMC genomics*, *16*, 882. https://doi.org/10.1186/s12864-015-2070-7

Yavatkar, A. S., Lin, Y., Ross, J., Fann, Y., Brody, T., & Odenwald, W. F. (2008). Rapid detection and curation of conserved DNA via enhanced-BLAT and EvoPrinterHD analysis. *BMC genomics*, *9*, 106. https://doi.org/10.1186/1471-2164-9-106

Zhang, S., Rasai, A., Wang, Y., Xu, J., Bannerman, P., Erol, D., Tsegaye, D., Wang, A., Soulika, A., Zhan, X., & Guo, F. (2018). The Stem Cell Factor Sox2 Is a Positive Timer of Oligodendrocyte Development in the Postnatal Murine Spinal Cord. *Molecular neurobiology*, *55*(12), 9001–9015. https://doi.org/10.1007/s12035-018-1035-7

Zhong, Y. F., & Holland, P. W. (2011). The dynamics of vertebrate homeobox gene evolution: gain and loss of genes in mouse and human lineages. *BMC evolutionary biology*, *11*, 169. https://doi.org/10.1186/1471-2148-11-169

Zhuang, B., & Sockanathan, S. (2006). Dorsal-ventral patterning: a view from the top. *Current opinion in neurobiology*, *16*(1), 20–24. https://doi.org/10.1016/j.conb.2005.11.001

Zinzen, R. P., Girardot, C., Gagneur, J., Braun, M., & Furlong, E. E. (2009). Combinatorial binding predicts spatio-temporal cis-regulatory activity. *Nature*, *462*(7269), 65–70. https://doi.org/10.1038/nature08531